

ISSN 1881-7815 Online ISSN 1881-7823

BST

BioScience Trends

Volume 6, Number 5
October, 2012



www.biosciencetrends.com

BST

BioScience Trends



ISSN: 1881-7815
Online ISSN: 1881-7823
CODEN: BTIRCZ
Issues/Year: 6
Language: English
Publisher: IACMHR Co., Ltd.

BioScience Trends is one of a series of peer-reviewed journals of the International Research and Cooperation Association for Bio & Socio-Sciences Advancement (IRCA-BSSA) Group and is published bimonthly by the International Advancement Center for Medicine & Health Research Co., Ltd. (IACMHR Co., Ltd.) and supported by the IRCA-BSSA and Shandong University China-Japan Cooperation Center for Drug Discovery & Screening (SDU-DDSC).

BioScience Trends devotes to publishing the latest and most exciting advances in scientific research. Articles cover fields of life science such as biochemistry, molecular biology, clinical research, public health, medical care system, and social science in order to encourage cooperation and exchange among scientists and clinical researchers.

BioScience Trends publishes Original Articles, Brief Reports, Reviews, Policy Forum articles, Case Reports, News, and Letters on all aspects of the field of life science. All contributions should seek to promote international collaboration.

Editorial Board

Editor-in-Chief:

Masatoshi MAKUUCHI
Japanese Red Cross Medical Center, Tokyo, Japan

Co-Editors-in-Chief:

Xue-Tao CAO
Chinese Academy of Medical Sciences, Beijing, China
Rajendra PRASAD
UP Rural Institute of Medical Sciences & Research, Uttar Pradesh, India
Arthur D. RIGGS
Beckman Research Institute of the City of Hope, Duarte, CA, USA

Chief Director & Executive Editor:

Wei TANG
The University of Tokyo, Tokyo, Japan

Managing Editor:

Munehiro NAKATA
Tokai University, Hiratsuka, Japan

Senior Editors:

Xunjia CHENG
Fudan University, Shanghai, China
Yoko FUJITA-YAMAGUCHI
Tokai University, Hiratsuka, Japan
Na HE
Fudan University, Shanghai, China
Kiyoshi KITAMURA
The University of Tokyo, Tokyo, Japan

Chushi KUROIWA
Yotsukaidou Tokushukai Medical Center, Yotsukaido, Japan
Misao MATSUSHITA
Tokai University, Hiratsuka, Japan
Takashi SEKINE
The University of Tokyo, Tokyo, Japan
Yasuhiko SUGAWARA
The University of Tokyo, Tokyo, Japan

Web Editor:

Yu CHEN
The University of Tokyo, Tokyo, Japan

Proofreaders:

Curtis BENTLEY
Roswell, GA, USA
Christopher HOLMES
The University of Tokyo, Tokyo, Japan
Thomas R. LEBON
Los Angeles Trade Technical College, Los Angeles, CA, USA

Editorial Office

Pearl City Koishikawa 603,
2-4-5 Kasuga, Bunkyo-ku,
Tokyo 112-0003, Japan
Tel: +81-3-5840-8764
Fax: +81-3-5840-8765
E-mail: office@biosciencetrends.com

BioScience Trends

Editorial and Head Office

Pearl City Koishikawa 603, 2-4-5 Kasuga, Bunkyo-ku,
Tokyo 112-0003, Japan

Tel: +81-3-5840-8764, Fax: +81-3-5840-8765
E-mail: office@biosciencetrends.com
URL: www.biosciencetrends.com

Editorial Board Members

Girdhar G. AGARWAL (Lucknow, India)	David M. HELFMAN (Daejeon, Korea)	Mark MEUTH (Sheffield, UK)	Puay Hoon TAN (Singapore, Singapore)
Hirotsugu AIGA (Geneva, Switzerland)	Takahiro HIGASHI (Tokyo, Japan)	Satoko NAGATA (Tokyo, Japan)	Koji TANAKA (Tsu, Japan)
Hidechika AKASHI (Tokyo, Japan)	De-Xing HOU (Kagoshima, Japan)	Miho OBA (Odawara, Japan)	John TERMINI (Duarte, CA, USA)
Moazzam ALI (Geneva, Switzerland)	Sheng-Tao HOU (Ottawa, Canada)	Xianjun QU (Ji'nan, China)	Usa C. THISYAKORN (Bangkok, Thailand)
Ping AO (Shanghai, China)	Yong HUANG (Ji'ning, China)	John J. ROSSI (Duarte, CA, USA)	Toshifumi TSUKAHARA (Nomi, Japan)
Michael E. BARISH (Duarte, CA, USA)	Hirofumi INAGAKI (Tokyo, Japan)	Carlos SAINZ-FERNANDEZ (Santander, Spain)	Kohjiro UEKI (Tokyo, Japan)
Boon-Huat BAY (Singapore, Singapore)	Masamine JIMBA (Tokyo, Japan)	Yoshihiro SAKAMOTO (Tokyo, Japan)	Masahiro UMEZAKI (Tokyo, Japan)
Yasumasa BESSHO (Nara, Japan)	Kimitaka KAGA (Tokyo, Japan)	Erin SATO (Shizuoka, Japan)	Junming WANG (Jackson, MS, USA)
Generoso BEVILACQUA (Pisa, Italy)	Ichiro KAI (Tokyo, Japan)	Takehito SATO (Isehara, Japan)	Ling WANG (Shanghai, China)
Shiuan CHEN (Duarte, CA, USA)	Kazuhiro KAKIMOTO (Osaka, Japan)	Akihito SHIMAZU (Tokyo, Japan)	Stephen G. WARD (Bath, UK)
Yuan CHEN (Duarte, CA, USA)	Kiyoko KAMIBEPPU (Tokyo, Japan)	Zhifeng SHAO (Shanghai, China)	Hisashi WATANABE (Tokyo, Japan)
Naoshi DOHMAE (Wako, Japan)	Haidong KAN (Shanghai, China)	Ri SHO (Yamagata, Japan)	Lingzhong XU (Ji'nan, China)
Zhen FAN (Houston, TX, USA)	Bok-Luel LEE (Busan, Korea)	Judith SINGER-SAM (Duarte, CA, USA)	Masatake YAMAUCHI (Chiba, Japan)
Ding-Zhi FANG (Chengdu, China)	Mingjie LI (St. Louis, MO, USA)	Raj K. SINGH (Dehradun, India)	Yun YEN (Duarte, CA, USA)
Yosiharu FUKUDA (Ube, Japan)	Ren-Jang LIN (Duarte, CA, USA)	Junko SUGAMA (Kanazawa, Japan)	George W-C. YIP (Singapore, Singapore)
Rajiv GARG (Lucknow, India)	Hongxiang LOU (Ji'nan, China)	Hiroshi TACHIBANA (Isehara, Japan)	Benny C-Y ZEE (Hong Kong, China)
Ravindra K. GARG (Lucknow, India)	Daru LU (Shanghai, China)	Tomoko TAKAMURA (Tokyo, Japan)	Xiaomei ZHU (Seattle, WA, USA)
Makoto GOTO (Yokohama, Japan)	Duan MA (Shanghai, China)	Tadatoshi TAKAYAMA (Tokyo, Japan)	
Demin HAN (Beijing, China)	Yutaka MATSUYAMA (Tokyo, Japan)	Shin'ichi TAKEDA (Tokyo, Japan)	
Jinxiang HAN (Ji'nan, China)	Qingyue MENG (Beijing, China)	Sumihito TAMURA (Tokyo, Japan)	

(as of October 2012)

Review

- 219 - 228 **Biomass fuel exposure and respiratory diseases in India.**
Rajendra Prasad, Abhijeet Singh, Rajiv Garg, Giridhar B. Hosmane

Brief Report

- 229 - 233 **Angiogenin expression in the sera and skin of patients with rheumatic diseases.**
Aki Kuwahara, Masatoshi Jinnin, Takamitsu Makino, Ikko Kajihara, Katsunari Makino, Noritoshi Honda, Wakana Nakayama, Kuniko Inoue, Satoshi Fukushima, Hironobu Ihn

Original Articles

- 234 - 240 **Density functional theory based quantitative structure-property relationship studies on coumarin-based prodrugs.**
Xinying Yang, Xuben Hou, Binghe Wang, Minyong Li, Hao Fang
- 241 - 247 **Fluorimetric assay for D-amino acid oxidase activity in rat brain homogenate by using D-kynurenine as a substrate.**
Anna Kozaki, Sumiko Iwasa, Shoko Hosoda, Yoshikazu Nishiguchi, Moe Nakakyama, Hideaki Ichiba, Takeshi Fukushima
- 248 - 261 **Identification of MIWI-associated Poly(A) RNAs by immunoprecipitation with an anti-MIWI monoclonal antibody.**
Takahiro Nishibu, Yukinobu Hayashida, Saori Tani, Sadamu Kurono, Kanako Kojima-Kita, Ryo Ukekawa, Tsutomu Kurokawa, Satomi Kuramochi-Miyagawa, Toru Nakano, Kunio Inoue, Susumu Honda
- 262 - 269 **Effects of Xiaoqinglong decoction on gene expression profiles in a rat chronic obstructive pulmonary disease model.**
Caiqing Zhang, Lili Feng, Ming Li, Chongjuan Dong, Wei Zhang
-

CONTENTS

(Continued)

- 270 - 275 **An *in vitro* study of pcDNA 3.0-hVEGF165 gene transfection in endothelial progenitor cells derived from peripheral blood of rabbits.**
Xiulian Gu, Xiaoyong Miao, Jia Xu, Jianping Cao

-
- 276 - 282 **Increased cerebrovascular resistance after retrograde cerebral perfusion: A Doppler study.**
Nobuhide Kin, Nagara Ono, Yoshiteru Mori, Jun Ninagawa, Yoshitsugu Yamada

Guide for Authors

Copyright

(This journal was partially supported by a Grant-in-Aid for Scientific Research from Japan Society for the Promotion of Science.)

Biomass fuel exposure and respiratory diseases in India

Rajendra Prasad^{1,*}, Abhijeet Singh², Rajiv Garg², Giridhar B. Hosmane³

¹ UP Rural Institute of Medical Sciences and Research, Safai, Etawah, India;

² Department of Pulmonary Medicine, CSM Medical University, Lucknow, India;

³ Department of TB, Chest & Respiratory Diseases, KS Hegde Medical Academy, Mangalore, India.

Summary

One half of the world's population relies on biomass fuel as the primary source of domestic energy. Biomass fuel exposure causes a high degree of morbidity and mortality in humans. This is especially true in the context of developing countries, which account for 99% of the world's biomass fuel use. Biomass fuel consists of fire wood, dung cakes, agricultural crop residues such as straw, grass, and shrubs, coal fuels and kerosene. Together, they supply 75% of the domestic energy in India. An estimated three-quarters of Indian households use biomass fuel as the primary means for domestic cooking. Ninety percent of rural households and 32% of urban households cook their meals on a biomass stove. There are wide variations between the rural and urban households regarding the specific type of biomass fuel used. Globally, almost 2 million deaths per year are attributable to solid fuel use, with more than 99% of these occurring in developing countries. Biomass fuel accounts for 5-6% of the national burden of disease. Burning biomass fuels emits toxic fumes into the air that consist of small solid particles, carbon monoxide, polyorganic and polyaromatic hydrocarbons, and formaldehyde. Exposure to biomass fuels has been found to be associated with many respiratory diseases such as acute lower respiratory infections, chronic obstructive pulmonary disease, lung cancer, pulmonary tuberculosis, and asthma. Biomass fuel exposure is closely related to the burden of disease in India. Hopes are that future studies will examine the morbidity associated with biomass exposure and seek to prevent it. Concerted efforts to improve stove design and transition to high-efficiency low-emission fuels may reduce respiratory disease associated with biomass fuel exposure.

Keywords: Biomass fuels, chronic obstructive pulmonary disease (COPD), tuberculosis, cancer

1. Introduction

One half of the world's population relies on biomass fuel as the primary source of domestic energy (1). Biomass fuel causes a high degree of morbidity and mortality in humans. This is especially true in the context of developing countries, which account for 99% of the world's biomass fuel use (2). Biomass fuel consists of firewood, dung cakes, agricultural crop residues (such as straw, grass, and shrubs), coal fuels, and kerosene. Together, they supply 75% of the domestic energy in India. The rest of the country relies on cleaner fuels, namely liquified petroleum gas (LPG)

and natural gas.

2. Biomass fuel use in India

An estimated three-quarters of Indian households use biomass fuel as the primary means for domestic cooking. Ninety percent of rural households and 32% of urban households cook their meals on a biomass stove. Only 25% of the cooking is done with cleaner gases. Ninety percent of households using biomass fuels cook on an open fire. There are wide variations between rural and urban households regarding the specific type of biomass fuel used. In rural India, 62% of households use firewood and 14% cook with dung cakes while 13% use straw, shrubs, grass and agricultural crop residues to fire their stoves. In urban India, 22% use firewood, 8% use kerosene, and the rest uses cleaner fuels like LPG or natural gas (3). According to World Health Organization, an estimated 58% of the Indian

*Address correspondence to:

Dr. Rajendra Prasad, UP Rural Institute of Medical Sciences and Research, Safai, Etawah, India.

E-mail: rprasadkgmc@gmail.com

population depended on solid fuels for domestic use in 2010 (4). Seventy-five percent of rural households reported firewood as their primary cooking fuel as compared to only 22% of urban households. Clearly, factors such as affordability, education, availability, constraints on cooking space, social customs, and demographics (e.g. working women) play a significant role in the choice of fuel in urban areas (5).

3. Morbidity and mortality

Globally, almost 2 million deaths per year are attributable to solid fuel use, with more than 99% of these occurring in developing countries (1). The number of disability-adjusted life years (DALYs) attributable to indoor air pollution from solid fuel for all uses is calculated to be 40 million. India's figures are very alarming. With a yearly death toll of 662,000 attributed to biomass fuel exposure, India tops the list of fuel-related deaths in the South Asian region (2). Biomass fuel attributes for 5-6% of the national burden of disease (6). Indoor air pollution from solid fuel use in all developing countries was estimated to account for about 1.6 million deaths annually in 2004 and about 500,000 in India in 2010, suggesting a serious impact on health (7,8).

4. Emissions from a biomass stove and exposure-determining factors

When firewood (an essential biomass fuel) is burnt, its combustion efficiency is far less than 100%. This indicates that biomass fuels are at the high end of the fuel ladder in terms of pollution emissions and at the low end in terms of combustion efficiency (9). Typical biomass cook stoves convert 6-20% of the fuel carbon to toxic substances. What fuels actual cooking is only 18%, whereas 74% of the carbon is dissipated as waste heat (10). Burning biomass fuels emits toxic fumes into the air, and the content of these fumes will now be described in detail.

4.1. Small solid particles

Particles with a diameter smaller than 10 μm (PM10), and particularly those with a diameter smaller than 2.5 μm (PM2.5), can penetrate deeply into the lungs and appear to have the greatest potential for damaging health. Several studies have shown remarkable consistency in the relationship between change in daily ambient suspended particulate levels and subsequent changes in mortality (11). The range of risk was found to be 1.2-4.4% increased mortality per 10 mg/m^3 increase in concentration of respirable suspended particles. The concentration distribution of indoor particles less than 10 μm (PM10) measured over 24 h in Indian households using solid fuels was over

2,000 $\mu\text{g}/\text{m}^3$ compared to 30 $\mu\text{g}/\text{m}^3$ in the US (11). The determination of the concentration of suspended particles offers the best indicator of health risk (12). A simple Monte Carlo single-box model is presented as a recent approach to examine the relationship between emissions of pollutants from fuel as well as stove combinations and the resulting Indoor Air Pollution (IAP) concentrations (13). This model combines stove emission rates with expected distributions of kitchen volumes and air exchange rates in the context of a developing country to produce a distribution of IAP concentration estimates that can be used to predict if IAP concentrations will meet air quality guidelines, including those recommended by the WHO for fine particulate matter (PM2.5) (14). The modeled distributions of indoor PM2.5 concentration estimated that only 4% of homes using fuel wood in a rocket-style cook stove, even under ideal conditions, would meet the WHO Interim-1 annual PM2.5 guideline of 35 mg/m^3 . According to the model, the PM2.5 emissions that would be required for even 50% of homes to meet this guideline (0.055 g MJ-delivered-1) are lower than those for an advanced gasifier fan stove, while emissions levels akin to those of liquefied petroleum gas (0.018 g MJ-delivered-1) would be required for 90% of homes to meet the guideline. Although the predicted distribution of PM concentrations (median-1,320 $\mu\text{g}/\text{m}^3$) from inputs for traditional wood stoves was within the range of reported values for India (108-3,522 $\mu\text{g}/\text{m}^3$), the model likely overestimates IAP concentrations.

4.2. Carbon monoxide

An estimated 38 g, 17 g, 5 g, and 2 g/meal of carbon monoxide is released during household cooking using dung, crop residues, wood, and kerosene, respectively (15). The short-term health effects of CO exposure include dizziness, headaches, nausea, and feeling weak. An association between long-term exposure to carbon monoxide from cigarette smoke and heart disease and fetal development has been noted (16).

4.3. Polyorganic and polyaromatic hydrocarbons

Polyaromatic hydrocarbons include a large class of compounds released during the incomplete combustion of organic matter (17). Benzopyrene is one of the most important carcinogens in this group (18). In addition to PAH, azo and amino compounds have also been found to be potentially carcinogenic. A study by the National Institute of Occupational Health showed that the indoor levels of PAH (total) in air during use of dung, wood, coal, kerosene, and LPG were 3.56, 2.01, 0.55, 0.23, and 0.13 $\mu\text{g}/\text{m}^3$, respectively (19). These PAHs include fluorine, pyrene, chrysene, benzoanthracene, benzofluoranthene, benzofluoranthene, benzopyrene, dibenzanthracene, benzoperylene, and indenopyrene.

All but the first three of these PAHs have been classified as possible carcinogens.

4.4. Formaldehyde

The mean levels of formaldehyde emitted from cattle dung ($670 \mu\text{g}/\text{m}^3$), wood ($652 \mu\text{g}/\text{m}^3$), coal ($109 \mu\text{g}/\text{m}^3$), kerosene ($112 \mu\text{g}/\text{m}^3$), and LPG ($68 \mu\text{g}/\text{m}^3$) have been calculated (20). In an epidemiological study in the UK, significantly excess mortality from lung cancer was observed in workers exposed to high levels of formaldehyde (21). Formaldehyde is recognized as an acute irritant and long-term exposure to it can cause a reduction in vital capacity and chronic bronchitis. It is known to form crosslinks with biologic macromolecules. Inhaled formaldehyde forms DNA and DNA-protein cross-links in the nasal respiratory mucosa (22). Studies in workers occupationally exposed to formaldehyde have consistently noted a higher incidence of leukemia (23).

Biomass smoke has a pathological effect. The toxic fumes released from a biomass stove contain organic chemicals that are known mutagens, immune system suppressants, severe irritants, blood poisons, inflammatory agents, CNS depressants, cilia toxins, endocrine disruptors, and neurotoxins. A number of other chemicals released have been demonstrated to be human carcinogens. Several toxic inorganic chemicals are known to cause asphyxiation, stillbirth, infant death, heart disease, and severe acute and chronic lung disease. Many mechanisms of cell injury are still unexplained.

5. Household composition and biomass smoke exposure

The level of exposure to the toxic fumes from a biomass stove varies widely with the house architecture and household composition. Quantitative exposure assessments have been conducted in various households in different parts of India in order to determine exposure-response relationships. The climatic and cultural variations between northern and southern India have influenced outcomes significantly. Cooking areas in many Indian households tend to be poorly ventilated, and about one-half of all households do not have a separate kitchen. Most households lack a chimney or other means of ventilation. One study conducted in Porur, Chennai reported that 36% of households use biomass fuels to cook in indoor kitchens without partitions, 30% cook in a separate kitchen inside the house, 19% cook in a separate kitchen outside the house, and 16% cook in an outdoor kitchen (24). The level of individual exposure to respirable particles in biomass smoke does not significantly differ for cooks using an indoor kitchen with or without partitions and cooks using a separate kitchen outside the house but

it does differ significantly ($p < 0.05$) for cooks using open outdoor kitchens as emissions are dispersed more outdoors. Therefore cooks using an open outdoor kitchen have less exposure than cooks using an enclosed kitchen. Households with kitchens without partitions have higher concentrations of particles in living areas. Young children and the elderly often occupy living areas and are exposed to higher levels of smoke in unpartitioned indoor kitchens. Among individuals not cooking in a household using solid fuels, women who were not involved in cooking and men with outdoor jobs had the lowest exposure, while women who assisted with cooking and men staying at home had the highest exposure. The level of exposure does not appear to be significantly associated with the length of cooking, the number of meals cooked, outdoor area measurements, or the presence or absence of chimneys (10,24).

6. Respiratory effects of biomass fuels

Many respiratory diseases have been found to be associated with exposure to biomass fuels. The strength of association varies for diseases like acute respiratory infections (ALRI), chronic obstructive pulmonary disease (COPD), lung cancer, pulmonary tuberculosis (TB), asthma, and interstitial lung disease (ILD). The evidence relates to this strength of association is depicted in Table 1 (25). The relative risks shown in the table are generally applicable since they are based on the entire evidence base. The relative risks include the results of formal meta-analyses with regard to ALRI, COPD, and lung cancer (from exposure to coal smoke). More recent studies including meta-analyses of the available epidemiological evidence have been conducted in India, as summarized in Table 2.

6.1. ALRI in children under 5 years of age

ALRI accounts for 13% of deaths and 11% of the national burden of disease (6). One of the major diseases associated with indoor air quality is ALRI. It includes infections from a wide range of viruses and bacteria but with similar symptoms and risk factors (26). Many studies have found that various respiratory symptoms (coughing, wheezing, etc.) are associated with solid fuel smoke exposure. However, none have provided sufficient evidence to calculate odds ratios. A host of odd's ratios ranging from 1.9-2.7 have been calculated (25). These ratios pertain to children with ALRI younger than 5 years only. Other factors might strongly influence the incidence of ALRI, such as housing type, cooking location, and cultural practices (27). Some of the studies in India have reported no association between use of biomass fuels and ALRI in children. In a case-controlled study of children under five years of age in southern Kerala, India, children

Table 1. Evidence relating to the strength of the association between biomass fuels and some common respiratory diseases in developing countries

Evidence	Health outcome	Group (age) (ys)	Relative risk	95% CI	Studies	Location	Ref.
Strong ^a	ALRI	Children < 5	2.3	1.9-2.7	Campbell, Armsrong & Bypass (1989)	Gambia	(45)
					Armstrong & Campbell (1991)	Gambia	(46)
					Cerquero (1990)	Argentina	(47)
					Collings, Sithole & Martin (1990)	Zimbabwe	(48)
					De Francisco (1993)	Gambia	(49)
					Ezzati & Kammen (2001)	Kenya	(50)
					Johnson & Aderere (1992)	Nigeria	(51)
					Kossove (1982)	S. Africa	(52)
					Morris (1990)	USA	(53)
					Mtango (1992)	Tanzania	(54)
					O'Dempsey (1996)	Gambia	(55)
					Pandey (1989)	Nepal	(56)
					Robin (1996)	USA	(57)
					Shah (1994)	India	(28)
Victora (1994)	Brazil	(58)					
Strong ^a	COPD	Women ≥ 30	3.2	2.3-4.8	Albalak, Frisancho & Keeler (1999)	Bolivia	(59)
					Behera, Dash & Yadav (1991)	India	(60)
					Dennis (1996)	Colombia	(61)
					Dossing & Khan (1994)	Saudi Arabia	(62)
					Dutt (1996)	India	(63)
					Gupta & Mathur (1997)	India	(30)
Moderate-I ^b	COPD	Men ≥ 30	1.8	1.0-3.2	Malik (1985)	India	(64)
					Menezes, Victora & Rigatto (1994)	Brazil	(65)
					Pandey (1984)	Nepal	(66)
					Perez-Padilla (1996)	Mexico	(67)
					Qureshi (1994)	India	(68)
Strong ^a	Lung Cancer (Coal smoke exposure)	Women ≥ 30	1.9	1.1-3.5	Dai (1996)	China	(69)
					Du (1988)	China	(70)
					Du (1996)	China	(71)
Moderate-I ^b	Lung Cancer (Coal smoke exposure)	Men ≥ 30	1.5	1.0-2.5	Gao (1987)	China	(72)
					Huang (1999)	China	(73)
					Ko (1997)	Taiwan	(74)
Moderate-II ^c	Lung Cancer (Biomass smoke exposure)	Women ≥ 30	1.5	1.0-2.1	Lei (1996)	China	(75)
		Children 5-14	1.6	1.0-2.5	Liu, He & Chapman (1991)	China	(76)
					Liu (1993)	China	(77)
					J. Liu & H. Hu (Unpublished data)	China	(78)
					Luo (1996)	China	(79)
					Shen (1996)	China	(80)
					Sobue (1990)	Japan	(81)
					Wang, Zhou & Shi (1996)	China	(82)
					Wu (1985)	USA	(83)
					Wu-Williams (1990)	China	(84)
					Wu (1999)	China	(85)
					Xu (1996)	China	(86)
					Yang, Jiang & Wang (1988)	China	(87)
Moderate-II ^c	Asthma	All ≥ 15	1.2	1.0-1.5	Azizi, Zulkifi & Kasim (1995)	Malaysia	(88)
					Mohamed (1995)	Kenya	(89)
					Xu, Niu & Christian (1996)	China	(90)
Moderate-II ^c	Tuberculosis	All ≥ 15	1.5	1.0-2.4	Gupta & Mathur (1997)	India	(30)
					Mishra, Retherford & Smith (1999)	India	(98)
					Perez-Padilla (1996)	Mexico	(67)
					Perez-Padilla (2001)	Mexico	(91)

^a "Strong" indicates that the results of studies on household pollution in developing countries reveal a consistent, sizeable, plausible, and coherent relationship, with supporting evidence from studies of outdoor air pollution, active and passive smoking, and laboratory animals. "Moderate" indicates a relatively small number of suggestive findings from studies on household pollution in developing countries, and some evidence from studies on outdoor air pollution, smoking, or laboratory animals indicating further more studies are required to strengthen the evidence base and pinpoint risks. Moderate can be further classified as: ^b "Moderate-I" indicates an association between solid fuel use and a health outcome for which there is strong evidence for specific age and sex groups; ^c "Moderate-II" indicates that there is as yet no strong evidence. Note: Studies conducted in India are shown in bold. Adapted from Desai MA, Mehta S, Smith KR. WHO protection of the human environment, Geneva, 2004 (25) and Smith KR. National burden of disease in India from indoor air pollution. Proc Natl Acad Sci. 2000 (6).

Table 2. Major Indian studies depicting the association between current solid fuel use relative to cleaner burning fuel or electricity and the risk of common respiratory diseases

Respiratory disease	Authors	Study type	Outcome	Odds ratio/Incidence risk ratio (95% CI)	Ref.
Tuberculosis	Gupta <i>et al.</i> (1997)	Case-control India	Clinical pulmonary	2.54 (1.07-6.04)	(30)
	Mishra <i>et al.</i> (1999)	Cross-sectional: India (National Family Health Survey)	Self-reported	2.58 (1.98-3.37)	(98)
	Shetty <i>et al.</i> (2006)	Case-control India	Clinical Pulmonary	3.26 (1.25-8.46)	(93)
	Mageshwari U <i>et al.</i> (2008)	Case-control India	Clinical Pulmonary	0.22 (0.12-0.41)	(102)
	Kolappan <i>et al.</i> (2009)	Case-control India	Clinical pulmonary	2.9 (1.8-4.7)	(36)
	Behera D <i>et al.</i> (2010)	Case-control India	Clinical pulmonary	0.60 (0.22-1.63)	(95)
	Lakshmi <i>et al.</i> (2012)	Case-control India	Clinical pulmonary	2.33 (1.18-4.59)	(94)
ALRI	Mishra <i>et al.</i> (2005)	Cross-sectional survey	Self-reported symptoms	1.58 (1.28-1.95)	(98)
	Dherani <i>et al.</i> (2008)	Meta-analysis	24 studies for calculation of OR	1.78 (1.45-2.18)	(96)
	Ramaswamy P <i>et al.</i> (2011)	Longitudinal cohort	Clinical symptoms and estimation of the incidence risk ratio among children from households using biomass fuels relative to cleaner fuels	1.33 (1.02-1.73)	(103)
Lung cancer	Gupta D <i>et al.</i> (2001)	Case-control India	Clinical, radiological, and histopathological assessment	1.52 (0.33-6.98)	(99)
	Behera D <i>et al.</i> (2005)	Case-control India	Clinical, radiological, and histopathological assessment	3.59 (1.07-11.97)	(33)
	Sapkota A <i>et al.</i> (2008)	Case-control India	Clinical, radiological, and histopathological assessment	3.76 (1.64-8.63)	(34)
	Hosgood HD <i>et al.</i> (2011)	Meta-analysis	25 studies for estimation of OR	2.15 (1.61-2.89)	(100)
COPD	Behera D <i>et al.</i> (1991)	Descriptive study	Clinical assessment	3.04 (2.15-4.31)	(101)
	Qureshi <i>et al.</i> (1994)	Case-control India	Clinical assessment	2.10 (1.50-2.94)	(68)
	Kurmi OP <i>et al.</i> (2010)	Meta-analysis	12 studies for estimation of OR	2.80 (1.85-4.0)	(97)

with severe pneumonia (meeting WHO criteria) were compared to those with non-severe ALRI seen as outpatients. According to the study, cooking fuel was not a major risk factor for severe ALRI (28). In a cross-sectional study involving 642 infants dwelling in urban slums of Delhi where wood and kerosene were used, Sharma *et al.* found no significant difference in the prevalence of ALRI infections and the type of fuel (27).

6.2. COPD

COPD accounts for 1.5% of deaths and represents 0.9% of the national burden of disease in India (6). Both men and women have similar rates of incidence of chronic cor pulmonale. This is despite the fact that only 10% of women are smokers compared to 75% of men. Another point to note is that chronic cor pulmonale occurs 10-15 years earlier in women than in men (29). Various Indian studies have calculated a relative risk of 2-4 for biomass fuel exposure (6). Despite the progress made in highlighting the association between biomass fuel exposure and COPD, many problems still exist. Smoking is an important confounding variable for COPD and particularly so when men are included in the analyses. Another major confounding factor is age. The risk of COPD increases with age and many age-matched studies have provided insufficient quantitative evidence to develop an odds ratio. The overall risk of

COPD in women exposed to biomass fuel has been estimated as 3.2 (95% CI 2.3-4.8) (25). There is much less evidence available about the impact on men, but the risk seems to be lower with an odds ratio (OR) of 1.8 (95% CI 1.0-3.2). This may be attributed to the lower exposure of men to biomass fumes (30).

6.3. Lung cancer

Lung cancer in women is an amply demonstrated outcome of cooking with open coal stoves in China (31). Indian women generally have low lung cancer rates (32). This may be attributed to the minimal use of coal for cooking in Indian households. Nevertheless, a few studies in India have suggested an association with lung cancer even after adjusting for active and passive smoking. An odds ratio of 3.59 (95% CI 1.07-11.97) has been calculated (33). In conclusion, there is a general lack of epidemiological evidence associating lung cancer with biomass fuel exposure. The few cases reported have been linked to exposure to coal fires (34).

6.4. TB

TB is a major public health problem in India. Out of the 9.4 million new cases recorded globally, 1.98 million are reported from India (35). An estimated 276,000 deaths occur annually due to TB in India. There is a

strong association between the use of biomass fuel and pulmonary TB. A high risk of pulmonary TB exists in individuals using wood and cow dung cake as cooking fuel (36). Lowered immunodefense mechanisms of the lung may why the disease develops. Biomass fuel poses a higher risk (969/100,000) of TB compared to cleaner fuels (378/100,000). Fifty-one percent of active TB in individuals over 20 is believed to be attributed to smoke from cooking with biomass fuels (37).

A study in Nepal implicated the use of kerosene stoves and wick lamps in the development of TB. Compared to use of a cleaner fuel like LPG or biogas, the adjusted OR for using a biomass fuel stove was 1.21 (95% CI 0.48-3.05). A kerosene fuel stove had an OR of 3.36 (95% CI 1.01-11.22). The OR of biomass fuel for heating was 3.45 (95% CI 1.44-8.27). Kerosene lamps used for lighting had an OR of 9.43 (95% CI 1.45-61.32). This study further found that use of indoor biomass fuel for heating purposes is associated with TB in women (38). This is supported by a recent study in India (94). Given the prevalence of TB in India and its likeliness to increase with HIV, these findings need to be followed up with more detailed studies.

6.5. Pneumoconiosis and ILD

Pneumoconiosis has been reported from Ladakh, a hilly region in northernmost India (39). This place is completely devoid of industries or mines, and yet cases of a disease resembling miner's pneumoconiosis have been reported. Another factor for this respiratory morbidity is exposure to dust from dust storms. In the spring, dust storms blanket villages in fine dust. The practice of not allowing wood to burn quickly and allowing it to smoulder to conserve fuel adds to the high level of respirable particles indoors. Low oxygen levels or some other factor associated with a high altitude may contribute to pneumoconiosis because miners working at high altitudes are more prone to develop pneumoconiosis than their counterparts who are exposed to the same levels of dust and work in mines at normal altitudes (40). Biomass fuel exposure has not been proven to cause pneumoconiosis (39). Although a few case reports have similarly linked ILD and biomass fuel exposure, the validity of the association is still debatable (41).

7. Toxicological evidence of the strength of the association between biomass fuels and respiratory diseases

Toxicological studies are quite useful to study the effects of air pollutants on humans but cannot be conducted directly because of limitations such as societal concerns, ethical and legal issues, and cost. Therefore, predictive health assessments of inhaled pollutants need to include information gained from

animal exposure studies and, in some cases, *in vitro/ex vivo* assay systems in order to overcome these limitations. These animal studies contribute to a better understanding of the possible mechanism(s) by which smoke, and its associated PM, may act to bring about increased pulmonary morbidity in exposed individuals and also have the potential to help uncover information concerning the mechanisms of toxicity and relative toxicity of different mixtures and sources. Few toxicological studies in India have indicated that exposure to smoke results in significant impacts on the respiratory immune system and can produce long-term or permanent lesions in lung tissues at high doses. These effects seem to be most strongly associated with the particle phase. Lal *et al.* examined the hematological and histopathologic responses of rats exposed repeatedly to smoke generated from the combustion of wood dust and they found that the rats had cell desquamation, pulmonary edema, and perivascular infiltration of neutrophils upon acute exposure and emphysematous alveolar destruction as well as eosinophilia upon chronic exposure (42). Bhattacharyya *et al.* examined the effects of pinewood smoke exposure on rabbit tracheal explants for 20 minutes and found degeneration of the mucociliary epithelial sheath although shorter exposure to smoke of 10 minutes resulted in retained tissue integrity but altered epithelial morphology (43). Thus, these toxicological studies indicate biological plausibility of the epidemiologic evidence suggesting that exposure to smoke emissions adversely affects human health. Clearly, short-term inhalation of smoke appears to compromise pulmonary immune defense mechanisms that are vital to maintaining host resistance against pulmonary infections. These studies lend support to the notion that inhaled smoke contributes to the increased incidence of infectious respiratory disease reported in children living in developing nations and/or near homes heated by wood burning devices (44). Data are currently insufficient to reliably distinguish the toxicological effects of different types of biomass smoke. More work in this area is needed to better understand the mechanisms by which adverse effects observed in exposed individuals might occur.

8. Conclusion

In conclusion, biomass fuel exposure contributes substantially to the burden of disease in India. Many studies in this vein have discovered significant associations with diseases like ALRI and COPD. More evidence is needed to establish the association between solid fuel smoke and other diseases. Implementing strategies to reduce or eliminate exposure is very challenging because it must consider the level of individual exposure as well as cultural and economic aspects at the individual and local levels, including the

level of development, resources, technical capacity, domestic energy needs, the sustainability of the sources of energy considered, and protection of the environment. Substantial improvement can be brought about by health education and cultural changes, modification of stove design, and switching over to cleaner fuels or other high-efficiency low-emission fuels for cooking. Physicians and health administrators should have a heightened awareness of the health effects of solid fuel smoke inhalation as this may spur research and preventive measures and facilitate the diagnosis and treatment of future patients. Hopes are that future studies will examine the morbidity associated with biomass exposure and seek to prevent it. This is a pressing issue given the great risk posed by solid fuels in rural India.

References

- World Health Organization. The World health report: 2004: Changing history. <http://www.who.int/whr/2004/en/> (accessed February 12, 2012).
- World Health Organization. The World Health Report 2007: A safer future: Global public health security in the 21st century. http://www.who.int/whr/2007_en (accessed February 22, 2012).
- International Institute of Population Sciences (IIPS). National Family Health Survey (MCH and Family Planning): India 2005-2006. Bombay: International Institute of Population Sciences, 2007.
- World Health Organization. The World health statistics: 2012. <http://www.who.int/whosis/whostat/2012/en/> (accessed September 24, 2012).
- Government of India, Ministry of Statistics and program, New Delhi, India. Service sector implementation, NSSO Enterprises (extending trade) and consumer expenditure. National Sample Survey report, 63rd round, 2006-2007.
- Smith KR. National burden of disease in India from indoor air pollution. *Proc Natl Acad Sci.* 2000; 97:13286-13293.
- Smith KR, Mehta S, Maeusezahl-Feuz M. Indoor smoke from household solid fuels. In: Ezzati M, Rodgers AD, Lopez AD, *et al.*, eds. Comparative quantification of health risks: Global and regional burden of disease due to selected major risk factors, Vol. 2. Geneva: World Health Organization, 2004; pp. 1435-1493.
- Wilkinson P, Smith KR, Davies M, *et al.* Household energy, series on the impact on public health of strategies to reduce greenhouse gases. *Lancet.* 2009; 374:1917-1929.
- Smith KR. Biomass, air pollution, and health; a global review. Plenum Press, New York, NY, USA, 1987.
- Balakrishnan K, Sankar S, Padmavathi R, Smith KR. Respirable particulate levels in rural households of Andhra Pradesh, India: Daily concentrations and exposures. *J of Env Studies and Policy.* 2002; 5:87-97.
- Smith KR. Indoor air pollution in developing countries: Growing evidence of its role in the global disease burden. In: *Indoor Air, 96: Proceedings of 7th International Conference on Indoor Air and Climate.* Ikeda K, Iwata T, eds. Institute of Public Health, Tokyo, Japan, 1996; p. 33.
- World Health Organization. A methodology for estimating air pollution health effects. WHO, 1996. (WHO/EHG/96.5)
- Johnson M, Lam N, Brant S, Gray C, Pennise D. Modeling indoor air pollution from cook stove emissions in developing countries using a Monte Carlo single-box model. *Atmospheric Environment.* 2011; 45:3237-3243.
- WHO, 2010. WHO guidelines for indoor air quality: Selected pollutants. World Health Organization Regional Office for Europe, Bonn.
- World Health Organization. International Programme on Chemical Safety; Environmental Health Criteria 202: Selected Non-heterocyclic, Polycyclic Aromatic Hydrocarbons. WHO, Geneva, 1998; 3:63.
- The Health Consequences of Smoking – Cardiovascular Diseases. A Report of the Surgeon General. US Department of Health and Human Services, Rockville, MD, 1983.
- Perera FP, Hemmlinki K, Young TL, Brenner D, Kelly G, Santella RM. Detection of poly-aromatic hydrocarbon-DNA adducts in white blood cells of foundry workers. *Cancer Res.* 1988; 48:2288-2291.
- Schwarz-Miller J, Rom WN, Brandt-Rauf PW. Polycyclic aromatic hydrocarbons. In: *Environmental and Occupational Health*, Rom RN, ed. Little Brown & Co., London, UK, 1991; p. 873.
- Raiyani CV, Jani JP, Desai NM, Shah SH, Shah PG, Kashyap SK. Assessment of indoor exposure to polycyclic aromatic hydrocarbons for urban poor using various types of cooking fuels. *Bull Environ Contam Toxicol.* 1993; 50:757-763.
- Patel TS, Raiyani CV. Indoor air quality: Problems and perspectives. In: *Energy Strategies and Green House Gas Mitigation*, Shukla PR, ed. Allied Publishers, New Delhi, India, 1995; p. 72.
- Acheson ED, Barnes HR, Gardner MJ, Osmond C, Pannet B, Taylor CP. Formaldehyde process, workers and lung cancer. *Lancet.* 1984; 1:1066-1067.
- Swenberg JA, Barrow M, Starr TB. Nonlinear biologic responses to formaldehyde and their implications for carcinogenic risk assessment. *Carcinogenesis.* 1983; 4:945-952.
- Blair A, Saracci I, Stewart PA, Hayes RB, Shy C. Epidemiologic evidence of the relationship between formaldehyde exposure and cancer. *Scand J Work Environ Health.* 1990; 16:381-393.
- Balakrishnan K, Sankar S, Parikh J, Padmavathi R, Srividya K, Venugopal V, Prasad S, Pandey VL. Daily average exposures to respirable particulate matter from combustion of biomass fuels in rural households of Southern India. *Environ Health Perspect.* 2002; 110:1069-1075.
- Desai MA, Mehta S, Smith KR. Indoor smoke from solid fuels: Assessing the environmental burden of disease at national and local levels; Environmental burden of disease series No. 4. WHO protection of the human environment, Geneva, 2004.
- Smith KR, Samet JM, Romieu I, Bruce N. Indoor air pollution in developing countries and ALRI in children. *Thorax.* 2000; 55:518-532.
- Sharma S, Sethi GR, Rohtagi A, Chaudhary A, Shankar R, Bapna JS, Joshi V, Sapir DG. Indoor air quality and acute lower respiratory infection in Indian urban slums. *Environ Health Perspect.* 1998; 106:291-297.
- Shah N, Ramankutty V, Pramila PG, Sathy N. Risk factors for severe pneumonia in children in South Kerala:

- A hospital based case-control study. *J Trop Paediatric*. 1994; 40:201-206.
29. Padmavati S, Pathak SN. Chronic cor pulmonale in Delhi. *Circulation*. 1959; 20:343-352.
 30. Gupta B, Mathur N, Mahendra P, Srivastava A, Swaroop V, Agnihotri M. A study of the household environmental risk factors pertaining to respiratory disease. *Energy Environ Rev*. 1997; 13:61-67.
 31. Smith KR, Liu Y. In *The Epidemiology of Lung Cancer*, Samet J, ed. Dekker, New York, NY, USA, 1994; pp. 151-184.
 32. Alberg AJ, Samet JM. Epidemiology of lung cancer. *Chest*. 2003; 123 (1 Suppl):21S-49S
 33. Behera D, Balamugesh T. Indoor air pollution as a risk factor for lung cancer in women. *J Assoc Physicians India*. 2005; 53:190-192.
 34. Sapkota A, Gajalakshmi V, Jetli DH, Chowdhary SR, Dikshit RP, Brennan P, Hashib M, Boffetta P. Indoor air pollution from solid fuels and risk of hypopharyngeal/laryngeal and lung cancers: A multicentric case-control study from India. *Int J Epidemiology*. 2008; 2:1-8.
 35. Government of India, Central TB Division, Ministry of Health and Family Welfare, New Delhi, India. RNTCP TB status report, 2010.
 36. Kolappan C, Subramani R. Association between biomass fuel and pulmonary tuberculosis: A nested case-control study. *Thorax*. 2009; 64:705-708.
 37. Misra VK, Ratherford RD, Smith KR. Biomass cooking fuels and prevalence of tuberculosis in India. *Int J Infect Dis*. 1999; 3:119-129.
 38. Pokhrel AK, Bates MN, Verma SC, Joshi HC, Sreeramareddy CT, Smith KR. Tuberculosis and indoor biomass and kerosene use in Nepal: A case-control study. *Environ Health Perspect*. 2010; 118:558-564.
 39. Saiyed HN, Sharma YK, Sadhu HG, Norboo T, Patel PD, Patel TS, Venkaiah K, Kashyap SK. Non-occupational pneumoconiosis at high altitude villages in central Ladakh. *Br J Ind Med*. 1991; 48:825-829.
 40. Odinaev FI. The characteristics of development and course of pneumoconiosis under the conditions of a mountain climate. *Grig Tr Prof Zabol*. 1992; 7:13-14. (in Russian).
 41. Dhar SN, Pathania AG. Bronchitis due to biomass fuel burning: 'Gujjar lung' an extreme effect. *Semin Respir Med*. 1991; 12:69-74.
 42. Lal K, Dutta KK, Vachhrajani KD, Gupta GS, Srivastava AK. Histomorphological changes in lung of rats following exposure to wood smoke. *Indian J Exp Biol*. 1993; 31:761-764.
 43. Bhattacharyya SN, Manna B, Smiley R, Ashbaugh P, Coutinho R, Kaufman B. Smoke-induced inhalation injury: Effects of retinoic acid and antisense oligodeoxynucleotide on stability and differentiated state of the mucociliary epithelium. *Inflammation*. 1998; 22:203-214.
 44. Naeher LP, Brauer M, Lipsett M, Zelikoff JT, Simpson CD, Koenig JQ, Smith KR. Woodsmoke health affects: A review. *Inhal Toxicol*. 2007; 19:67-106.
 45. Campbell H, Armstrong JR, Byass P. Indoor air pollution in developing countries and acute respiratory infection in children. *Lancet*. 1989; 1:1012.
 46. Armstrong JR, Campbell H. Indoor air pollution exposure and lower respiratory infections in young Gambian children. *Int J Epidemiol*. 1991; 20:424-429.
 47. Cerqueira MC, Murtagh P, Halac A, Avila M, Weissenbacher M. Epidemiologic risk factors for children with acute lower respiratory tract infection in Buenos Aires, Argentina: A matched case-control study. *Rev Infect Dis*. 1990; 12 (Suppl 8):S1021-S1028.
 48. Collings DA, Sithole SD, Martin KS. Indoor wood smoke pollution causing lower respiratory disease in children. *Trop Doct*. 1990; 20:151-155.
 49. De Francisco A, Morris J, Hall AJ, Armstrong-Schellenberg JR, Greenwood BM. Risk factors for mortality from acute lower respiratory tract infections in young Gambian children. *Int J Epidemiol*. 1993; 22:1174-1182.
 50. Ezzati M, Kammen DM. Quantifying the effects of exposure to indoor air pollution from biomass combustion on acute respiratory infections in developing countries. *Environ Health Perspect*. 2001; 109:481-488.
 51. Johnson AW, Aderole WI. The association of household pollutants and socio-economic risk factors with the short-term outcome of acute lower respiratory infections in hospitalized pre-school Nigerian children. *Ann Trop Paediatr*. 1992; 12:421-432.
 52. Kossove D. Smoke-filled rooms and lower respiratory disease in infants. *S Afr Med J*. 1982; 61:622-624.
 53. Morris K, Morgenlander M, Coulehan JL, Gahagen S, Arena VC, Morganlander M. Wood-burning stoves and lower respiratory tract infection in American Indian children. *Am J Dis Child*. 1990;144:105-108.
 54. Mtango FD, Neuvians D, Broome CV, Hightower AW, Pio A. Risk factors for deaths in children under 5 years old in Bagamoyo district, Tanzania. *Trop Med Parasitol*. 1992; 43:229-233.
 55. O'Dempsey T, McArdle TF, Morris J, Lloyd-Evans N, Baldeh I, Laurence BE, Secka O, Greenwood BM. A study of risk factors for pneumococcal disease among children in a rural area of west Africa. *Int J Epidemiol*. 1996; 25:885-893.
 56. Pandey MR, Boleij JS, Smith KR, Wafula EM. Indoor air pollution in developing countries and acute respiratory infection in children. *Lancet*. 1989;1:427-429.
 57. Robin LF, Less PS, Winget M, Teinhoff M, Moulton LH, Santosham M, Correa A. Wood-burning stoves and lower respiratory illnesses in Navajo children. *Pediatr Infect Dis J*. 1996; 15:859-865.
 58. Victora C, Fuchs S, Flores J, Fonseca W, Kirkwood B. Risk factors for pneumonia among children in a Brazilian metropolitan area. *Pediatrics*. 1994; 93:977-985.
 59. Albalak RA, Frisancho R, Keeler GJ. Domestic biomass fuel combustion and chronic bronchitis in two rural Bolivian villages. *Thorax*. 1999; 54:1004-1008.
 60. Behera D, Dash S, Yadav SP. Carboxyhaemoglobin in women exposed to different cooking fuels. *Thorax*. 1991; 46:344-346.
 61. Dennis RJ, Maldonado D, Norman S, Baena E, Martinez G. Woodsmoke exposure and risk for obstructive airways disease among women. *Chest*. 1996; 109:115-119.
 62. Døssing M, Khan J, al-Rabiah F. Risk factors for chronic obstructive lung disease in Saudi Arabia. *Respir Med*. 1994; 88:519-522.
 63. Dutt D, Srinivasa DK, Rotti SB, Sahai A, Konar D. Effect of indoor air pollution on the respiratory system of women using different fuels for cooking in an urban slum of Pondicherry. *Natl Med J India*. 1996; 9:113-117.
 64. Malik SK. Exposure to domestic cooking fuels and chronic bronchitis. *Indian J Chest Dis Allied Sci*. 1985; 27:171-174.

65. Menezes AM, Victora CG, Rigatto M. Prevalence and risk factors for chronic bronchitis in Pelotas, RS, Brazil: A population-based study. *Thorax*. 1994; 49:1217-1221.
66. Pandey MR. Prevalence of chronic bronchitis in a rural community of the hill region of Nepal. *Thorax*. 1984; 39:331-336.
67. Perez-Padilla R, Regalado J, Vedal S, Pare P, Chapela R, Sansores R, Selman M. Exposure to biomass smoke and chronic airway disease in Mexican women: A case-control study. *Am J Respir Crit Care Med*. 1996; 154:701-706.
68. Qureshi KA. Domestic smoke pollution and prevalence of chronic bronchitis/asthma in a rural area of Kashmir. *Indian J Chest Dis Allied Sci*. 1994; 36:61-72.
69. Dai XD, Lin CY, Sun XW, Shi YB, Lin YJ. The etiology of lung cancer in nonsmoking females in Harbin, China. *Lung Cancer*. 1996; 14 (Suppl 1):S85-S91.
70. Du E, Wang W, Zhang Q, Li Z, Wu Y, Zhao S. Survey of indoor air quality and human health in rural Changchun, Jilin Province, China. *Journal of Norman Bethune University of Medical Science*. 1988; 14:88-91. (in Chinese)
71. Du YX, Cha Q, Chen XW, Chen YZ, Huang LF, Feng ZZ, Wu XF, Wu JM. An epidemiological study of risk factors for lung cancer in Guangzhou, China. *Lung Cancer*. 1996; 14 (Suppl 1):S9-S37.
72. Gao YT, Blot WJ, Zheng W, Ershow AG, Hsu CW, Levin LI, Zhang R, Fraumeni JF Jr. Lung cancer among Chinese women. *Int J Cancer*. 1987; 40:604-609.
73. Huang ZB. A study on the risk factors and population attributable risk for primary lung cancer. *Journal of Guangxi Medical University*. 1999; 16:447-450. (in Chinese)
74. Ko YC, Lee CH, Chen MJ, Huang CC, Chang WY, Lin HJ, Wang HZ, Chang PY. Risk factors for primary lung cancer among non-smoking women in Taiwan. *Int J Epidemiol*. 1997; 26:24-31.
75. Lei YX, Cai WC, Chen YZ, Du YX. Some lifestyle factors in human lung cancer: A case-control study of 792 lung cancer cases. *Lung Cancer*. 1996; 14 (Suppl 1): S121-S136.
76. Liu J, Hu H. A case-control study on farmers' lung cancer mortality and its non-smoking risk factors in Shunyi County, Beijing. Department of Environmental Health, Beijing Medical University, Beijing, China.
77. Liu Q, Sasco AJ, Riboli E, Hu MX. Indoor air pollution and lung cancer in Guangzhou, People's Republic of China. *Am J Epidemiol*. 1993; 137:145-154.
78. Liu ZY, He XZ, Chapman RS. Smoking and other risk factors for lung cancer in Xuanwei, China. *Int J Epidemiol*. 1991; 20:26-31.
79. Luo RX, Wu B, Yi YN, Huang ZW, Lin RT. Indoor burning coal air pollution and lung cancer – a case-control study in Fuzhou, China. *Lung Cancer*. 1996; 14 (Suppl 1):S113-S119.
80. Shen XB, Wang GX, Huang YZ, Xiang LS, Wang XH. Analysis and estimates of attributable risk factors for lung cancer in Nanjing, China. *Lung Cancer*. 1996 14 (Suppl 1):S107-S112.
81. Sobue T. Association of indoor air pollution and lifestyle with lung cancer in Osaka, Japan. *Int J Epidemiol*. 1990; 19 (Suppl 1):S62-S66.
82. Wang TJ, Zhou BS, Shi JP. Lung cancer in nonsmoking Chinese women: A case-control study. *Lung Cancer*. 1996; 14 (Suppl 1):S93-S98.
83. Wu AH, Henderson BE, Pike MC, Yu MC. Smoking and other risk factors for lung cancer in women. *J Natl Cancer Inst*. 1985; 74:747-751.
84. Wu Y, Cao K, Ma G, Deng F, Liu Y, Zhou J, Wan D. A case-control study of the risk factors of male lung cancer in Guangzhou. *Cancer*. 1999; 18:535-537.
85. Wu-Williams AH, Dai XD, Blot W, *et al*. Lung cancer among women in north-east China. *Br J Cancer*. 1990; 62:982-987.
86. Xu ZY, Brown L, Pan GW, Li G, Feng YP, Guan DX, Liu TF, Liu LM, Chao RM, Sheng JH, Gao GC. Lifestyle, environmental pollution and lung cancer in cities of Liaoning in northeastern China. *Lung Cancer*. 1996; 14 (Suppl 1):S149-S160.
87. Yang R, Jiang W, Wang C. Characteristics of indoor air pollution in districts of high lung cancer incidence, Xuanwei, China. *Journal of Environment and Health*. 1988; 5:16-18. (in Chinese)
88. Azizi BH, Zulkifli HI, Kasim S. Indoor air pollution and asthma in hospitalized children in a tropical environment. *J Asthma*. 1995; 32:413-418.
89. Mohamed N, Ng'ang'a L, Odhiambo J, Nyamwaya J, Menzies R. Home environment and asthma in Kenyan schoolchildren: A case-control study. *Thorax*. 1995; 50:74-78.
90. Xu X, Niu T, Christiani DC, Weiss ST, Chen C, Zhou Y, Fang Z, Jiang Z, Liang W, Zhang F. Occupational and environmental risk factors for asthma in rural communities in China. *Int J Occup Environ Health*. 1996; 2:172-176.
91. Pérez-Padilla R, Pérez-Guzmán C, Báez-Saldaña R, Torres-Cruz A. Cooking with biomass stoves and tuberculosis: A case control study. *Int J Tuberc Lung Dis*. 2001; 5:441-447.
92. Pandey MR, Basnyat B, Neupane RP. Chronic bronchitis and cor pulmonale in Nepal. *Lung India* 1988; 6:209-210.
93. Shetty N, Shemko M, Vaz M, D'Souza G. An epidemiological evaluation of risk factors for tuberculosis in South India: A matched case control study. *Int J Tuberc Lung Dis*. 2006; 10:80-86.
94. Lakshmi PV, Virdi NK, Thakur JS, Smith KR, Bates MN, Kumar R. Biomass fuel and risk of tuberculosis: A case-control study from Northern India. *J Epidemiol Community Health*. 2012; 66:457-461.
95. Behera D, Aggarwal G. Domestic cooking fuel exposure and tuberculosis in Indian women. *Indian J Chest Dis Allied Sci*. 2010; 2:139-143.
96. Dherani M, Pope D, Mascarenhas M, Smith KR, Weber M, Bruce N. Indoor air pollution from unprocessed solid fuel use and pneumonia risk in children aged under five years: a systematic review and meta-analysis. *Bull World Health Organ*. 2008; 86:390-398.
97. Kurmi OP, Semple S, Simkhada P, Smith WC, Ayres JG. COPD and chronic bronchitis risk of indoor air pollution from solid fuel: A systematic review and meta-analysis. *Thorax*. 2010; 65:221-228.
98. Mishra V, Retherford RD, Smith KR. Cooking smoke and tobacco smoke as risk factors for stillbirth. *Int J Environ Health Res*. 2005; 15:397-410.
99. Gupta D, Boffetta P, Gaborieau V, Jindal SK. Risk factors of lung cancer in Chandigarh, India. *Indian J Med Res*. 2001; 113:142-150.
100. Hosgood HD 3rd, Wei H, Sapkota A, Choudhury I, Bruce N, Smith KR, Rothman N, Lan Q. Household coal use and lung cancer: systematic review and meta-analysis

- of case-control studies, with an emphasis on geographic variation. *Int J Epidemiol.* 2011; 40:719-728.
101. Behera D, Jindal SK. Respiratory symptoms in Indian women using domestic cooking fuels. *Chest.* 1991; 100:385-388.
102. Magheswari U, Johnson P, Ramaswamy P, *et al.* Exposure to Biomass Fuel Smoke and Tuberculosis-A Case-Control Study in India. *Epidemiology* 2007; 18: s122.
103. Ramaswamy P, Balakrishnan K, Ghosh S, *et al.* Indoor air pollution due to biomass fuel combustion and acute respiratory infection in children under 5 in Trichy district of rural Tamilnadu, India. *Epidemiology.* 2011; 22:s104.

(Received August 1, 2012; Revised October 6, 2012; Accepted October 16, 2012)

Brief Report

DOI: 10.5582/bst.2012.v6.5.229

Angiogenin expression in the sera and skin of patients with rheumatic diseases**Aki Kuwahara, Masatoshi Jinnin*, Takamitsu Makino, Ikko Kajihara, Katsunari Makino, Noritoshi Honda, Wakana Nakayama, Kuniko Inoue, Satoshi Fukushima, Hironobu Ihn***Department of Dermatology and Plastic Surgery, Faculty of Life Sciences, Kumamoto University, Kumamoto, Japan.***Summary**

Vascular abnormalities are one of the common features in rheumatic diseases, but their pathogenesis is still not known. Angiogenin, a molecule implicated in the angiogenic process, may play some roles in such vascular changes. Serum angiogenin concentrations were measured in 21 scleroderma patients, 10 patients with systemic lupus erythematosus (SLE), 21 patients with dermatomyositis (DM), 5 patients with polymyositis (PM), 11 patients with clinically amyopathic DM (CADM) and 12 normal subjects, with specific enzyme-linked immunosorbent assays. Angiogenin mRNA *in vivo* was determined in skin tissues of 5 DM patients, 4 CADM patients, 5 SLE patients and 7 normal subjects using quantitative real-time polymerase chain reactions. We could not find any significant differences in the serum angiogenin levels among normal subjects and patients with rheumatic diseases. However, when we evaluated the correlation of serum angiogenin levels with clinical features of 32 DM/CADM patients, the patients with increased angiogenin levels had significantly higher aldolase levels than those with decreased levels. On the other hand, angiogenin mRNA is significantly up-regulated in the involved skin of DM and CADM, suggesting that angiogenin expression is up-regulated locally in the skin but not in sera of patients with DM and CADM. In conclusion, dysregulated angiogenin expression may contribute to the pathogenesis of myositis as well as skin involvement *via* the vascular change in DM/CADM. Further studies with an increased number of patients may help to clarify the relationship between angiogenin and vascular abnormalities in rheumatic diseases and to develop new therapeutic strategies.

Keywords: Collagen disease, vascular disease, angiogenesis

1. Introduction

Vascular abnormalities such as Raynaud's phenomenon, nailfold bleeding, skin ulcers, antiphospholipid antibody syndrome, and hyper γ -globulinemia are common features of rheumatic diseases. However, the cause of these changes is still unknown.

Angiogenin is a non-glycosylated polypeptide consisting of 123 amino acid residues in length and contains three intra-chain disulfide bonds.

This molecule is classified as a member of the RISBASE family of ribonucleases, which exhibit both ribonuclease activity and special biological actions (1-3). Various cell types including vascular endothelial cells, smooth muscle cells, fibroblasts, and lymphocytes are thought to express angiogenin (4,5). In addition, circulating angiogenin has been detected in normal serum (6,7).

Angiogenin is implicated in the angiogenic process. The molecule first binds to actin, followed by dissociation of the actin-angiogenin complex from the cell surface and subsequent activation of tissue plasminogen activator. This then generates plasmin, which is known to degrade matrix of basement membrane (8,9). Destruction of the existing basement membrane may be a prerequisite for endothelial cell migration during *de novo* vascularization (10,11).

*Address correspondence to:

Dr. Masatoshi Jinnin, Department of Dermatology and Plastic Surgery, Faculty of Life Sciences, Kumamoto University, Honjo 1-1-1, Kumamoto 860-8556, Japan.
E-mail: mjin@kumamoto-u.ac.jp

Angiogenin may play some role in the pathogenesis of vascular changes seen in rheumatic diseases. However, no link between angiogenin and rheumatic diseases has been established. Therefore, to prove our hypothesis, we examined angiogenin levels in the sera and skin of patients with various rheumatic diseases.

2. Materials and Methods

2.1. Clinical assessment and patient material

Patients with scleroderma (SSc) or systemic lupus erythematosus (SLE) fulfilled the criteria proposed by the American College of Rheumatology (ACR) (12-14). Polymyositis (PM) and dermatomyositis (DM) were diagnosed based on the criteria proposed by Bohan and Peter (15,16). Patients with clinically and histopathologically typical cutaneous lesions but without myositis were diagnosed as clinically amyopathic DM (CADM) according to the previous criteria (17). Clinical and laboratory data reported in this study were obtained at the time of sampling of tissue or serum.

Skin samples were obtained from 5 DM patients, 4 CADM patients and 5 SLE patients. Seven control skin samples were obtained from routinely discarded skin of healthy human subjects undergoing skin grafts. Immediately after removal, skin biopsy specimens were fixed with formalin and embedded in paraffin. Sera were obtained from 21 patients with SSc, 10 SLE patients, 21 DM patients, 5 PM patients, 11 CADM patients and 12 normal control subjects. All serum samples were stored at -80°C prior to use. Institutional review board approval and written informed consent were obtained before patients and normal subjects were entered into this study according to the Declaration of Helsinki.

2.2. Antinuclear antibodies

Antinuclear antibodies (ANA) were detected by indirect immunofluorescence using HEP-2 cells as the substrate and double immunodiffusion, as described previously (18).

2.3. Serum angiogenin levels

Levels of serum angiogenin were measured with a specific ELISA kit (R & D Systems) (19). Briefly, anti-angiogenin monoclonal antibodies were precoated onto microtiter wells. Aliquots of serum were added to each well, followed by peroxidase-conjugated antibodies to angiogenin. Color was developed with hydrogen peroxide and tetramethylbenzidine peroxidase, and the absorbance at 450 nm was measured. Wavelength correction was performed using absorbance at 540 nm. The concentration of angiogenin in each sample was

determined by interpolation from a standard curve.

2.4. RNA isolation and quantitative real-time polymerase chain reaction (PCR)

Total RNA isolation from paraffin-embedded sections was performed with an RNeasy FFPE kit (Qiagen, Valencia, CA, USA) following the manufacturer's instructions. cDNA was synthesized from the total RNA with a PrimeScript RT reagent Kit (Takara Bio Inc, Shiga, Japan). Quantitative real-time PCR with Takara Thermal Cycler Dice (TP800)[®] used primers and templates mixed with the SYBR Premix Ex TaqII (Takara Bio Inc). Primer sets for angiogenin and 18S were purchased from Takara Bio Inc. DNA was amplified by denaturation for 5 sec at 95°C and annealing for 30 sec at 60°C . Data generated from each PCR reaction were analyzed using the Thermal Cycler Dice Real Time System ver2.10B (Takara Bio Inc.). The relative level of angiogenin was normalized to 18S levels in the same sample.

2.5. Statistical analysis

Statistical analysis was carried out with a Mann-Whitney's *U* test for the comparison of medians, and Fisher's exact probability test for the analysis of frequency. *p* values less than 0.05 were considered significant.

3. Results and Discussion

Serum samples were obtained from 32 DM patients including 11 CADM patients as well as 5 PM patients, 21 SSc patients, 10 SLE patients and 12 healthy normal subjects. The serum angiogenin levels in patients with these rheumatic diseases are shown in Figure 1. We could not find any significant difference in the angiogenin levels among normal subjects and patients with rheumatic diseases: the mean serum angiogenin in patients with DM (111.7 pg/mL) or CADM (107.7 pg/mL) was slightly lower than those in normal subjects (120.8 pg/mL), but not statistically significant.

Next, we evaluated the correlation of serum angiogenin levels with clinical features of 32 DM/CADM. The patients with increased angiogenin levels had significantly higher aldolase levels than those with decreased levels (47.2 vs. 7.1 U/I, $p < 0.05$, Table 1). Other myositis markers, CK and myoglobin, also tended to be higher in patients with increased angiogenin levels than those without, but were not statistically significant. There were no significant differences between the two patient groups in terms of other clinical/laboratory features including age at the time of serum sampling, duration of disease, the ratio of DM:CADM or IgG levels.

On the other hand, when skin samples were obtained

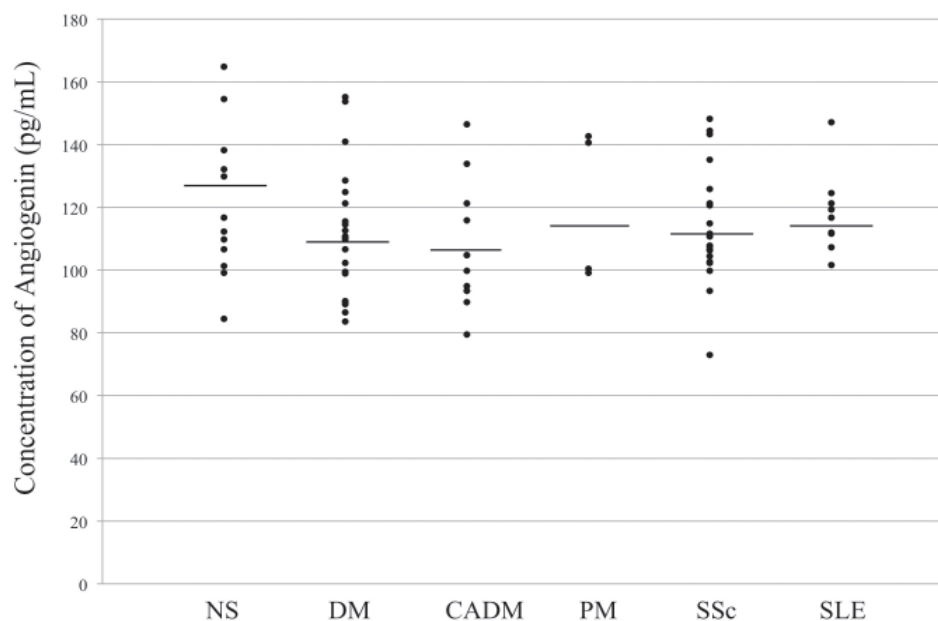


Figure 1. Serum concentrations of angiogenin in patients with rheumatic diseases. Serum concentrations of angiogenin determined by ELISA are shown on the ordinate; the horizontal bars show the mean value in each group. NS, normal subjects; DM, dermatomyositis; CADM, clinically amyopathic dermatomyositis; PM, polymyositis; SSc, systemic sclerosis; SLE, systemic lupus erythematosus.

Table 1. Correlation of serum angiogenin levels with clinical and serological features in patients with dermatomyositis (DM)

Items	Patients with decreased angiogenin levels (n = 16)	Patients with increased angiogenin levels (n = 16)
Age at the time of serum sampling (mean years)	58.3	54.6
Duration of disease (mean months)	6.1	5.2
Type (DM:CADM)	9:7	12:4
Clinical features		
Gottron's sign	62.5	62.5
Heliotrope	37.5	56.3
Laboratory features		
IgG (mg/dL)	1,453.6	1,523.9
CK (IU/L)	931.4	2,662.4
Myoglobin (ng/mL)	300.9	873.9
Aldolase (U/L)	7.1	47.2*
ANA	56.3	31.3
Organ involvement		
Muscle	50.0	68.8
Lung	43.8	25.0
Dysphagia	12.5	18.8
Joint	18.8	6.3

Unless indicated, values are percentages. DM, dermatomyositis; CADM, clinically amyopathic dermatomyositis; IgG, immunoglobulin; CK, creatine kinase; ANA, antinuclear antibodies. * $p < 0.05$ vs. patients with decreased angiogenin levels using Mann-Whitney U test.

from 5 DM patients, 4 CADM patients and 5 SLE patients, mean relative transcript levels of angiogenin in skin tissues from DM/CADM patients were significantly up-regulated compared with the values in normal skin ($p = 0.007$ and 0.014 , respectively) and SLE skin ($p = 0.009$ and 0.014 , respectively) (Figure 2). Our results suggest that angiogenin expression is up-regulated locally in the involved skin but not in sera of patients with DM and CADM.

In this study, we demonstrated three novel findings. First, there was no significant difference in the serum angiogenin levels among normal subjects and patients

with rheumatic diseases. Second, in DM/CADM patients, the levels of myopathic markers such as aldolase tended to be higher in patients with increased serum angiogenin levels than those without. Lastly, angiogenin mRNA is significantly up-regulated in the involved skin of DM and CADM patients *in vivo*.

It was reported that serum angiogenin levels increase in patients with cutaneous T cell lymphoma, and the molecule is thought to act as an inhibitor of polymorphonuclear leukocyte degranulation (20). Elevated levels of angiogenin have also been detected in the sera of patients with pancreatic cancer and

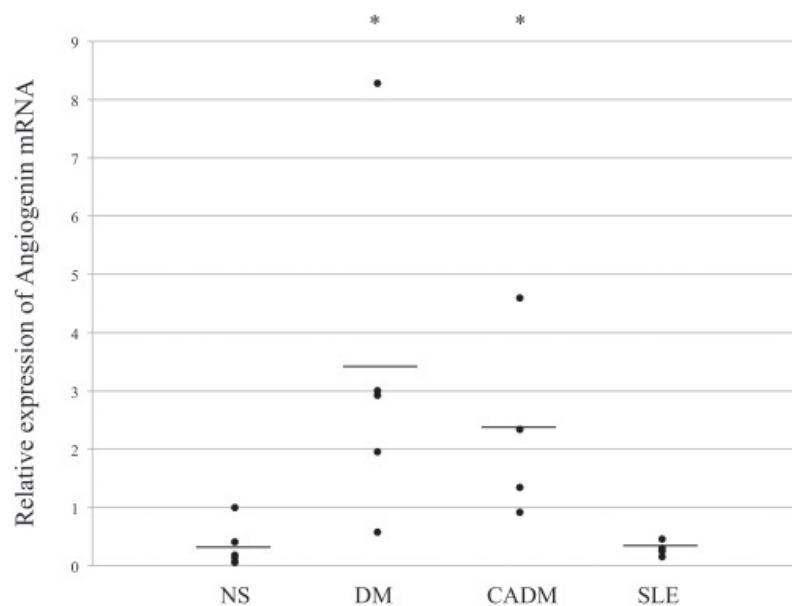


Figure 2. The mRNA expression of angiogenin in involved skin of rheumatic diseases. Mean relative transcript levels of angiogenin in skin tissues from 7 normal control subjects (NS), 5 dermatomyositis (DM) patients, 4 clinically amyopathic DM (CADM) patients, and 5 systemic lupus erythematosus (SLE) patients were determined by real-time quantitative PCR. The maximum value in samples from NS was set at 1.

arterial occlusive disease as well as inflammatory arthritis (21-24). Our research is the first to measure serum angiogenin levels in patients with PM/DM, SSc and SLE, but we did not find any significant difference between controls and these patients. This may be because of a small number of patients.

Vascular change is thought to be found frequently in the involved skin of DM/CADM; Crowson *et al.* described increased endothelial injury, increased vascular ectasia and reduced superficial vascular plexus density in skin lesions of DM/CADM compared with lupus erythematosus (25). Considering that uncontrolled activation of vascular endothelial growth factor (VEGF), one of the most potent angiogenic factors, rather than its inactivation is suggested to cause disturbed vessel morphology (26,27), and excessive expression of angiogenin in the skin of DM/CADM patients may also induce vascular change.

Similarly, histopathological findings of the muscles in DM are characterized by perivascular infiltration of CD4-positive T lymphocytes or macrophages (28,29). Furthermore, Pestronk *et al.* studied muscle specimens of DM and found reduction of vessel size and endothelial loss, as well as C5b9 complement deposition (30). Considering that patients with increased serum angiogenin had higher levels of myositis markers, the dysregulated angiogenin expression may contribute to the pathogenesis of muscle involvement *via* the vascular abnormality in DM. Further studies with an increased number of patients may help to clarify the relationship between angiogenin and vascular abnormalities in rheumatic diseases and to develop new therapeutic strategies.

Acknowledgements

This study was supported in part by project research from the Japanese Ministry of Health, Labour and Welfare.

References

- Shapiro R, Strydom DJ, Olson KA, Vallee BL. Isolation of angiogenin from normal human plasma. *Biochemistry*. 1987; 26:5141-5146.
- Bond MD, Strydom DJ, Vallee BL. Characterization and sequencing of rabbit, pig and mouse angiogenins: Discernment of functionally important residues and regions. *Biochim Biophys Acta*. 1993; 1162:177-186.
- D'Alessio G. New and cryptic biological messages from RNases. *Trends Cell Biol*. 1993; 4:106-109.
- Moenner M, Gusse M, Hatzi E, Badet J. The widespread expression of angiogenin in different human cells suggests a biological function not only related to angiogenesis. *Eur J Biochem*. 1994; 226:483-490.
- Rybak SM, Fett JW, Yao QZ, Vallee BL. Angiogenin mRNA in human tumor and normal cells. *Biochem Biophys Res Commun*. 1987; 146:1240-1248.
- Burgmann H, Hollenstein U, Maca T, Zedwitz-Liebenstein K, Thalhammer F, Koppensteiner R, Ehringer H, Graninger W. Increased serum laminin and angiogenin concentrations in patients with peripheral arterial occlusive disease. *J Clin Pathol*. 1996; 49:508-510.
- Shimoyama S, Gansauge F, Gansauge S, Negri G, Oohara T, Beger HG. Increased angiogenin expression in pancreatic cancer is related to cancer aggressiveness. *Cancer Res*. 1996; 56:2703-2706.
- Hu GF, Riordan JF. Angiogenin enhances actin acceleration of plasminogen activation. *Biochem*

- Biophys Res Commun. 1993; 197:682-687.
9. Lyons RM, Gentry LE, Purchio AF, Moses HL. Mechanism of activation of latent recombinant transforming growth factor β 1 by plasmin. *J Cell Biol.* 1990; 110:1361-1367.
 10. Hu G, Riordan JF, Vallee BL. Angiogenin promotes invasiveness of cultured endothelial cells by stimulation of cell-associated proteolytic activities. *Proc Natl Acad Sci U S A.* 1994; 91:12096-12100.
 11. Folkman J, Klagsbrun M. Angiogenic factors. *Science.* 1987; 235:442-447.
 12. Subcommittee for scleroderma criteria of the American Rheumatism Association Diagnostic and Therapeutic Criteria Committee. Preliminary criteria for the classification of systemic sclerosis (scleroderma). *Arthritis Rheum.* 1980; 23:581-590.
 13. Hochberg MC. Updating the American College of Rheumatology revised criteria for the classification of systemic lupus erythematosus. *Arthritis Rheum.* 1997; 40:1725.
 14. LeRoy EC, Black C, Fleischmajer R, Jablonska S, Krieg T, Medsger TA Jr, Rowell N, Wollheim F. Scleroderma (systemic sclerosis): Classification, subsets and pathogenesis. *J Rheumatol.* 1988; 15:202-205.
 15. Bohan A, Peter JB. Polymyositis and dermatomyositis (first of two parts). *N Engl J Med.* 1975; 292:344-347.
 16. Bohan A, Peter JB. Polymyositis and dermatomyositis (second of two parts). *N Engl J Med.* 1975; 292:403-407.
 17. Sontheimer RD. Cutaneous features of classic dermatomyositis and amyopathic dermatomyositis. *Curr Opin Rheumatol.* 1999; 11:475-482.
 18. Ihn H, Sato S, Tamaki T, Soma Y, Tsuchida T, Ishibashi Y, Takehara K. Clinical evaluation of scleroderma spectrum disorders using a points system. *Arch Dermatol Res.* 1992; 284:391-395.
 19. Aboulghar MA, Mansour RT, Serour GI, Elhelw BA, Shaarawy M. Elevated concentrations of angiogenin in serum and ascitic fluid from patients with severe ovarian hyperstimulation syndrome. *Hum Reprod.* 1998; 13:2068-2071.
 20. Miyagaki T, Sugaya M, Suga H, Akamata K, Ohmatsu H, Fujita H, Asano Y, Tada Y, Kadono T, Sato S. Angiogenin levels are increased in lesional skin and sera in patients with erythrodermic cutaneous T cell lymphoma. *Arch Dermatol Res.* 2012; 304:401-406.
 21. Burgmann H, Hollenstein U, Maca T, Zedwitz-Liebenstein K, Thalhammer F, Koppensteiner R, Ehringer H, Graninger W. Increased serum laminin and angiogenin concentrations in patients with peripheral arterial occlusive disease. *J Clin Pathol.* 1996; 49:508-510.
 22. Shimoyama S, Gansauge F, Gansauge S, Negri G, Oohara T, Beger HG. Increased angiogenin expression in pancreatic cancer is related to cancer aggressiveness. *Cancer Res.* 1996; 56:2703-2706.
 23. Lioté F, Champy R, Moenner M, Boval-Boizard B, Badet J. Elevated angiogenin levels in synovial fluid from patients with inflammatory arthritis and secretion of angiogenin by cultured synovial fibroblasts. *Clin Exp Immunol.* 2003; 132:163-168.
 24. Park MC, Chung SJ, Park YB, Lee SK. Relationship of angiogenic factors to disease activity and radiographic damage in rheumatoid arthritis. *Clin Exp Rheumatol.* 2008; 26:881-886.
 25. Crowson AN, Magro CM. The role of microvascular injury in the pathogenesis of cutaneous lesions of dermatomyositis. *Hum Pathol.* 1996; 27:15-19.
 26. Distler O, Distler JH, Scheid A, Acker T, Hirth A, Rethage J, Michel BA, Gay RE, Müller-Ladner U, Matucci-Cerinic M, Plate KH, Gassmann M, Gay S. Uncontrolled expression of vascular endothelial growth factor and its receptors leads to insufficient skin angiogenesis in patients with systemic sclerosis. *Circ Res.* 2004; 95:109-116.
 27. Davies CA, Jeziorska M, Freemont AJ, Herrick AL. The differential expression of VEGF, VEGFR-2, and GLUT-1 proteins in disease subtypes of systemic sclerosis. *Hum Pathol.* 2006; 37:190-197.
 28. Arahata K, Engel AG. Monoclonal antibody analysis of mononuclear cells in myopathies. I: Quantitation of subsets according to diagnosis and sites of accumulation and demonstration and counts of muscle fibers invaded by T cells. *Ann Neurol.* 1984; 16:193-208.
 29. Emslie-Smith AM, Engel AG. Microvascular changes in early and advanced dermatomyositis: A quantitative study. *Ann Neurol.* 1990; 27:343-356.
 30. Pestronk A, Schmidt RE, Choksi R. Vascular pathology in dermatomyositis and anatomic relations to myopathology. *Muscle Nerve.* 2010; 42:53-61.

(Received September 19, 2012; Revised October 25, 2012; Accepted October 28, 2012)

Density functional theory based quantitative structure-property relationship studies on coumarin-based prodrugs

Xinying Yang¹, Xuben Hou¹, Binghe Wang^{1,2}, Minyong Li^{1,*}, Hao Fang^{1,*}

¹ Department of Medicinal Chemistry, Key Laboratory of Chemical Biology (Ministry of Education), School of Pharmacy, Shandong University, Ji'nan, Shandong, China;

² Department of Chemistry and Center for Biotechnology and Drug Design, Georgia State University, Atlanta, GA, USA.

Summary

A coumarin-based prodrug system plays a significant role in preparing esterase-sensitive prodrugs of amines and peptides. The electronic structures of 27 coumarin-based prodrugs developed in our lab were calculated at a B3LYP/6-31+G (d,p) level with a Gaussian 03 program. The calculated structural parameters were taken as theoretical descriptors to establish five novel QSPR models. The SMLR linear model ($q^2 = 0.427$, $r^2 = 0.516$) and the PLS linear model ($q^2 = 0.584$, $r^2 = 0.663$) were developed with descriptors selected by an Unsupervised Forward Selection method. Another three nonlinear QSPR models were established by a Polynomial Neural Network (PNN) Simulation method ($q^2 = 0.692, 0.675, 0.663$; $r^2 = 0.700, 0.688, 0.672$). We suggest that the QSPR models derived here, especially the PNN models, can be used to predict the release kinetics of coumarin-based prodrugs as well as design new derivatives of coumarin-based prodrug candidates.

Keywords: Coumarin, prodrug, QSPR, quantitative structure-property relationship, DFT

1. Introduction

There is no doubt that prodrugs play an important role in current drug delivery and drug discovery (1-3). Our lab developed a coumarin-based prodrug system for preparing esterase-sensitive prodrugs of amines and peptides (4). This system has a *cis*-double bond which could facilitate the lactonization when an acyl group (R) is hydrolyzed by esterase (Scheme 1). To date, it has been used for the preparations of cyclic prodrugs of opioid peptides (5-8), such as DADLE (9-11) and DADLE analogs (12), and peptidomimetics, such as an RGD (Arg-Gly-Asp) analog MK-383 (13,14). Moreover, this system was also applied in the design of non-peptide prodrugs such as meptazinol, and the prodrug of meptazinol has shown a 4-fold increase in

oral bioavailability (15). The advantage of the coumarin system lies in the released final product, coumarin, which is known to be non-toxic in extensive studies. In addition, the release rate of the coumarin-based prodrug system can be further manipulated by the introduction of additional substituents on the aromatic ring or the acyl group. In our previous studies, a series of coumarin derivatives with different substitutions of R and R₁-R₆ were synthesized and evaluated for release kinetics (Table 1) (3,16-18). These release kinetic studies only obtained overall pseudo-first-order rate constants because the complex process involves an enzymatic reaction and multi-step chemical reactions (Scheme 1). Our preliminary results suggest that the acyl group (R) has a minor influence on the overall half-lives, but the substituents on the phenyl ring (R₁-R₄) and amine part (R₅ and R₆) have major and complicated effects which include an electronic effect, steric effect and so on. In order to clearly illustrate these issues, computer-based tools are needed to further analyze the structural effect on the release kinetics.

Quantitative structure-property relationship (QSPR) studies have been successfully used for the prediction of physicochemical properties of chemical compounds based on their structures (19-24). The biological counterpart of such studies, quantitative

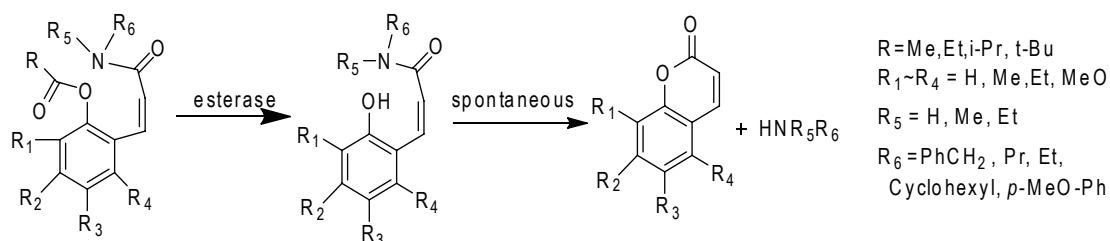
*Address correspondence to:

Dr. Fang Hao, Department of Medicinal Chemistry, School of Pharmacy, Shandong University, No. 44 Wenhua Road, Ji'nan, 250012, China.

E-mail: haofangen@sdu.edu.cn

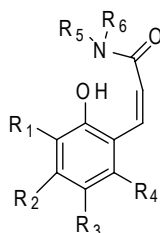
Dr. Minyong Li, Department of Medicinal Chemistry, School of Pharmacy, Shandong University, No. 44 Wenhua Road, Ji'nan, 250012, China.

E-mail: mli@sdu.edu.cn



Scheme 1. The illustration of a coumarin-based esterase-sensitive prodrug system and its derivatives.

Table 1. The structure of coumarin derivatives



Compound	R1	R2	R3	R4	R5	R6
1	H	H	H	H	H	Benzyl
2	H	H	H	H	H	Benzyl
3	H	H	H	H	H	Benzyl
4	H	H	H	H	H	Benzyl
5	H	H	H	H	H	Pr
6	H	H	H	H	H	Cyclohexyl
7	H	H	H	H	H	p-MeO-Ph
8	H	H	H	H	Me	Benzyl
9	H	H	H	H	Et	Et
10	Me	H	H	Me	Me	Benzyl
11	Me	H	H	Me	Et	Et
12	H	Me	H	Me	Me	Benzyl
13	H	Me	H	Me	Et	Et
14	Me	Me	H	H	Me	Benzyl
15	Me	Me	H	H	Et	Et
16	Me	H	Me	H	Me	Benzyl
17	Me	H	Me	H	Et	Et
18	Me	H	H	H	Me	Benzyl
19	Me	H	H	H	Et	Et
20	H	Me	Me	Me	Me	Benzyl
21	H	Me	Me	Me	Et	Et
22	H	H	Me	H	Me	Benzyl
23	H	H	Me	H	Et	Et
24	H	Me	H	H	Me	Benzyl
25	H	Me	H	H	Et	Et
26	H	MeO	H	H	Me	Benzyl
27	H	MeO	H	H	Et	Et

structure-activity relationships (QSAR), has also been extensively used with great success (25-28). So far, many efforts have successfully been made to investigate the spectral properties by using this kind of QSAR/QSPR approach (29-31). However, a common problem in QSAR/QSPR modeling is choosing a proper description of the variance between the individual molecular structures within a set of compounds. In our case, some commercially available 3D-QSAR methods, such as CoMFA and CoMSIA, cannot be used in such a complex system because these approaches mainly focus on interaction between macromolecules (receptors,

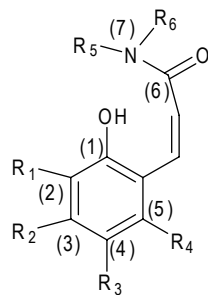
enzymes) and substrates, while the kinetics of the coumarin-based prodrug system is more complicated and consists of not only the enzyme hydrolysis interaction but also intramolecular lactonization steps. The latter lactonization step is also significantly different from molecular recognition in biological systems. Currently, quantum-mechanical descriptors calculated using density functional theory (DFT) have been successfully used in the modeling of reaction-related procedures, such as free-radical copolymerization (32), bond dissociation (33), and olefin metathesis (34). Therefore, the structure parameters of the coumarin-based prodrug, especially the parameters related to the lactonization step should be taken into account due to the chemical reactivity of bond making and bond breaking. In this paper, we will use the DFT-based QSPR computational tool and statistics method to study the relationships between the coumarin-based prodrug system and their kinetics.

2. Materials and Methods

2.1. DFT calculations

Electronic structure calculations have been performed using the Gaussian 03 program (35) on URSA, a 160-processor computer based on the Power5+ processor and IBM's P series architecture. The DFT method B3LYP (36,37) and the 6-31+G (d,p) basis set were used for all calculations, along with the PCM solvation model (38). The PCM solvation model is used in single-point energy calculations (PCM (sp)), and during the geometry optimizations and frequency calculations (PCM (opt)). All calculations using the PCM solvent model employ UAHF atomic radii when constructing the solvent cavity, as recommended in the Gaussian 03 user's reference when the "scfvac" keyword is used to obtain the free energy of solvation, as is the case in this study. All the geometries are fully optimized, and the character of the stationary points found is confirmed by a harmonic frequency calculation at the same theory level to ensure a minimum is located. Such a practice is also the same as we have done in past studies (39,40). The kinetic constants and all structure parameters related to enzyme hydrolysis interaction and intramolecular lactonization of each compound are listed in Table 2.

Table 2. Structure parameters of coumarin derivatives based on DFT calculations



No.	X1	X2	X3	X4	X5	X6	X7	X8	X9	X10	X11	X12	X13	X14	X15	X16	X17	Y
1	-11.28	-18.06	33.75	-34.77	7.80	6.78	3.84	5.92	-0.353	-0.571	0.263	-0.328	-0.148	-0.441	-0.707	-0.194	58.02	4.86
2	-11.24	-17.96	33.73	-34.82	7.80	6.72	3.75	5.80	-0.350	-0.571	0.261	-0.330	-0.149	-0.434	-0.715	-0.191	61.16	4.81
3	-11.22	-17.95	33.74	-34.81	7.80	6.73	3.77	5.82	-0.353	-0.571	0.261	-0.328	-0.154	-0.430	-0.723	-0.191	61.04	4.76
4	-11.23	-17.96	33.73	-34.80	7.81	6.74	3.77	5.83	-0.345	-0.570	0.259	-0.329	-0.148	-0.431	-0.719	-0.191	61.14	4.76
5	-7.67	-14.42	29.30	-28.13	5.56	6.74	4.27	5.71	0.088	-0.546	-0.164	-0.232	-0.122	-0.374	-0.033	-0.287	45.05	4.97
6	-10.81	-16.87	32.15	-32.89	6.81	6.07	3.52	4.66	-0.429	-0.529	0.238	-0.356	-0.065	-0.397	-0.040	-0.329	49.87	4.36
7	-9.43	-16.58	34.96	-34.19	6.38	7.15	5.11	7.04	-0.267	-0.544	0.056	-0.358	0.066	-0.468	-0.224	-0.322	57.13	5.72
8	-7.93	-16.47	35.39	-34.42	7.57	8.54	2.72	3.76	-0.266	-0.564	0.272	-0.411	-0.167	-0.192	-0.349	-0.067	55.55	4.55
9	-8.05	-14.61	30.70	-30.47	6.33	6.56	2.81	3.97	-0.153	-0.560	0.198	-0.221	-0.291	-0.123	-0.375	-0.010	53.60	3.79
10	-5.14	-14.75	39.58	-37.74	7.77	9.61	2.58	3.56	0.404	-0.504	1.002	-0.767	0.273	0.064	-0.624	-0.036	70.12	5.15
11	-2.36	-9.15	33.91	-33.60	6.47	6.78	5.09	7.24	0.002	-0.594	1.191	-0.770	-0.124	0.585	-0.375	-0.058	60.12	5.01
12	-5.31	-15.71	39.56	-37.27	8.10	10.40	2.64	3.66	0.079	-0.521	0.097	0.226	-0.126	0.348	-0.354	-0.070	61.93	5.26
13	-6.08	-13.67	34.98	-34.07	6.69	7.60	3.03	4.30	0.232	-0.518	-0.280	0.239	0.305	0.052	-0.366	-0.006	61.52	4.79
14	-4.53	-14.87	39.38	-36.24	7.20	10.34	3.49	4.63	0.029	-0.493	-0.126	0.543	-0.268	-0.079	-0.466	0.005	64.87	5.56
15	-6.01	-13.20	34.86	-34.23	6.56	7.19	2.75	3.80	0.187	-0.522	0.878	0.139	-0.767	0.184	-0.469	0.011	57.31	4.99
16	-5.74	-14.95	39.78	-38.10	7.53	9.22	2.73	3.50	-0.473	-0.565	1.269	-1.240	0.733	-0.653	-0.670	-0.037	77.09	5.14
17	-4.91	-12.82	35.01	-33.49	6.39	7.91	2.88	4.11	-0.954	-0.522	0.970	-0.533	-0.022	0.836	-0.449	-0.012	58.25	4.40
18	-4.86	-14.60	37.37	-34.67	7.04	9.74	3.77	4.89	0.271	-0.515	0.124	-0.050	-0.430	-0.006	-0.134	-0.039	64.68	5.20
19	-5.88	-12.90	32.96	-32.24	6.29	7.01	2.43	3.52	-0.193	-0.550	0.943	-0.678	-0.237	-0.016	-0.447	0.005	55.02	4.58
20	-4.71	-15.71	41.38	-38.57	8.19	10.99	2.91	4.04	-0.242	-0.512	-0.142	0.512	0.064	0.680	-0.411	-0.051	70.81	5.09
21	-6.02	-13.74	36.53	-35.67	6.85	7.71	3.28	4.66	-0.112	-0.508	-0.091	0.712	-0.084	0.438	-0.434	-0.028	68.56	4.40
22	-7.35	-16.52	37.11	-35.66	7.72	9.17	2.95	4.13	-0.209	-0.569	0.291	-0.558	0.440	-0.375	-0.433	-0.061	54.45	4.63
23	-7.19	-14.55	32.74	-31.84	6.47	7.37	3.18	4.46	-0.170	-0.572	0.264	-0.722	0.461	-0.329	-0.410	-0.040	50.68	3.76
24	-7.37	-16.51	37.57	-36.34	7.92	9.15	2.91	3.94	-0.093	-0.565	0.481	-0.024	-0.714	0.120	-0.398	-0.060	58.73	4.56
25	-7.91	-14.80	32.94	-32.78	6.73	6.89	2.85	3.97	-0.031	-0.565	-0.144	0.300	-0.415	0.211	-0.478	0.002	52.46	3.72
26	-9.29	-18.43	38.82	-37.66	7.98	9.13	2.74	3.37	-0.541	-0.571	1.000	-0.515	-0.492	-0.018	-0.371	-0.072	65.78	4.52
27	-9.22	-15.99	34.30	-34.25	6.72	6.77	3.68	5.24	-0.133	-0.558	0.109	-0.269	0.243	-0.387	-0.473	-0.031	61.87	3.76

Y: $\log K$ ($\times 10^4/s$), represent the observed release kinetic value (k_{obs}) of coumarin-based prodrugs; X1: ΔG (kcal/mol), X2: Total electrostatic energy (kcal/mol), X3: Cavitation energy (kcal/mol), X4: Dispersion energy (kcal/mol), X5: Repulsion energy (kcal), X6: Total non electrostatic energy (kcal/mol), X7: dipole in vacuo (Debye), X8: dipole in solution (Debye), X9: atomic Mulliken charge of atom C(1), X10: atomic Mulliken charge of O(1), X11: atomic Mulliken charge of C(2), X12: atomic Mulliken charge of C(3), X13: atomic Mulliken charge of C(4), X14: atomic Mulliken charge of C(5), X15: atomic Mulliken charge of C(6), X16: atomic Mulliken charge of N(7), X17: surface of added spheres.

2.2. Rational selection of descriptors

After identification of a large number of descriptors, a rational descriptor selection was carried out to reduce the number of descriptors to an acceptable level containing no redundancy and a minimal amount of multicollinearity. In this selection, a novel descriptor reduction algorithm, unsupervised forward selection (UFS) (41), was employed to determine suitable descriptors. This method has been successfully used in our previous study for modeling the excitation wavelengths of boronic acids (42). UFS could select from a data matrix a maximal linearly independent set of columns with a minimal amount of multiple correlations, and therefore it was designed for use in the development of QSPR models, where the m by n data matrix contains the values of n variables (typically molecular properties) for m objects (typically

compounds). In the descriptor selection, variables with small variance (not significant at the 5% level) were then removed. The UFS procedure was then applied repeatedly using values of R^2_{max} stepping from 0.1 to 0.9 with an increment of 0.1, together with $R^2_{max} = 0.99$. The UFS calculation was performed on a Virtual Computational Chemistry Laboratory at <http://www.vcllab.org> (43).

2.3. Polynomial neural network (PNN) simulation

The PNN algorithm is also known as an iterational algorithm of group methods of data handling (GMDH) (44). PNN provides a robust nonlinear polynomial regression identification for numerical data with unknown dependencies (45). Moreover it is insensible to outliers and irrelevant variables, and provides fast learning and numerical stability. PNN is a robust

Table 3. Three neural network models and statistical data

Model	Equation	q^2	r^2	RMSE	F	MAE
SMLR	$Y = 0.286 \times X_6 + 0.312 \times X_8 + 0.984$	0.427	0.516	0.380	26.60	--
PLS	$Y = 0.164 \times X_6 + 0.121 \times X_8 + 0.423 \times X_9 + 7.088 \times X_{10} + 0.066 \times X_{15} - 1.269 \times X_{16} + 6.697$	0.584	0.663	0.310	49.08	--
PNN 1	$Y = 5.31 \times X_{14} \times X_{16} + 0.381 \times (X_{11})^2 + 0.293 \times X_8 + 0.387 \times X_6$	0.692	0.700	0.291	58.10	0.204
PNN 2	$Y = 7.07 \times (X_{16})^2 - 0.762 \times X_{11} \times X_{15} + 0.375 \times X_6 + 0.313 \times X_8$	0.675	0.688	0.299	54.67	0.207
PNN 3	$Y = 4.31 \times X_{14} \times X_{16} - 0.667 \times X_{11} \times X_{15} + 0.311 \times X_8 + 0.381 \times X_6$	0.663	0.672	0.304	51.10	0.211

method that can be used even in the presence of outliers in the training set and provides reliable results even for such difficult cases. PNN correlates input and target variables using (non) linear regression. The PNN simulation was performed on a Virtual Computational Chemistry Laboratory at <http://www.vcclab.org> (43).

3. Results

3.1. Selection of descriptors

In the first step, UFS was used to optimize the number of descriptors. After UFS, only 11 descriptors, X4, X6, X8, X9, X10, X11, X13, X14, X15, X16, and X17, were significantly correlated with Y at a 95% level among all descriptors. These 11 descriptors were then used as input for the development of the linear and nonlinear QSPR models of coumarin-based prodrug. The UFS selected descriptors, classes and references are shown in Table 1.

3.2. SMLR linear model

Based on these 11 descriptors after selection, 27 compounds were then used to develop an optimal SMLR linear model. For the development of the linear model, leave-one-out (LOO) cross-validation statistical parameters were calculated to evaluate the model quality. Finally, a two-descriptor (X6 and X8) correlation model was obtained as represented in Table 3. The obtained squared correlation (r^2) was 0.516 and the LOO squared correlation (q^2) was 0.427. The standard error (RMSE) was 0.38 and the F-value was 26.60. The estimated values based on the SMLR linear model are listed in Table 4. Figure 1 depicts the estimated *versus* experimental values for all compounds.

3.3. PLS linear model

The linear model was also developed by PLS using 11 selected descriptors. In this case a correlation model including six descriptors, X6, X8, X9, X10, X15, and X16, was obtained as shown in Table 3. The number of PLS components is 3. In this linear model, r^2 was 0.663 and q^2 was 0.584. RMSE was 0.310 and the F-value was 49.68. The estimated results of the PLS model are shown in Table 4. The experimental and estimated

Table 4. Experimental versus estimated data

No.	Experimental	SMLR	PLS	PNN		
				Model 1	Model 2	Model 3
1	4.86	4.77	4.88	4.84	4.81	4.91
2	4.81	4.71	4.84	4.77	4.74	4.84
3	4.76	4.72	4.85	4.77	4.75	4.85
4	4.76	4.73	4.86	4.78	4.75	4.86
5	4.97	4.69	4.88	4.86	4.89	4.80
6	4.36	4.17	4.55	4.43	4.51	4.33
7	5.72	5.22	5.37	5.63	5.63	5.57
8	4.55	4.59	4.43	4.50	4.49	4.54
9	3.79	4.09	3.95	3.72	3.76	3.79
10	5.15	4.84	5.30	5.13	5.21	5.17
11	5.01	5.18	4.63	5.10	5.17	4.98
12	5.26	5.10	5.22	4.97	5.11	5.02
13	4.79	4.49	4.62	4.23	4.12	4.16
14	5.56	5.38	5.49	5.36	5.29	5.34
15	4.99	4.22	4.40	4.20	4.20	4.20
16	5.14	4.71	4.61	5.34	5.21	5.27
17	4.40	4.52	4.37	4.57	4.59	4.54
18	5.20	5.29	5.22	5.21	5.21	5.24
19	4.58	4.08	4.02	4.08	4.05	4.04
20	5.09	5.38	5.41	5.26	5.36	5.25
21	4.40	4.64	4.78	4.29	4.33	4.30
22	4.63	4.89	4.68	4.91	4.86	4.96
23	3.76	4.48	4.25	4.26	4.26	4.32
24	4.56	4.83	4.67	4.75	4.84	4.81
25	3.72	4.19	4.07	3.84	3.78	3.81
26	4.52	4.64	4.39	4.91	4.80	4.78
27	3.76	4.55	4.39	4.22	4.23	4.29

values are shown in Figure 1.

3.4. PNN simulation of QSPR

In this case a nonlinear PNN model of QSPR was developed with the same selected subset of 6 descriptors from those linear models. The estimated results of the PNN model are given in Table 4. Figure 1 represents the estimated *versus* experimental values using the PNN nonlinear model.

3.5. Interpretation of descriptors

From Table 4, descriptors X3, X9, X15, and X16 existed in the three PNN non-linear models. Descriptors X5 and X12 showed their influence on PNN model 3 and model 1 respectively. Both the cavitation energy (X3) and repulsion energy (X5) belong to the components of free energy of solvation. Cavitation energy described the energy required to push aside the solvent molecules and then making a cavity to place a

solute molecule. Repulsion energy (X5) reflects the Van der Waals effect on solvation.

4. Discussion

To discuss the descriptors X9, X12, X15, and X16 in the PNN models, it is necessary to illustrate the mechanism of the coumarin-based esterase sensitive prodrug systems (Scheme 2). It was reported that the acyl group R of 28 would be easily hydrolyzed by esterase at physiological pH and generate 29 with an unmasked phenol group. Due to the *cis*-geometry of the double bond in the structure of 29, the spontaneous lactonization was easily triggered by the phenolic hydroxyl group attacking the carbonyl group of C-6 to form the tetrahedral 30. Then, the collapse of tetrahedral 30 would yield *cis*-coumarinic acid 31 and amine (3).

According to the mechanism of the coumarin-based prodrug, the carbonyl of C-1 would be hydrolyzed by esterase and the positive charge in C-1 will benefit hydrolysis of the acyl group. Therefore, the atomic charge of C-1 (X9) should have an influence on the

release kinetics of the coumarin prodrug system. In addition, considering the carbonyl group of the amide at C-6 would be attacked by the unmasked phenolic hydroxyl group in the lactonization step of 29, the positive atomic charge in C-6 (X15) should no doubt lead to enhance the release kinetics of the coumarin prodrug system for the same reason. Then, the atomic charge on C-3 (X12) only existed in model 1, which perhaps exerts an effect on the unmasked phenolic hydroxyl group with an inductive or conjugated effect. It was reported that stabilizing a developing negative charge on the nitrogen (N-1) would facilitate lactonization during the collapse of the tetrahedral intermediate 30 (3). Furthermore, the nitrogen charges also related to the *pKa* value of the amine which could affect the release rate of the coumarin system in our preliminary study. Therefore, the atomic charge of nitrogen (X16) is an important descriptor in three models of PNN.

In conclusion, the present report demonstrates that DFT-based QSPR models can be used successfully to predict the release kinetics of the coumarin-based prodrug system. Among these models, the nonlinear

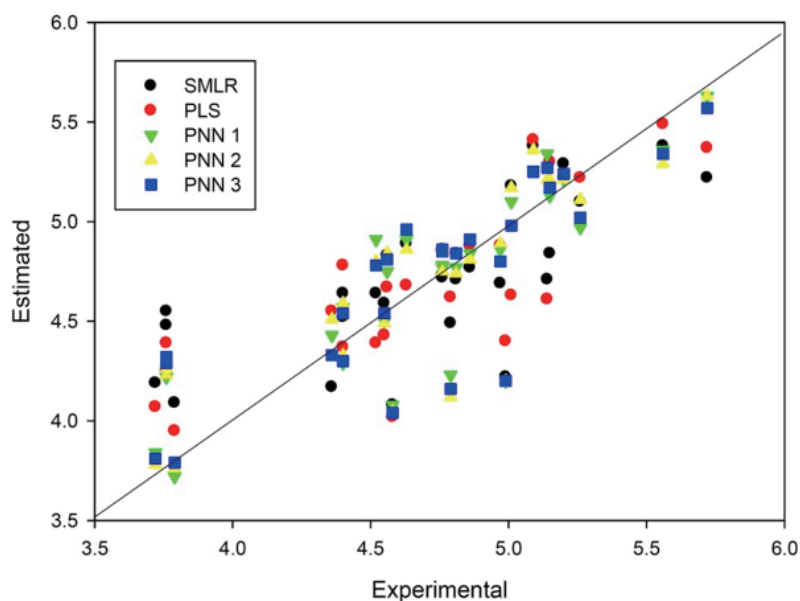
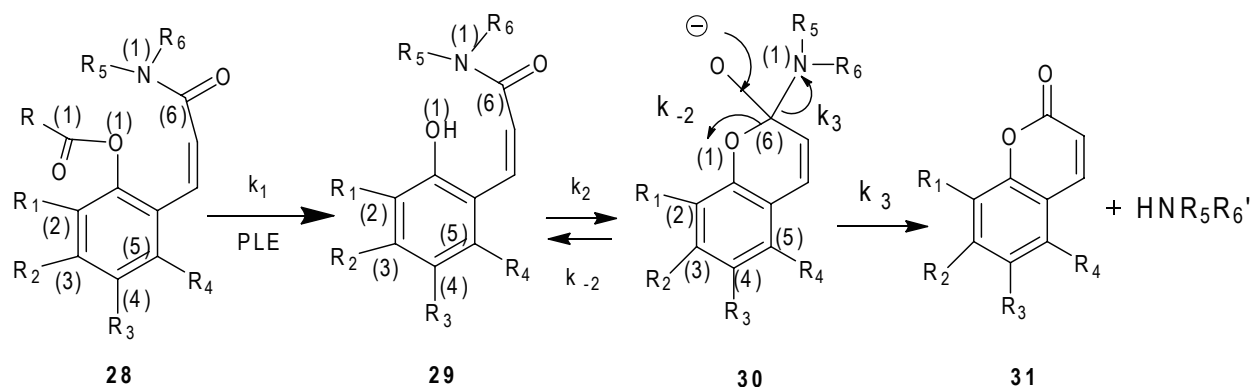


Figure 1. Estimated versus experimental values using three different models.



Scheme 2. The mechanism of the coumarin-based esterase sensitive prodrug system.

PNN models can provide estimated results in good agreement with experimental values. The descriptor of atomic charge of C-1, C-6 and N-1 exhibited more contributions to the prodrug release rate. In summary, this DFT-based QSPR approach can be a convenient way to predict release kinetics of coumarin prodrugs and the relative descriptors can also contribute to exploration of new derivatives of coumarin-based prodrug candidates.

Acknowledgements

This work was supported by a grant from NIH under Grant P20 GM065762 in USA, Scientific Research Foundation for Returned Overseas Chinese Scholars, State Education Ministry and Independent Innovation Foundation of Shandong University (IIFSDU, Grant No. 2012JC003) in China.

References

- Huttunen KM, Rautio J. Prodrugs – an efficient way to breach delivery and targeting barriers. *Curr Top Med Chem.* 2011; 11:2265-2287.
- Barot M, Bagui M, Gokulgandhi MR, Mitra AK. Prodrug strategies in ocular drug delivery. *Med Chem.* 2012; 8:753-768.
- Fang H, Kaur G, Wang B. Functional Group Approaches to Prodrugs: Functional Groups in Peptides. In *Prodrugs: Challenges and Rewards Part 2, Volume 5* (Stella VJ, Borchardt RT, Hageman MJ, Oliyai R, Tilley J, eds.). Springer, Berlin, German, 2007.
- Wang B, Zhang H, Wang W. Chemical feasibility studies of a potential coumarin-based prodrug system. *Bioorg Med Chem Lett.* 1996; 6:945-950.
- Gudmundsson OS, Jois SD, Vander Velde DG, Siahaan TJ, Wang B, Borchardt RT. The effect of conformation on the membrane permeation of coumarinic acid- and phenylpropionic acid-based cyclic prodrugs of opioid peptides. *J Pept Res.* 1999;53:383-392.
- Gudmundsson OS, Pauletti GM, Wang W, Shan D, Zhang H, Wang B, Borchardt RT. Coumarinic acid-based cyclic prodrugs of opioid peptides that exhibit metabolic stability to peptidases and excellent cellular permeability. *Pharm Res.* 1999; 16:7-15.
- Zych LA, Yang WQ, Liao Y, Griffin KR, Wang B. The effect of substitution patterns on the release rates of opioid peptides DADLE and [Leu(5)]-enkephalin from coumarin prodrug moieties. *Bioorg Chem.* 2004; 32:109-123.
- Wang B, Siahaan T, Soltero R. *Drug Delivery: Principles and Applications.* John Wiley & Sons, Inc., New York City, NY, USA, 2005.
- Ouyang H, Andersen TE, Chen W, Nofsinger R, Steffansen B, Borchardt RT. A comparison of the effects of p-glycoprotein inhibitors on the blood-brain barrier permeation of cyclic prodrugs of an opioid peptide (DADLE). *J Pharm Sci.* 2009; 98:2227-2236.
- Tang F, Borchardt RT. Characterization of the efflux transporter(s) responsible for restricting intestinal mucosa permeation of the coumarinic acid-based cyclic prodrug of the opioid peptide DADLE. *Pharm Res.* 2002; 19:787-793.
- Zych LA, Yang W, Liao Y, Griffin KR, Wang B. The effect of substitution patterns on the release rates of opioid peptides DADLE and [Leu(5)]-enkephalin from coumarin prodrug moieties. *Bioorg Chem.* 2004; 32:109-123.
- Nofsinger R, Fuchs-Knotts T, Borchardt RT. Factors that restrict the cell permeation of cyclic prodrugs of an opioid peptide, part 3: Synthesis of analogs designed to have improved stability to oxidative metabolism. *J Pharm Sci.* 2012; 101:3486-3499.
- Wang W, Jiang J, Ballard CE, Wang B. Prodrug approaches to the improved delivery of peptide drugs. *Curr Pharm Des.* 1999; 5:265-287.
- Wang W, Camenisch G, Sane DC, Zhang H, Hugger E, Wheeler GL, Borchardt RT, Wang B. A coumarin-based prodrug strategy to improve the oral absorption of RGD peptidomimetics. *J Control Release.* 2000; 65:245-251.
- Xie Q, Wang X, Wang X, Jiang Z, Qiu Z. Design, synthesis, and bioavailability evaluation of coumarin-based prodrug of meptazinol. *Bioorg Med Chem Lett.* 2005; 15:4953-4956.
- Liao Y, Hendrata S, Bae SY, Wang B. The effect of phenyl substituents on the release rates of esterase-sensitive coumarin-based prodrugs. *Chem Pharm Bull (Tokyo).* 2000; 48:1138-1147.
- Liao Y, Wang B. Substituted coumarins as esterase-sensitive prodrug moieties with improved release rates. *Bioorg Med Chem Lett.* 1999; 9:1795-1800.
- Wang B, Wang W, Camenisch GP, Elmo J, Zhang H, Borchardt RT. Synthesis and evaluation of novel coumarin-based esterase-sensitive cyclic prodrugs of peptidomimetic RGD analogs with improved membrane permeability. *Chem Pharm Bull (Tokyo).* 1999; 47:90-95.
- Jorgensen WL. QSAR/QSPR and proprietary data. *J Chem Inf Model.* 2006; 46:937.
- Dyckjaer JD, Jonsdottir SO. QSPR models for various physical properties of carbohydrates based on molecular mechanics and quantum chemical calculations. *Carbohydr Res.* 2004; 339:269-280.
- Fayet G, Rotureau P, Joubert L, Adamo C. Development of a QSPR model for predicting thermal stabilities of nitroaromatic compounds taking into account their decomposition mechanisms. *J Mol Model.* 2011; 17:2443-2453.
- Katritzky AR, Stoyanova-Slavova IB, Tämm K, Tamm T, Karelson M. Application of the QSPR approach to the boiling points of azeotropes. *J Phys Chem A.* 2011; 115:3475-3479.
- Peng S, Jian-Wei Z, Peng Z, Lin X. QSPR modeling of bioconcentration factor of nonionic compounds using Gaussian processes and theoretical descriptors derived from electrostatic potentials on molecular surface. *Chemosphere.* 2011; 83:1045-1052.
- Zeng XL, Wang HJ, Wang Y. QSPR models of n-octanol/water partition coefficients and aqueous solubility of halogenated methyl-phenyl ethers by DFT method. *Chemosphere.* 2012; 86:619-625.
- Selassie CD, Mekapati SB, Verma RP. QSAR: Then and now. *Curr Top Med Chem.* 2002; 2:1357-1379.
- Brown N, Lewis RA. Exploiting QSAR methods in lead optimization. *Curr Opin Drug Discov Devel.* 2006; 9:419-424.
- Hou X, Du J, Fang H, Li M. 3D-QSAR study on a series of Bcl-2 protein inhibitors using comparative molecular

- field analysis. *Protein Pept Lett.* 2011; 18:440-449.
28. Zhang L, Fang H, Zhu HW, Wang Q, Xu WF. QSAR studies of histone deacetylase (HDAC) inhibitors by CoMFA, CoMSIA, and molecular docking. *Drug Discov Ther.* 2009; 3:41-48.
 29. Hui-Ying X, Jian-Wei Z, Gui-Xiang H, Wei W. QSPR/QSAR models for prediction of the physico-chemical properties and biological activity of polychlorinated diphenyl ethers (PCDEs). *Chemosphere.* 2010; 80:665-670.
 30. Mercader AG, Duchowicz PR, Fernandez FM, Castro EA. Replacement method and enhanced replacement method *versus* the genetic algorithm approach for the selection of molecular descriptors in QSPR/QSAR theories. *J Chem Inf Model.* 2010; 50:1542-1548.
 31. Rayne S. Comment on "QSPR/QSAR models for prediction of the physicochemical properties and biological activity of polybrominated diphenyl ethers" by X. Hui-Ying, Z. Jian-Wei, Y. Qing-Sen, W. Yan-Hua, Z. Jian-Ying, and J. Hai-Xiao" [*Chemosphere* 66 (10) (2007) 1998-2010]. *Chemosphere.* 2010; 81:553.
 32. Yu X, Liu W, Liu F, Wang X. DFT-based theoretical QSPR models of Q-e parameters for the prediction of reactivity in free-radical copolymerizations. *J Mol Model.* 2008; 14:1065-1070.
 33. Bosque R, Sales J. A QSPR study of O-H bond dissociation energy in phenols. *J Chem Inf Comput Sci.* 2003; 43:637-642.
 34. Occhipinti G, Bjorsvik HR, Jensen VR. Quantitative structure-activity relationships of ruthenium catalysts for olefin metathesis. *J Am Chem Soc.* 2006; 128:6952-6964.
 35. M. J. Frisch, G. W. Trucks, H. B. Schlegel, *et al.* Gaussian 03, Revision C.02. Volume 24. Wallingford CT: Gaussian, Inc., Pittsburgh, PA, USA, 2004.
 36. Axel DB. Density-functional thermochemistry. III. The role of exact exchange. *J Chem Phys.* 1993; 98:5648-5652.
 37. Lee C, Yang W, Parr RG. Development of the Colle-Salvetti correlation-energy formula into a functional of the electron density. *Phys Rev B.* 1988; 37:785.
 38. Cancès E, Mennucci B, Tomasi J. A new integral equation formalism for the polarizable continuum model: Theoretical background and applications to isotropic and anisotropic dielectrics. *J Chem Phys.* 1997; 107:3032-3041.
 39. Jin S, Wang J, Li M, Wang B. Synthesis, evaluation, and computational studies of naphthalimide-based long-wavelength fluorescent boronic Acid reporters. *Chem Eur J.* 2008; 14:2795-2804.
 40. Jin S, Li M, Zhu C, Tran V, Wang B. Computer-based *de novo* design, synthesis, and evaluation of boronic acid-based artificial receptors for selective recognition of dopamine. *Chembiochem.* 2008; 9:1431-1438.
 41. Whitley DC, Ford MG, Livingstone DJ. Unsupervised forward selection: A method for eliminating redundant variables. *J Chem Inf Comput Sci.* 2000; 40:1160-1168.
 42. Li M, Ni N, Wang B, Zhang Y. Modeling the excitation wavelengths (λ_{ex}) of boronic acids. *J Mol Model.* 2008; 14:441-449.
 43. Tetko IV, Gasteiger J, Todeschini R, Mauri A, Livingstone D, Ertl P, Palyulin VA, Radchenko EV, Zefirov NS, Makarenko AS, Tanchuk VY, Prokopenko VV. Virtual computational chemistry laboratory – design and description. *J Comput Aided Mol Des.* 2005; 19:453-463.
 44. Tetko IV, Aksenova TI, Volkovich VV, Kasheva TN, Filipov DV, Welsh WJ, Livingstone DJ, Villa AEP. Polynomial neural network for linear and non-linear model selection in quantitative-structure activity relationship studies on the internet. *SAR QSAR Environ Res.* 2000; 11:263-280.
 45. Aksyonova TI, Volkovich VV, Tetko IV. Robust polynomial neural networks in quantitative-structure activity relationship studies. *Syst Anal Model Simul.* 2003; 43:1331-1339.

(Received August 13, 2012; Revised September 20, 2012; Accepted September 24, 2012)

Fluorimetric assay for D-amino acid oxidase activity in rat brain homogenate by using D-kynurenine as a substrate

Anna Kozaki¹, Sumiko Iwasa¹, Shoko Hosoda¹, Yoshikazu Nishiguchi², Moe Nakayama¹, Hideaki Ichiba¹, Takeshi Fukushima^{1,*}

¹Department of Analytical Chemistry, Faculty of Pharmaceutical Sciences, Toho University, Chiba, Japan;

²Department of Pharmaceutical Practice, Faculty of Pharmaceutical Sciences, Toho University, Chiba, Japan.

Summary

An easy fluorimetric assay for measuring D-amino acid oxidase (DAAO) activity by using one of the D-amino acids – D-kynurenine (D-KYN) – as a substrate was applied to assess DAAO activity in the cerebrum, cerebellum, and brainstem of Sprague-Dawley (SD) male rats. In this assay, DAAO produces kynurenic acid (KYNA) from D-KYN, and the fluorescence originating from KYNA can then be used to evaluate DAAO activity. Here, pellet fractions obtained by centrifugation of brain homogenates were allowed to react enzymatically with D-KYN. The addition of specific DAAO inhibitors, such as 3-methylpyrazole-5-carboxylic acid and 4*H*-thieno [3, 2-*b*] pyrrole-5-carboxylic acid (Compound 8), significantly attenuated the fluorescence intensity of KYNA, suggesting that DAAO present in the rat brain homogenates was responsible for the production of KYNA. In contrast, an inhibitor of aminotransferase (AT), aminooxyacetic acid, did not decrease KYNA production from D-KYN, meaning that AT could not metabolize D-KYN to KYNA under the present conditions. Moreover, the DAAO activity measured by the proposed assay correlated well with DAAO mRNA expression ($r = 0.9982$) determined by real-time polymerase chain reaction. Taken together, these findings show that the proposed fluorimetric assay can be used to evaluate DAAO activity in rat brain.

Keywords: D-amino acid oxidase, D-kynurenine, kynurenic acid, rat brain, fluorescence

1. Introduction

D-Amino acid oxidase (DAAO) (E.C. 1.4.3.3) can decompose neutral and basic D-amino acid oxidatively to generate hydrogen peroxide (H₂O₂), ammonia, and the corresponding α -keto acid (1,2). In mammalian brain tissue, D-serine, an endogenous co-agonist for the ionotropic glutamate receptor *N*-methyl-D-aspartate (NMDA) receptor (3), is decomposed by DAAO located in astroglial cells (3,4). Thus, the brain D-serine concentration controlled by DAAO is crucial for regular neurotransmission *via* the NMDA receptor,

and it has been suggested that a decrease in the D-serine concentration could induce NMDA receptor dysfunction. An example of this is the "glutamate hypothesis", which postulates that the cause of schizophrenia might arise from hypofunction of the NMDA receptor (5-7). In fact, the D-serine concentration in serum (8) and cerebrospinal fluids (9) is significantly decreased in schizophrenia patients. In addition, it has recently been reported that DAAO activity is significantly increased in the post-mortem brains of schizophrenia patients compared to controls (10).

DAAO activity in a tissue homogenate is usually assessed by measuring the H₂O₂ (11-14) or α -keto acid that is generated after addition of a substrate, D-alanine, or D-proline (10,15-17). Using the increased H₂O₂, an oxidative reaction that generates a colorimetric or fluorescent compound in the presence of a peroxidase is performed. Alternatively, the produced α -keto acid is reacted with a hydrazine compound to produce fluorescent or colorimetric substances. The generated

*Address correspondence to:

Dr. Takeshi Fukushima, Department of Analytical Chemistry, Faculty of Pharmaceutical Sciences, Toho University, 2-2-1 Miyama, Funabashi-shi, Chiba 274-8510, Japan.

E-mail: t-fukushima@phar.toho-u.ac.jp

substances are then quantified spectrophotometrically. However, both generated H_2O_2 and α -keto acid require the addition of next-step reagents, such as 2,4-dinitrophenyl hydrazine (DNPH) or Amplex Red[®], for the colorimetric or fluorimetric reaction to proceed.

A previous study by our group has shown that D-kynurenine (D-KYN) is oxidatively deaminated by a standard of pig kidney (pk) DAAO to produce a fluorescent compound, 4-hydroxyquinoline-2-carboxylic acid (kynurenic acid, KYNA) by one-step enzymatic reaction. The corresponding α -keto acid, 2-oxo-4-(2-aminophenyl)-4-oxobutanoic acid may be instantaneously produced as an intermediate in this reaction, but the α -keto acid appears to be immediately thereafter transformed to KYNA by intramolecular cyclization (18). Thus, the fluorescence intensity of KYNA can be utilized in conjunction with a standard of pig kidney (pk) DAAO in a fluorimetric assay to evaluate several compounds including drugs inhibiting DAAO activity (18,19).

The purpose of this study was to investigate the applicability of the proposed assay to rat brain homogenate. Here, we measured DAAO activity in the brain tissues of Sprague-Dawley (SD) rats according to our previously described *in vitro* assay using D-KYN as the substrate (18). The inhibition of the DAAO activity by 2 kinds of commercial DAAO inhibitors, as well as the correlation between DAAO mRNA expression and the enzyme activity was examined to determine the reliability of the proposed DAAO assay.

2. Materials and Methods

2.1. Chemicals

D-KYN, KYNA, 3-methylpyrazole-5-carboxylic acid (MPC), 3-methylpyrazole-4-carboxylic acid, Trizma[®] base (Tris) (min. 99.9%), D-alanine, and bovine serum albumin (BSA) were obtained from Sigma (St. Louis, MO, USA). Flavin adenine dinucleotide (FAD) and dimethylsulfoxide (DMSO) were obtained from Nacal Tesque (Kyoto, Japan). Zinc sulfate heptahydrate was obtained from Kanto Chemical Co. Ltd. (Tokyo, Japan). 2-Aminoxyacetic acid (AOAA) and catalase were purchased from Wako Pure Chemical Industries, Ltd. (Osaka, Japan). Compound 8 was from Santa Cruz Biotechnology, Inc. (Santa Cruz, CA, USA), and 2,4-dinitrophenyl hydrazine (DNPH) was purchased from Tokyo Chemical Industry Co., Ltd. (Tokyo, Japan). Water was purified using a Milli-Q system (Millipore Co. Ltd., Bedford, MA, USA). All other reagents were of reagent grade and were used without further purification.

2.2. Animal experiments

All animal experiments were approved by the Committee

of Animal Care, Toho University (No. 12-51-165). Male Sprague-Dawley (SD) rats were purchased from Charles River Japan (Kanagawa, Japan) and were housed in an environmentally controlled room for at least 1 week before use.

2.3. Tissue homogenate preparation

The rats were sacrificed by drawing blood from the abdominal aorta under diethyl-ether anesthesia. The rat brain tissue was immediately dissected and rinsed in a chilled physiological saline. The brain was then divided into cerebrum, cerebellum, and brainstem on an ice-cooled plate. After weighing each piece, the tissue was homogenized in 10 volumes of chilled Tris buffer (pH 8.3) using a potter-type homogenizer under ice cooling. The prepared homogenates were stored at $-80^{\circ}C$ until analysis.

2.4. DAAO assay with D-KYN as a substrate

After thawing at $4^{\circ}C$, an aliquot of 2.0 mL of the homogenate was centrifuged at $600 \times g$ for 30 min, and the obtained supernatant was further centrifuged at $20,000 \times g$ for 20 min. The pellet was suspended in 150 μL of 0.4 M Tris-buffer (pH 8.3) and subjected to the DAAO assay as an enzyme source. The DAAO assay was carried out according to the previously published method (18,19) with minor modifications.

In brief, 20 μL of the pellet fraction was mixed with 50 μL of 200 μM FAD solution, 20 μL of 2.0 mg/mL BSA in H_2O , and 390 μL of 0.4 M Tris buffer solution (pH 8.3). Subsequently, the mixed solution was incubated at $37^{\circ}C$ for 15 min. In some cases, 370 μL of 0.4 M Tris buffer solution (pH 8.3) was used instead of 390 μL , and 20 μL of inhibitor solution (in DMSO) was added before the incubation. The inhibitors used in the present study were AOAA (0, 1.0, 2.0, 4.0, 6.0, 8.0, and 10 mM), MPC (100 μM), 3,4-MPC (100 μM), and compound 8 (100 μM). Next, 20 μL of 7.0 mM D-KYN dissolved in Tris buffer (20 μL) were added, and the mixtures were then incubated at $37^{\circ}C$ for 120 min. To determine the optimum D-KYN concentration, different concentrations (0, 1.4, 4.2, and 7.0 mM) of D-KYN were added. After the enzymatic reaction, 1.0 mL of $CH_3CN/MeOH$ (1:1, v:v) was added and vortex-mixed. The mixture was then added to 500 μL of 0.4 M Tris buffer solution (pH 8.3) and 50 μL of 300 mM zinc sulfate dissolved in H_2O . The final solution was vortex-mixed and filtered (Millex[®] GV, 0.22 μm , Nihon Millipore, Tokyo, Japan) to remove proteins denatured by $CH_3CN/MeOH$ (1:1, v:v).

The fluorescence of the resultant solution was measured by a HITACHI F-7000 fluorescence spectrophotometer (Hitachi Co. Ltd., Tokyo, Japan). The fluorescence intensity of each solution was measured at an excitation wavelength of 346 nm and

an emission wavelength of 396 nm. According to the following equation (1), the ΔF value was determined:

$$\Delta F = F - F_0 \quad (1)$$

where F and F_0 are fluorescence intensities of the sample and blank sample (a sample treated without rat brain homogenate), respectively. Based on the ΔF value, the amount of KYNA produced (pmol) was calculated by the calibration curve for KYNA (Figure 1). Finally, DAAO activity was expressed as the production rate of KYNA per μg protein (fmol KYNA/min/ μg protein), where the protein concentration of the homogenate was determined by the Bradford method according to our previous paper (20). In the inhibition experiment, the mean fluorescence intensity (ΔF) value of the control sample, *i.e.*, the sample without inhibitor, was designated as 100%, and the inhibition degree was expressed as a percentage.

2.5. DAAO assay with D-alanine as a substrate

In the conventional DAAO assay using D-alanine as a substrate (10,16), 20 μL of the pellet fraction was mixed with 20 μL of 0.1 mg/mL catalase, 50 μL of 200 μM FAD solution, 20 μL of 2.0 mg/mL BSA in H_2O , and 390 μL of 0.4 M Tris buffer solution (pH 8.3). After incubation of the mixed solution at 37°C for 15 min, 20 μL of 50 mM D-alanine was added instead of D-KYN, and incubated for another 120 min. After the enzymatic reaction, 1.0 mL of $\text{CH}_3\text{CN}/\text{MeOH}$ (1/1) and 700 μL of 0.6 M NaOH solution were added and vortex-mixed. The final solution was filtered (Millex[®] GV, 0.22 μm , Nihon Millipore, Tokyo, Japan), and the absorbance of the resultant solution was measured at 445 nm (21,22) using a JASCO V-650 spectrophotometer (JASCO Corporation, Tokyo, Japan) using a quartz cell (1 cm \times 1 cm).

2.6. Stability of KYNA

In the incubated mixture described in 2.4. Section, 20 μL of KYNA (0.8 mg/mL, 4.2 μM) was added instead of 7.0 mM D-KYN after incubation at 37°C for 15 min. Samples were then incubated at 37°C for another 120 min and assayed as previously described. The mean fluorescence intensity (ΔF) value of the control sample, *i.e.*, the sample without a pellet fraction, was designated as 100%, and the decreased degree of ΔF was expressed as a percentage.

2.7. Real-time quantitative PCR

Total RNAs were extracted from each brain tissue using RNeasy Plus Universal kits (Qiagen, Courtaboeuf, France). Complementary DNAs (cDNAs) were made with a QuantiTect Reverse Transcription kit (Qiagen). DAAO gene expression was determined by RT-PCR using the glyceraldehyde 3-phosphate dehydrogenase

(GAPDH; accession number NM017008) gene as an internal control and primers specific for DAAO (accession number NM053626) mRNAs. Upstream primers were CCCTTTCTGGAAAAGCACAG (DAAO) and GTGGACCTCATGGCCTACAT (GAPDH), and downstream primers were CTCCTC TCACCACCTCTTCG (DAAO) and TGTGAGGGA GATGCTCAGTG (GAPDH). Expression of genes was assessed by real-time RT-PCR using the iQ SYBR Green Supermix and Chrome 4 (Bio-Rad Laboratories Inc., California, CA, USA) running 45 cycles of the following protocol: 3 min predenaturation at 95°C, 10 sec denaturation at 95°C, 10 sec at 62°C, followed by a 1 min extension at 65°C. The PCR products, DAAO and GAPDH, were purified by 2% agarose gel electrophoresis and subcloned into the pTZ19R vector. After transformation of these recombinants into XL1-Blue by the calcium chloride method, plasmid DNAs were recovered, and their nucleotide sequences were determined by a DNA sequencer, Model 4000 (LI-COR Inc., Lincoln, NE, USA).

3. Results and Discussion

3.1. DAAO activity

In our previous paper, we reported an easy fluorimetric assay for measuring compounds that can inhibit pig kidney DAAO using D-KYN as the substrate (18,19). The kynurenic acid (KYNA) produced enzymatically from D-KYN by DAAO emits an intense fluorescence at 396-398 nm in the presence of zinc ions. Thus, the inhibition potency of various compounds against DAAO can be evaluated by the degree of fluorescence produced.

In the present study, this fluorimetric assay was applied to assess the DAAO activity in rat brain tissues. As reported, KYNA emits fluorescence at 396-398 nm with an excitation wavelength at 251 nm (19,23) or 344-346 nm (24,25). An excitation wavelength of 346 nm was used in the present study to increase the signal to noise ratio and to avoid interference fluorescence stemming from endogenous substances included in the brain homogenate. Under the present conditions, a linear calibration curve for standard KYNA in the range of 26.1-81.2 pmol per assay tube was obtained (Figure 1), and this calibration curve was used to calculate KYNA production.

To assess DAAO activity in rat brain tissues, the brain tissue homogenates were centrifuged as previously described (15,17), and the pellet fraction was then used as an enzyme source for the proposed assay. Increasing concentrations of D-KYN were added to the reactions to determine its optimum concentration as a substrate, which was set at the plateau level of 7.0 mM (Figure 2). The pellet fraction was incubated with the D-KYN substrate in Tris buffer (pH 8.3), and

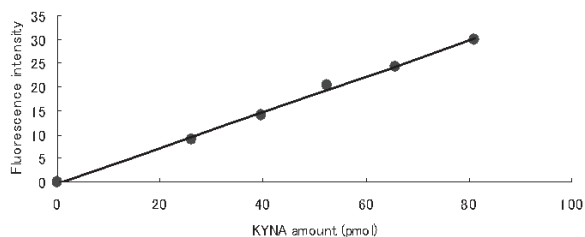


Figure 1. Calibration curve for standard KYNA.

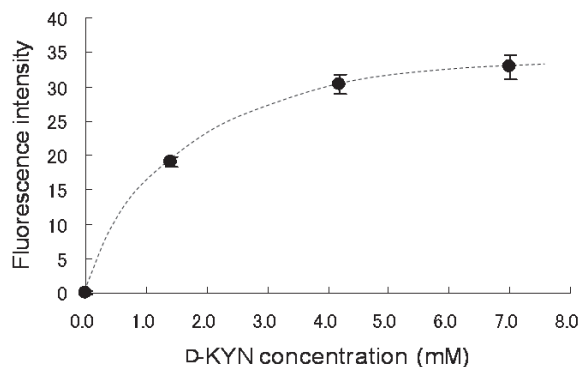


Figure 2. Effect of D-KYN concentration on the fluorescence intensity of the produced KYNA.

the fluorescence intensity of KYNA produced from D-KYN was measured. As shown in Figure 3, the fluorescence of KYNA at 396 nm increases linearly with time, suggesting that the added D-KYN was converted to KYNA by DAAO present in the pellet fraction. Conversely, incubation with D-KYN alone for 120 min in the absence of the pellet fraction gradually showed fluorescence at 396 nm. Based on this finding, the fluorescence derived from KYNA produced enzymatically from D-KYN by DAAO was calculated by subtracting the fluorescence value without the pellet fraction (blank) from the sample fluorescence intensity at 396 nm. As might be expected, DAAO activity expressed as fmol KYNA/min/ μ g protein was the highest in rat cerebellum, followed by brain stem and cerebrum (Figure 4), in agreement with previous reports (26,27).

Although endogenous KYNA is present in rat brain tissues, the concentration is reported to be relatively low, approximately 200-600 fmol/mg protein among the tissues assayed here (28). In this previous study, a centrifugation fractionation procedure was not carried out, while the assay here uses the pellet fraction by centrifugation. As a result, endogenous KYNA present in the brain tissues hardly affected the fluorescence intensity under the present experimental conditions. Indeed, a blank sample without adding D-KYN consistently showed a background level of fluorescence (Figure 3).

To determine whether the KYNA produced from D-KYN was further metabolized into other metabolites under the present experimental conditions, a standard

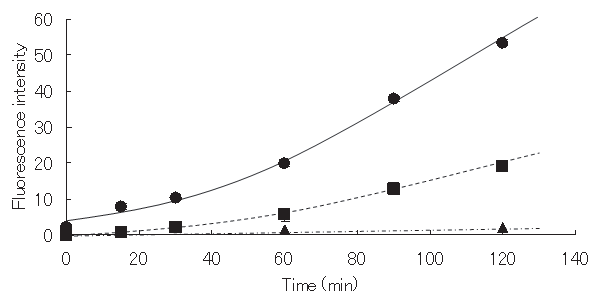


Figure 3. Changes in the fluorescence intensity at 396 nm with an excitation wavelength of 346 nm as a function of time. A closed circle with a solid line and a closed square with a dotted line represent the fluorescence intensities of a sample with D-KYN in the presence or absence of brainstem homogenate, respectively. A closed triangle represents the fluorescence intensity of the sample without D-KYN in the presence of brainstem homogenate.

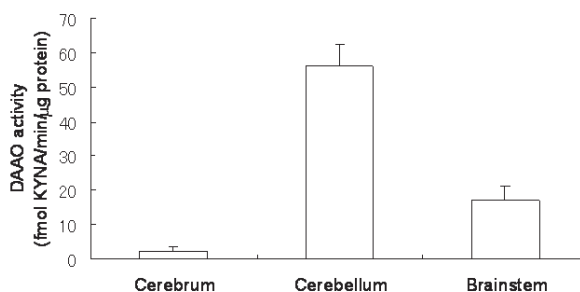


Figure 4. DAAO activity (fmol KYNA/min/ μ g protein) determined by the proposed method in rat cerebrum, cerebellum, and brainstem ($n = 5$).

of 4.2 μ M KYNA instead of D-KYN was added to the enzymatic reaction, and stability of KYNA was investigated. No remarkable decrease in fluorescence intensity of KYNA after the enzymatic reaction at 37°C for 120 min was observed (Figure 5). In addition, to our knowledge, no information on the metabolites of KYNA in the brain has been reported. Considering these observations, KYNA itself does not appear to be drastically metabolized or decomposed under the present conditions. In the fluorimetric assay, the stability of KYNA that is produced provides an advantage over H_2O_2 or α -keto acids. Thus, the fluorescence originating from the produced KYNA can be used as a reliable indicator of DAAO activity.

To compare the present data with data obtained by the conventional method, the homogenate sample was also reacted with D-alanine, followed by the addition of 2,4-DNPH, and the absorbance was measured at 445 nm as previously described (21,22). Unfortunately, the conventional method failed to assess DAAO activity since the obtained absorbance value hardly differed from the blank value (data not shown). Thus, a more concentrated homogenate sample might be needed to determine DAAO activity by the conventional method. In contrast, the proposed method employs fluorescence detection, allowing brain DAAO activity to be determined in spite of a small amount of homogenate

sample.

3.2. Inhibition of brain DAAO activity by specific inhibitors

To examine whether the enzymatic formation of KYNA from D-KYN was indeed caused by DAAO or other unknown enzymes, specific inhibitors for DAAO (12,16) were added to the reaction mixture. 3-Methylpyrazole-5-carboxylic acid (MPC) (12) and 4*H*-thieno [3,2-*b*] pyrrole-5-carboxylic acid (Compound 8) (17) were chosen as specific inhibitors in the present study because both compounds are commercially available. Both MPC and Compound 8 (each 100 μ M) could completely attenuate the DAAO activity (Figure 6). It has been reported that the IC_{50} value of Compound 8 is 114 nM (17), while that of MPC is 0.91 μ M (12), indicating that Compound 8 is a more potent inhibitor of DAAO activity. However, the results from this study (Figure 6) indicated that both specific inhibitors (100 μ M) appropriately inhibited the DAAO activity. In contrast, 3-methylpyrazole-4-carboxylic acid (3,4-MPC), a structural isomer of MPC, failed to inhibit the production of KYNA (Figure 6). In agreement with

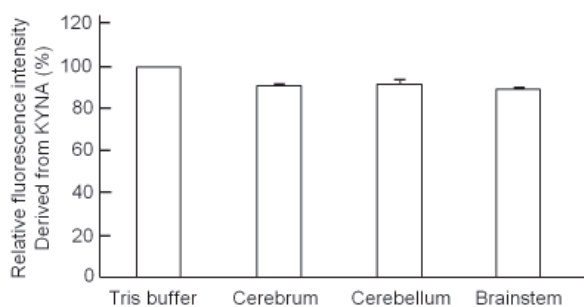


Figure 5. Relative fluorescence intensity of added KYNA in rat cerebrum, cerebellum, and brain stem after the enzymatic reaction of the pellet fraction ($n = 3$). The fluorescence intensity of the added KYNA in Tris buffer (pH 8.3) was designated as 100%.

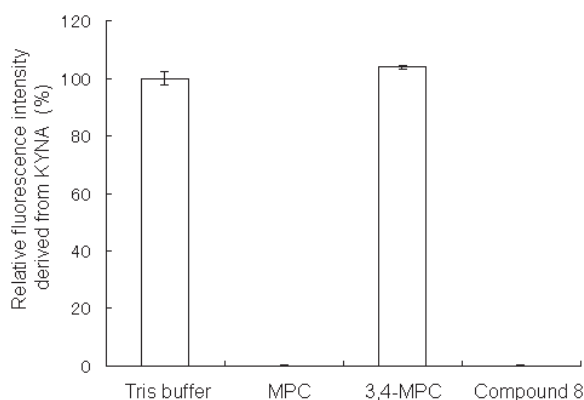


Figure 6. Relative fluorescence intensity of the produced KYNA after the enzymatic reaction of D-KYN with rat brainstem homogenates in the presence or absence of inhibitors, 3,4-MPC, MPC, and Compound 8 (each 100 μ M; $n = 3$).

this finding, 3,4-MPC has previously been shown to hardly inhibit pk DAAO in an *in vitro* study (19). Taken together, these findings suggest that DAAO in the pellet fraction is responsible for the enzymatic production of KYNA from D-KYN.

Recently, an *in vivo* microdialysis study demonstrated that D-KYN was metabolized to KYNA in rat striatum by kynurenine aminotransferase (KAT) based on evidence showing that addition of an inhibitor of KAT, AOAA, remarkably inhibited KYNA production from D-KYN (29). Considering this recent report, the effect of AOAA on the production of KYNA from D-KYN in our brain homogenates was investigated. As shown in Figure 7, however, no considerable decrease in the production of KYNA by D-KYN was observed in the present study with the addition of AOAA. Therefore, it seems unlikely that KAT contributed to the production of KYNA under the present experimental conditions. The reason for this discrepancy is unknown, but it may stem from differences between the *in vivo* state examined in the first study and the homogenates examined here, which are not at physiological pH, but at a weakly basic pH in Tris buffer (pH 8.3).

3.3. mRNA expression

In addition to DAAO activity, DAAO mRNA expression was also investigated by real-time quantitative PCR. Table 1 shows DAAO activity and mRNA expression in the cerebrum, brainstem, and cerebellum of SD rats. The present data revealed a similar tendency to those reported previously (30,31), namely, the highest DAAO mRNA expression was found in the cerebellum, while slight expression was observed in the cerebrum. DAAO mRNA expression plotted against DAAO activity, as shown in Figure 8, reveals a linear relationship between DAAO mRNA and DAAO activity ($r = 0.9982$), indicating that the DAAO activity shown by the present assay might be reflected in DAAO expression in rat brain.

In summary, DAAO activity in the cerebrum,

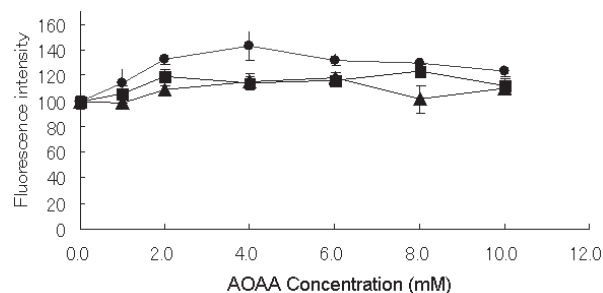
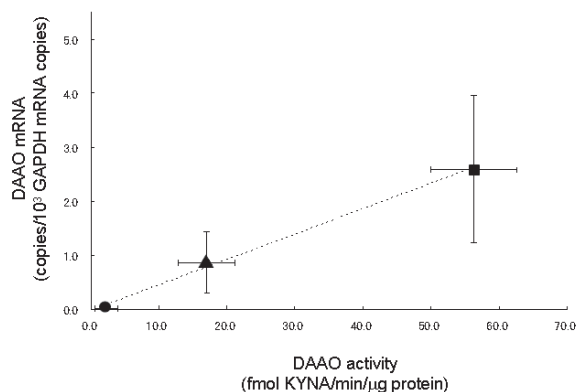


Figure 7. Fluorescence intensity at 396 nm with an excitation wavelength of 346 nm after the enzymatic reaction of D-KYN with rat cerebrum (circle), cerebellum (square), and brainstem (triangle) in the presence of several concentrations of an aminotransferase inhibitor, AOAA ($n = 3$).

Table 1. DAAO activity and mRNA expression in the cerebrum, brainstem, and cerebellum of control rats (n = 5)

Items	Activity (fmol KYNA/min / μ g protein)	mRNA(copies/ 10^3 GAPDH mRNA copies)
Cerebrum	2.24 \pm 1.67	0.0143 \pm 0.00623
Brainstem	17.0 \pm 4.15	0.858 \pm 0.567
Cerebellum	56.3 \pm 6.31	2.59 \pm 1.36

**Figure 8. Expression of DAAO mRNA plotted against the DAAO activity in the cerebrum (circle), brainstem (triangle), and cerebellum (square) determined by the proposed assay (n = 5).**

cerebellum, and brainstem of rats can be measured by an easy fluorimetric assay using D-KYN as a substrate. The produced KYNA was stable in the homogenate under the current experimental conditions. Recently, Wong *et al.* reported a microplate fluorescence assay for KAT I using fluorescence originating from KYNA (32). Since the fluorimetric assay proposed here also uses the fluorescence of KYNA, a rapid microplate version of this assay will be performed with a plate reader in the future.

Acknowledgements

The authors thank Ms. Koshikawa, Ms. Kume, and Mr. Yoshihara for their technical assistance. This study was financially supported in part by a Nukada scholarship in Toho University and Grant-in-Aid for Scientific Research (C) (22590147) from the Japan Society for the Promotion of Science (JSPS).

References

1. Khoronenkova SV, Tishkov VI. D-Amino acid oxidase: Physiological role and applications. *Biochemistry (Moscow)*. 2008; 73:1511-1518.
2. Pollegioni L, Piubelli L, Sacchi S, Pilone MS, Molla G. Physiological functions of D-amino acid oxidases: From yeast to humans. *Cell Mol Life Sci*. 2007; 64:1373-1394.
3. Schell MJ, Molliver ME, Snyder SH. D-serine, an endogenous synaptic modulator: Localization to astrocytes and glutamate-stimulated release. *Proc Natl Acad Sci U S A*. 1995; 92:3948-3952.
4. Park HK, Shishido Y, Ichise-Shishido S, Kawazoe T,

- Ono K, Iwana S, Tomita Y, Yorita K, Sakai T, Fukui K. Potential role for astroglial D-amino acid oxidase in extracellular D-serine metabolism and cytotoxicity. *J Biochem*. 2006; 139:295-304.
5. Lindsley CW, Shipe WD, Wolkenberg SE, Theberge CR, Williams DL, Sur C, Kinney GG. Progress towards validating the NMDA receptor hypofunction hypothesis of schizophrenia. *Curr Topics Med Chem*. 2006; 6:771-785.
6. Paz RD, Tardito S, Atzori M, Tseng KY. Glutamatergic dysfunction in schizophrenia: From basic neuroscience to clinical psychopharmacology. *Eur Neuropsychopharmacol*. 2008; 18:773-786.
7. Verrall L, Burnet PWJ, Betts JF, Harrison PJ. The neurobiology of D-amino acid oxidase (DAO) and its involvement in schizophrenia. *Mol Psychiatry*. 2010; 15:122-137.
8. Hashimoto K, Fukushima T, Shimizu E, Komatsu N, Watanabe H, Shinoda N, Nakazato M, Kumakiri C, Okada S, Hasegawa H, Imai K, Iyo M. Decreased serum levels of D-serine in patients with schizophrenia – Evidence in support of the N-methyl-D-aspartate receptor hypofunction hypothesis of schizophrenia. *Arch Gen Psychiatry*. 2003; 60:572-576.
9. Hashimoto K, Engberg G, Shimizu E, Nordin C, Lindstrom LH, Iyo M. Reduced D-serine to total serine ratio in the cerebrospinal fluid of drug naive schizophrenic patients. *Prog Neuropsychopharmacol Biol Psychiatr*. 2005; 29:767-769.
10. Madeira C, Freitas ME, Vargas-Lopes C, Wolosker H, Panizzutti R. Increased brain D-amino acid oxidase (DAAO) activity in schizophrenia. *Schizophrenia Res*. 2008; 101:76-83.
11. Watanabe T, Motomura Y, Suga T. A new colorimetric determination of D-amino acid oxidase and urate oxidase activity. *Anal Biochem*. 1978; 86:310-315.
12. Adage T, Trillat AC, Quattropani A, Perrin D, Cavarec L, Shaw J, Guerassimenko O, Giachetti C, Gréco B, Chumakov I, Halazy S, Roach A, Zaratin P. *In vitro* and *in vivo* pharmacological profile of AS057278, a selective D-amino acid oxidase inhibitor with potential antipsychotic properties. *Eur Neuropsychopharmacol*. 2008; 18:200-214.
13. Khoronenkova SV, Tishkov VI. High-throughput screening assay for D-amino acid oxidase. *Anal Biochem*. 2008; 374:405-410.
14. Duplantier AJ, Becker SL, Bohanon MJ, *et al.* Discovery, SAR, and pharmacokinetics of a novel 3-hydroxyquinoline-2(1H)-one series of potent D-amino acid oxidase (DAAO) inhibitors. *J Med Chem*. 2009; 52:3576-3585.
15. D'Aniello A, D'Onofrio G, Pischetola M, D'Aniello G, Vetere A, Petrucelli L, Fisher GH. Biological role of D-amino acid oxidase and D-aspartate oxidase. *J Biol Chem*. 1993; 268:26941-26949.
16. Zhao W, Konno R, Zhou XJ, Yin M, Wang YX. Inhibition of D-Amino-acid oxidase activity induces pain relief in mice. *Cell Mol Neurobiol*. 2008; 28:581-591.
17. Smith SM, Uslaner JM, Yao L, *et al.* The behavioral and neurochemical effects of a novel D-amino acid oxidase inhibitor Compound 8 [4H-thieno[3,2-b]pyrrole-5-carboxylic acid] and D-serine. *J Pharmacol Exp Ther*. 2009; 328:921-930.
18. Song Z, Ogaya T, Ishii K, Ichiba H, Iizuka H, Fukushima T. Utilization of kynurenic acid produced

- from D-kynurenine in an *in vitro* assay of D-amino acid oxidase activity. *J Health Sci.* 2010; 56:341-346.
19. Iwasa S, Tabara H, Song Z, Nakabayashi M, Yokoyama Y, Fukushima T. Inhibition of D-amino acid oxidase activity by antipsychotic drugs evaluated by a fluorimetric assay using D-kynurenine as substrate. *Yakugaku Zasshi.* 2011; 131:1111-1116.
 20. Song Z, Ge D, Ishii K, Yamada H, Toriumi K, Watanabe H, Nabeshima T, Fukushima T. Determination of *N*-acetylaspartic acid concentration in the mouse brain using HPLC with fluorescence detection. *Biomed Chromatogr.* 2012; 26:147-151.
 21. Oguri S, Watanabe K, Nozu A, Kamiya A. Screening of D-amino acid oxidase inhibitor by a new multi-assay method. *Food Chem.* 2007; 100:616-622.
 22. Katsuki H, Yoshida T, Tanegashima C, Tanaka S. Improved direct method for determination of keto acids by 2,4-dinitrophenylhydrazine. *Anal Biochem.* 1971; 43:349-356.
 23. Mitsuhashi S, Fukushima T, Kawai J, Tomiya M, Santa T, Imai K, Toyo'oka T. Improved method for the determination of kynurenic acid in rat plasma by column-switching HPLC with post-column fluorescence detection. *Anal Chim Acta.* 2006; 562:36-43.
 24. Inuma F, Tabara M, Yashiro K, Watanabe M. Fluorometric determination of kynurenic acid in urine with zinc (II) acetate. *Bunseki Kagaku.* 1985; 34:483-486.
 25. Shibata K. Fluorimetric micro-determination of kynurenic acid, an endogenous blocker of neurotoxicity, by high-performance liquid chromatography. *J Chromatogr.* 1988; 430:376-380.
 26. Weimar WR, Neims AH. The development of D-amino acid oxidase in rat cerebellum. *J Neurochem.* 1977; 29:649-656.
 27. Horiike K, Tojo H, Arai R, Nozaki M, Maeda T. D-Amino-acid oxidase is confined to the lower brain stem and cerebellum in rat brain: Regional differentiation of astrocytes. *Brain Res.* 1994; 652:297-303.
 28. Fukushima T, Mitsuhashi S, Tomiya M, Kawai J, Hashimoto K, Toyo'oka T. Determination of rat brain kynurenic acid by column-switching HPLC with fluorescence detection. *Biomed Chromatogr.* 2007; 21:514-519.
 29. Perez-De la C, Amroi L, Sathyaikumar KV, Wang X, Notarangelo FM, Wu HQ, Schwarcz R. Enzymatic transamination of D-kynurenine generates kynurenic acid in rat and human brain. *J Neurochem.* 2012; 120:1026-1035.
 30. Takeyama K, Yoshikawa M, Oka T, Kawaguchi M, Suzuki T, Hashimoto A. Ketamine enhances the expression of serine racemase and D-amino acid oxidase mRNAs in rat brain. *Eur J Pharmacol.* 2006; 540:82-86.
 31. Watanabe M, Yoshikawa M, Takeyama K, Hashimoto A, Kobayashi H, Suzuki T. Subchronic administration of ketamine decreases the mRNA expression of serine racemase in rat brain. *Tokai J Exp Clin Med.* 2010; 35:137-143.
 32. Wong J, Ray WJ, Kornilova AY. Development of a microplate fluorescence assay for kynurenine aminotransferase. *Anal Biochem.* 2011; 409:183-188.

(Received August 13, 2012; Accepted October 25, 2012)

Identification of MIWI-associated Poly(A) RNAs by immunoprecipitation with an anti-MIWI monoclonal antibody

Takahiro Nishibu^{1,2,*}, Yukinobu Hayashida¹, Saori Tani², Sadamu Kurono^{3,4}, Kanako Kojima-Kita⁵, Ryo Ukekawa¹, Tsutomu Kurokawa¹, Satomi Kuramochi-Miyagawa⁶, Toru Nakano^{5,6}, Kunio Inoue², Susumu Honda¹

¹Life Science Research Laboratories, Wako Pure Chemical Industries Ltd., Hyogo, Japan;

²Graduate School of Science, Kobe University, Kobe, Japan;

³BMS Center, Wako Pure Chemical Industries Ltd., Osaka, Japan;

⁴Joint Research Laboratory of Molecular Signature Analysis, Graduate School of Medicine, Division of Health Sciences, Osaka University, Osaka, Japan;

⁵Graduate School of Frontier Biosciences, Osaka University, Osaka, Japan;

⁶Graduate School of Medical Sciences, Osaka University, Osaka, Japan.

Summary

MIWI is one of the PIWI subfamily of proteins mainly expressed in mouse germ cells, and associates with pachytene piRNAs. MIWI has been thought to play an essential role in spermatogenesis and spermiogenesis *via* biogenesis and/or stability of pachytene piRNAs, retrotransposon silencing, and post-transcriptional regulation of target mRNAs. However, MIWI's detailed role and function are not well understood. In this study, we produced an anti-MIWI mouse monoclonal antibody and identified MIWI-associated poly(A) RNAs by immunoprecipitation from adult mouse testes lysates. Approximately 70% of the MIWI-associated poly(A) RNAs were known mRNAs and 30% of them were unknown non-coding RNAs. These poly(A) RNAs contained piRNA-encoding RNAs transcribed from piRNA cluster regions and piRNA-encoding mRNA, such as *Aym1* mRNA. Mature piRNAs specifically encoded in these piRNA-encoding RNAs were generated in pachytene spermatocytes and not detected in *Miwi*-deficient (*Miwi*^{-/-}) testes. Moreover, MIWI associated with a large number of known mRNAs whose expression levels were increased in pachytene spermatocytes, and the expression of these mRNAs was decreased in *Miwi*^{-/-} testes at 20 days postpartum when pachytene spermatocytes were most abundant. These results strongly suggest that MIWI is involved in pachytene piRNA biogenesis and the positive regulation of target mRNA metabolism in pachytene spermatocytes *via* association with pachytene piRNA precursors and target mRNAs.

Keywords: MIWI, PIWI, piRNA, pachytene, spermatogenesis

1. Introduction

Argonaute family proteins, classified into AGO and PIWI subfamily proteins by amino acid sequence homology, play an important role in small RNA-mediated regulation of target gene expression. AGO subfamily proteins are ubiquitously expressed, whereas

PIWI subfamily proteins are expressed mainly in germ cells (1). AGO subfamily proteins bind to microRNA (miRNA) or small interfering RNA of approximately 22 nucleotides in length, and function predominantly in post-transcriptional repression of target RNAs, *via* cleavage, translational repression and degradation mediated by the associated small RNA (2-4). On the other hand, PIWI subfamily proteins bind to PIWI-interacting RNAs (piRNAs) of approximately 25-31 nucleotides in length, but their functions have not been elucidated in detail (5-9).

There are three murine PIWI subfamily proteins, MIWI, MILI, and MIWI2. Each protein shows different

*Address correspondence to:

Dr. Takahiro Nishibu, Life Science Research Laboratories, Wako Pure Chemical Industries Ltd., 6-1 Takada-cho, Amagasaki, Hyogo 661-0963, Japan.
E-mail: nishibu.takahiro@wako-chem.co.jp

expression patterns during spermatogenesis. MIWI is expressed from meiotic pachytene spermatocytes to elongating spermatids, and *Miwi*-deficient (*Miwi*^{-/-}) mice display spermatogenic arrest at the round spermatid stage (10). MILI is expressed from primordial germ cells to round spermatids and MIWI2 is expressed in gonocytes (11-14). *Mili*^{-/-} or *Miwi2*^{-/-} mice display spermatogenic arrest between the early and mid-pachytene stage of meiosis (11,12,14). Thus, these three PIWI subfamily proteins are thought to play essential roles in spermatogenesis at different stages.

MILI and MIWI2 have been reported to associate with fetal piRNAs derived from repetitive retrotransposon genes in fetal gonocytes and to play an important role in gene silencing of retrotransposons via DNA methylation (12,13,15,16). Fetal piRNAs are generated from retrotransposon transcripts via the primary processing pathway and the secondary ping-pong amplification cycle pathway, and MILI and MIWI2 are directly involved in these pathways (13). In addition to MILI and MIWI2, other proteins, such as the TDRD family, MVH, GASZ, SUN1, and MOV10L1, are required for biogenesis of piRNAs and gene silencing of retrotransposons (17-26). These findings have begun to reveal the mechanisms of retrotransposon gene silencing mediated by MILI and MIWI2 in the primordial testis.

MIWI associates with pachytene piRNAs derived from various genomic regions that are unrelated to retrotransposons (6,8). The function of MIWI is therefore not thought to be limited to gene silencing of retrotransposons, although most recently MIWI has been reported to function in LINE1 retrotransposon silencing via its slicer activity (27). MIWI is concentrated in the chromatoid bodies, a germ cell-specific cytoplasmic structure that appears in the stages from pachytene spermatocytes to round spermatids. These chromatoid bodies contain RNA-processing proteins, such as Dicer, AGO2, and GW182. Therefore, MIWI is predicted to function in post-transcriptional control of target mRNAs (28). Certain mRNAs associated with MIWI are severely down-regulated in *Miwi*^{-/-} mutants, suggesting that MIWI is required for target mRNA stability (10). As MIWI associates with mRNAs and piRNAs in the polysome fraction, MIWI is also thought to function in translational control of mRNAs (29). The detailed function of MIWI in post-transcriptional control of target mRNAs is unclear. In addition, MIWI has been reported to be required for the biogenesis and/or stability of pachytene piRNAs based on the result that pachytene piRNAs are not detected in *Miwi*^{-/-} mutants (7). However, the function of MIWI in pachytene piRNA biogenesis is also still unknown.

AGO2, one of the AGO subfamily members, is a component of the chromatoid body similar to MIWI and plays an important role in post-transcriptional regulation of target mRNA mediated by miRNA.

However, since spermatogenesis is not arrested in conditional *Ago2*^{-/-} testes, AGO2 is not thought to be essential for spermatogenesis (30).

In this study, we analyzed poly(A) RNA present in MIWI complexes obtained by immunoprecipitation of adult mouse testes lysates, and compared them to poly(A) RNAs present in AGO2 complexes to reveal the function of MIWI. Our results suggest that MIWI may play an important role in pachytene piRNA biogenesis and the positive regulation of target mRNAs in pachytene spermatocytes.

2. Materials and Methods

2.1. Ethics Statement

Animal experiments were approved by the Institutional Animal Care and Use Committee of Wako Pure Chemical Industries Ltd. (approval ID: 19-5, 20-4, and 20-12).

2.2. Production of monoclonal antibodies

To produce anti-HIWI/MIWI and anti-mouse AGO2 monoclonal antibodies, a HIWI N-terminal region peptide TGRARARARGRARGQETAQ-bovine thyroglobulin (BTG) conjugate and a mouse AGO2 N-terminal region peptide YSGAGPVLASPAPTTSPIP-BTG conjugate were respectively injected into BALB/c mice. The B lymphocytes derived from the immunized mice were fused with P3U1 myeloma cells (ATCC). The resulting hybridomas were screened by enzyme-linked immunosorbent assays and immunoprecipitation assays using lysates of HEK293T cells (ATCC) that expressed FLAG-tagged HIWI or FLAG-tagged mouse AGO2, and an anti-HIWI/MIWI monoclonal antibody (2C12) and anti-mouse AGO2 monoclonal antibody (3E7) were established. The 2C12 hybridoma and the 3E7 hybridoma were injected into the abdominal cavity of adult mice and the ascites fluid was collected. Each monoclonal antibody was purified from the ascites fluid by affinity purification using Protein A Sepharose (GE Healthcare, Milwaukee, WI, USA).

2.3. Immunoprecipitation and RNA purification

Adult mouse testes (approximately 50 mg) were homogenized in 1 mL of cell lysis buffer (20 mM Tris-HCl, pH 7.4, 2.5 mM MgCl₂, 200 mM NaCl, 0.05% NP40), and the cell lysate was cleared by centrifugation at 20,000 × g for 20 min at 4°C. After filtration of the cell lysate using a 0.45 μm filter, 20 μL of Protein G-coupled beads (Life Technologies) bound with 5 μg of 2C12, 3E7, or non-specific mouse IgG was added to the cell lysate and mixed by rotation for 3 h at 4°C. The beads were washed three times with 1 mL of cell lysis buffer, and the immunoprecipitated protein-RNA

complex was eluted with 0.5% SDS. RNA contained in the eluted immunoprecipitated complex was extracted with phenol/chloroform, and precipitated with ethanol and Ethachinmate (Nippon Gene). The RNA sample was resuspended in nuclease-free water.

Total RNA was extracted from mouse testes samples with ISOGEN (Nippon Gene) according to the manufacturer's instructions. The extracted RNA was treated with Turbo DNase (Life Technologies) for 30 min at 37°C. After an additional phenol/chloroform extraction, the RNA was precipitated with ethanol and Ethachinmate, and was resuspended in nuclease-free water.

2.4. cDNA synthesis and cloning

The RNA purified from each immunoprecipitated product derived from approximately 50 mg of adult mouse testes was used as a template for cDNA synthesis. cDNA synthesis and PCR amplification were performed using a Target mRNA Cloning Kit (Wako, Osaka, Japan) according to the manufacturer's instructions and reference (31). PCR-amplified cDNA fragments were subcloned into the pGEM-T easy vector (Promega), and sequenced using a BigDye Terminator Cycle Sequencing Kit (Life Technologies). The sequence of these cDNA clones was analyzed by BLAST searches of DDBJ (<http://blast.ddbj.ac.jp/>) and NCBI (<http://blast.ncbi.nlm.nih.gov/>), BLAT searches of UCSC (<http://genome.ucsc.edu/>) and homology searches of piRNABank (<http://pirnabank.ibab.ac.in/>).

2.5. Gel electrophoresis and Western blotting

The immunoprecipitated protein derived from approximately 25 mg of adult mouse testes was applied to SDS-PAGE using a 7.5% polyacrylamide gel followed by staining with a silver staining kit (Wako, Osaka, Japan). Western blotting was performed using anti-mouse AGO2 mouse monoclonal antibody 2D4 (1:1,000; Wako) as the primary antibody and horseradish peroxidase (HRP)-conjugated anti-mouse IgG rabbit polyclonal antibody (1:5,000; Dako) as the secondary antibody, or anti-MIWI rabbit polyclonal antibody MIWI-C (11) (1:1,000) as the primary antibody and HRP-conjugated anti-rabbit IgG goat polyclonal antibody (1:2,000; Dako) as the secondary antibody. The immunopurified RNA derived from approximately 25 mg of adult mouse testes was applied to gel electrophoresis in 0.5× Tris-borate-EDTA (TBE) buffer using a 10% polyacrylamide TBE-urea gel followed by staining with Clear Stain Ag (Nippon Gene). The PCR-amplified product of the cDNA derived from the poly(A) RNA in each immunoprecipitation product was analyzed by capillary electrophoresis with a Bioanalyzer DNA 1000 kit and a Bioanalyzer 2100 system (Agilent Technologies).

2.6. Mass spectrometric analysis

The protein bands stained with the Silver Stain MS Kit (Wako, Osaka, Japan) were excised and destained with De-staining Soln reagent in the Silver Stain MS Kit. The destained gel bands were rinsed in 50% acetonitrile/100 mM ammonium bicarbonate, dehydrated with acetonitrile and dried in a SpeedVac Concentrator (Thermo Electron). For in-gel protein digestion, Trypsin Gold, Mass Spectrometry Grade (Promega, Madison, WI, USA), was applied to each gel piece, followed by incubation in 50 µL of 10% acetonitrile/40 mM ammonium bicarbonate, overnight at 37°C. The extracted tryptic peptide solutions were dried and dissolved in 10 µL of 0.1% trifluoroacetic acid. The peptide solution was analyzed with a nano liquid chromatography (LC, UltiMate 3000, Dionex)-electrospray ionization-ion trap-mass spectrometer (ESI-IT-MS, HCTultra, Bruker Daltonics) or a matrix-assisted laser desorption/ionization time-of-flight mass spectrometer (MALDI-TOF-MS, AXIMA-CFR Plus, Shimadzu/Kratos Analytical). The data were entered into the Peptide Mass Fingerprint or the MS/MS Ion Search in the Mascot Search (Matrix Science) for a NCBI protein database search to characterize the protein.

2.7. Microarray analysis

Total RNA (0.1 µg) and immunopurified RNA (0.1 µg) were amplified and labeled using an Amino Alkyl MessageAmp™ II aRNA Amplification Kit (Life Technologies) according to the manufacturer's instructions. The aRNA derived from the total RNA and the immunopurified RNA were labeled with Cy3 and Cy5, respectively. Each labeled aRNA (1 µg) was hybridized to a 3D-Gene® Mouse Oligo chip 25k (Toray Industries Inc.) at 37°C for 16 h and the DNA chip was washed and dried according to the manufacturer's protocols. The fluorescence intensities of each probe were detected using a ScanArray scanner (PerkinElmer). The tiff image was analyzed using GenePix Pro® 6.0 (MDS Analytical Technologies). The data were filtered to remove low-confidence measurements, and were normalized by subtraction with the mean intensity of the background signal determined by the 95% confidence intervals of all the blank spots' signal intensities. The raw data intensities greater than two standard deviations from the background signal intensity were considered valid. Detected signals for each gene were normalized using the global normalization method according to the manufacturer's instructions. The data are MIAME compliant and the raw data have been deposited into the GEO database (Accession number: GSE27582). The pathway analysis of mRNAs that were enriched in the MIWI-IP products and the AGO2-IP products was performed using GenMAPP pathway profiler (<http://www.genmapp.org/>).

2.8. Quantitative PCR

The whole sample of immunopurified RNA derived from approximately 50 mg of adult mouse testes, and 1 µg of total RNA derived from mouse testes samples were used as templates for reverse transcription, which was performed with a SuperScript VILO cDNA Synthesis Kit (Life Technologies) according to the manufacturer's instructions. Eight-fold and 40-fold diluted reverse transcription products derived from the immunopurified RNA and the total RNA, respectively, were used as a template for quantitative PCR, which was performed with gene-specific primer pairs and 2× Power SYBR Master Mix (Life Technologies) on an ABI 7500 real-time PCR system (Life Technologies) according to the manufacturer's instructions. The sequences of the primers are described in Table S1.

2.9. Northern blotting

Six micrograms of total RNA purified from each testes sample were separated on a 12% denaturing polyacrylamide gel and blotted onto a nylon membrane (Biodyne plus; Pall Corporation). The blots were prehybridized in hybridization buffer (50% formamide, 5× saline-sodium citrate (SSC), 2% blocking solution, 0.1% N-lauroyl sarcosine, 0.1% SDS, 200 µg/mL yeast tRNA) for 1 h at 60°C. LNA-modified DNA probes labeled with digoxigenin at the 5' end were added to the hybridization buffer and incubated with the blots overnight at 60°C. The nucleotide sequences of the LNA probes were for piR-108116, 5'-TAGGCGACTAAGTG TGTTGTGCAAAATGTA-3' and for U6 snRNA, 5'-ATCGTTCCAATTTTGTATATGTGCTGCCG-3'. The concentrations of the probe used for piR-108116 and U6 snRNA were 0.1 nM and 0.05 nM, respectively. After hybridization, the blots were washed twice with 2× SSC containing 0.1% SDS and once with 1× SSC containing 0.1% SDS at room temperature for 15 min each, and with 0.2× SSC containing 0.1% SDS and 0.1× SSC containing 0.1% SDS at 65°C for 30 min each. After a brief wash with maleic acid buffer (0.15 M NaCl, 0.1 M maleic acid, pH 7.5), the blots were incubated in 1% blocking reagent (Roche) in maleic acid buffer for 30 min, washed twice in maleic acid buffer containing 0.3% Tween 20, washed briefly in AP buffer (0.1 M NaCl, 0.1 M Tris-HCl, pH 9.5), incubated with CSPD-star chemiluminescent substrate (Roche) and finally the luminescent signal was detected with an ImageQuant LAS4000 mini image analyzer (GE Healthcare).

3. Results

3.1. Isolation of MIWI complexes by immunoprecipitation

To isolate MIWI complexes by immunoprecipitation, we produced an anti-HIWI/MIWI monoclonal antibody

(2C12). As an antigen, we used a HIWI N-terminal region peptide with high homology to MIWI and low homology to other PIWI subfamily proteins, and this region is outside of the PAZ domain that serves as binding site for small RNA (Figures S1A and S1B). To isolate AGO2 complexes to compare with MIWI complexes, we also produced an anti-mouse AGO2 monoclonal antibody (3E7) in a similar manner using a mouse AGO2 N-terminal region peptide whose sequence showed low homology to other AGO subfamily proteins, and this region is also outside of the PAZ domain (Figures S2A and S2B). Using these antibodies, we performed immunoprecipitation experiments with adult mouse testes. Western blotting with anti-MIWI rabbit polyclonal antibody (MIWI-C) and anti-mouse AGO2 mouse monoclonal antibody (2D4) showed that 2C12 and 3E7 immunoprecipitated MIWI and AGO2, respectively (Figure 1A). Mass spectrometric analysis showed multiple protein bands except for the AGO2-band detected in anti-AGO2-immunoprecipitated (AGO2-IP) products containing HSPA2 (heat shock protein 2) that is a family protein of heat shock protein 70 reported to associate with human AGO2 (32). However, the other co-precipitated proteins are unknown to associate with AGO2 (data not shown), and it is possible that these proteins were bound to 3E7 or AGO2 non-specifically. Two protein bands detected at around 90 to 100 kDa in anti-MIWI-immunoprecipitated (MIWI-IP) products by silver staining (Figure 1A) were identified as TUBGCP2 (tublin, gamma complex associated protein 2) (asterisk) and MIWI (double asterisks) by mass spectrometric analysis. Moreover, the other protein bands detected at around 70 kDa and 200 kDa in the MIWI-IP products were identified as HSPA2 and a hypothetical protein LOC230393, respectively (data not shown). Since the interaction of MIWI with TUBGCP2 was observed in transiently expressed HEK293T cells and in adult mouse testes (Figures S3A and S3B), MIWI is considered to specifically interact with TUBGCP2. When we substituted Empigen BB, a strong zwitterionic detergent, for immunoprecipitation in place of NP-40, silver staining detected a major protein band of MIWI and a minor protein band of HSPA2 considered as a chaperone protein, (Figure S4). These results showed that 2C12 specifically binds to MIWI.

Using denaturing polyacrylamide gel electrophoresis, we detected small RNAs of approximately 30 nucleotides in length in the MIWI-IP products, which corresponded to piRNAs. In contrast, we detected small RNAs of approximately 22 nucleotides in length, which corresponded to miRNAs, in AGO2-IP products (Figure 1B). We cloned the small RNAs in the MIWI-IP products and characterized 93 clones in detail. Twenty-five percent of these small RNAs showed no homology to known piRNAs but matched perfectly to genomic sequences while 72%

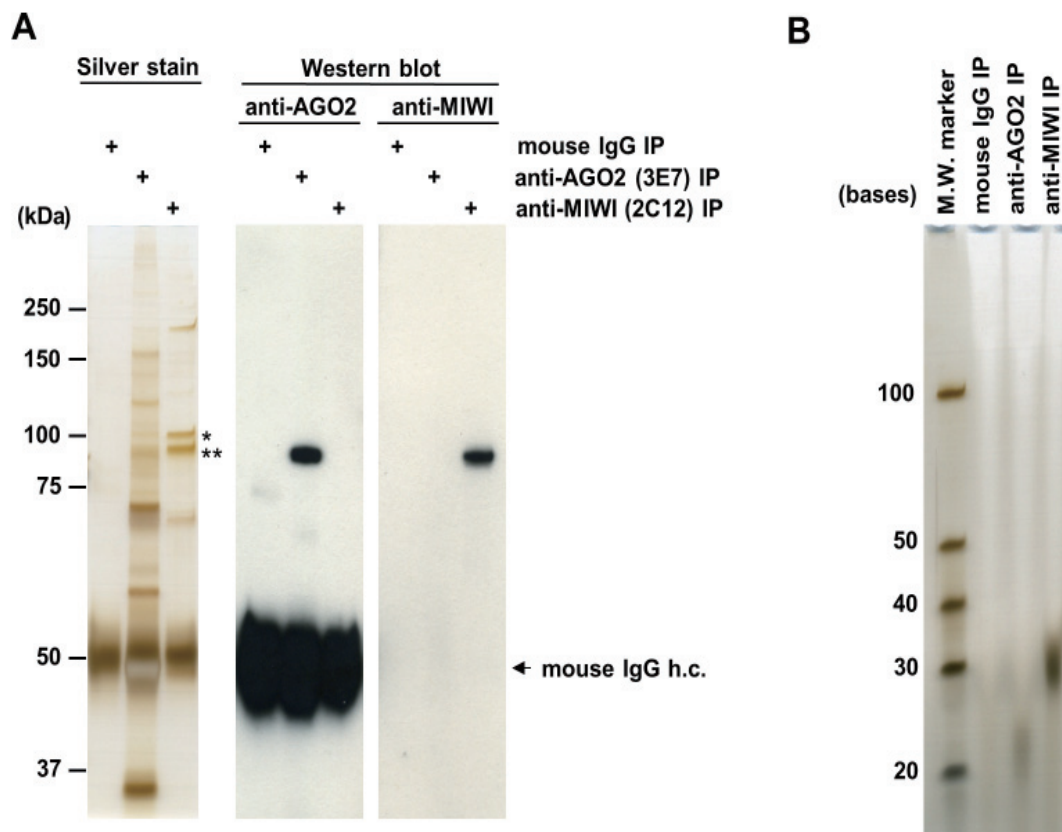


Figure 1. Isolation of the MIWI complex by immunoprecipitation. (A) Silver staining and Western blotting of immunoprecipitated (IP) proteins. The proteins immunoprecipitated from adult mouse testes using an anti-mouse AGO2 monoclonal antibody (3E7) or an anti-MIWI monoclonal antibody (2C12) were analyzed by SDS-polyacrylamide gel electrophoresis followed by silver staining (left panel), and Western blotting using an anti-mouse AGO2 mouse monoclonal antibody (2D4) (central panel) and an anti-MIWI rabbit polyclonal antibody (MIWI-C) (right panel). Immunoprecipitation with non-specific mouse IgG was performed as a negative control. Two silver stained protein bands of nearly 100 kDa in anti-MIWI-immunoprecipitated (MIWI-IP) products (left panel) were identified as TUBGCP2 (tublin, gamma complex associated protein 2) (asterisk) and MIWI (double asterisks) by mass spectrometric analysis. Silver stained protein bands of approximately 50 kDa (left panel) corresponded to the heavy chain (h.c.) of mouse IgG, which was detected by Western blotting using a HRP-conjugated anti-mouse IgG rabbit polyclonal antibody as the secondary antibody (central panel), but was not detected by Western blotting using a HRP-conjugated anti-rabbit IgG goat polyclonal antibody as the secondary antibody (right panel). (B) Silver staining of immunoprecipitated small RNAs. The small RNAs immunoprecipitated from adult mouse testes using 3E7 and 2C12 were analyzed by denaturing polyacrylamide gel electrophoresis followed by silver staining. Immunoprecipitation with non-specific mouse IgG was performed as a negative control. M.W., molecular weight.

showed substantial homology to known piRNAs (Figure S5A). The average length of the 93 clones was 30.1 ± 1.4 nucleotides, which corresponds to pachytene piRNAs (6,7), and only approximately 10% of these clones showed substantial homology to retrotransposon sequences in contrast to the fetal piRNAs and pre-pachytene piRNAs that include many sequences derived from retrotransposons (12,13,15,16). In the primary processing pathway of piRNA biogenesis, single-stranded piRNA precursor transcripts generate a diverse set of piRNA sequences that share a preference for uridine at the 5' end (1st U) (5,6). On the other hand, secondary piRNAs generated by the ping-pong amplification cycle have a strong preference for adenine at position 10 (10th A) (13,33,34). In this study approximately 80% of the 93 clones had a 1st U (Figure S5B), indicating that these clones encode piRNAs generated by the primary processing pathway. These results suggest that MIWI-associated

small RNAs isolated from mouse adult testes by immunoprecipitation with 2C12 are pachytene piRNAs.

3.2. Isolation of poly(A) RNAs contained in the MIWI-IP products

We previously established a cDNA cloning method utilizing an adaptor ligation to identify poly(A) RNA in immunoprecipitated products, and succeeded in identifying target mRNA candidates of miRNAs in the AGO2-IP products of HeLa cells and HepG2 cells (31). In order to examine whether poly(A) RNAs are contained in the MIWI-IP and AGO2-IP products of adult mouse testes, we performed cDNA cloning of poly(A) RNAs in both products using the same method. We detected PCR amplification products in both IPs but did not detect any amplification from the control non-specific mouse IgG-immunoprecipitated (mouse IgG-IP) products (Figure 2A). Therefore, poly(A) RNAs

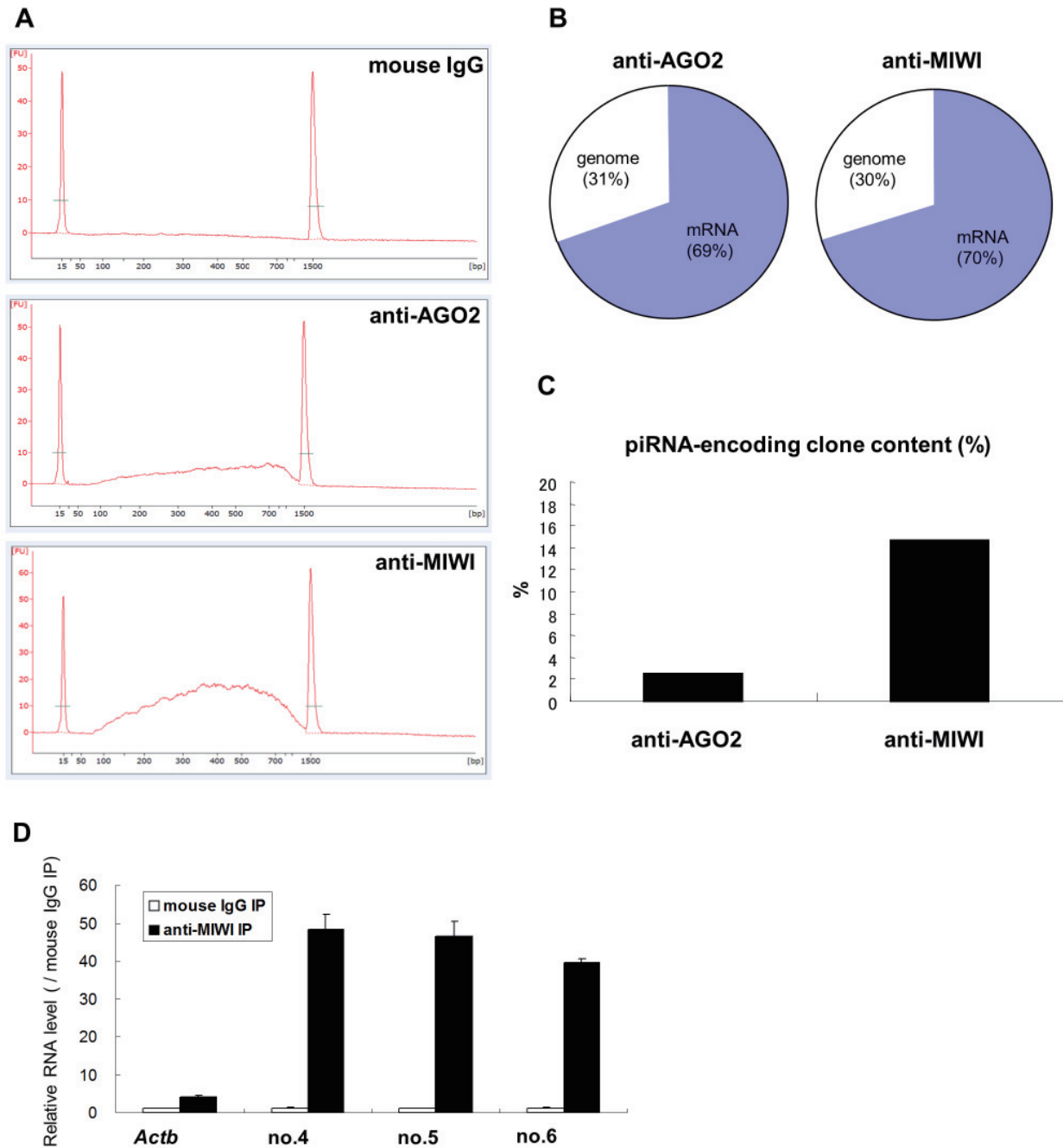


Figure 2. cDNA cloning of poly(A) RNAs contained in the MIWI-IP products. (A) Electropherograms of PCR-amplified cDNA products derived from IP poly(A) RNAs. The PCR products of cDNA derived from poly(A) RNAs that were immunoprecipitated from adult mouse testes with 3E7 and 2C12 were analyzed by capillary electrophoresis. The peaks at 15 bp and 1,500 bp correspond to the lower and upper markers, respectively. Immunoprecipitation with non-specific mouse IgG was performed as a negative control. (B) Composition of 278 cDNA clones derived from AGO2-IP poly(A) RNAs and 280 cDNA clones derived from MIWI-IP poly(A) RNAs. All cDNA clones were categorized as clones that matched mRNAs ("mRNA") or clones that showed no homology to known mRNAs but matched perfectly to the genomic sequence ("genome"). (C) Proportion of piRNA-encoding clones among the "genome" clones derived from AGO2-IP poly(A) RNAs and MIWI-IP poly(A) RNAs. (D) Enrichment levels of piRNA-encoding RNAs in the MIWI-IP products. The RNA levels of three piRNA-encoding RNAs (clone Nos. 4, 5 and 6) and *Actb* mRNA in mouse IgG-IP RNA and MIWI-IP RNA isolated from adult testes were analyzed by quantitative PCR and normalized to those of *Gapdh*. The normalized levels in MIWI-IP RNA were compared with those in mouse IgG-IP RNA.

were present in the MIWI-IP products as well as in the AGO2-IP products. We analyzed the sequence of 280 cDNA clones obtained from the MIWI-IP products and the 278 cDNA clones obtained from the AGO2-IP products. In both sets of IP products, approximately

70% of cDNA clones showed substantial homology to known mRNAs and the remainder showed no homology to known mRNAs, but matched perfectly to the genomic sequence (Figure 2B). These results indicated that mRNAs and non-coding poly(A) RNAs

are included in the MIWI complex as well as in the AGO2 complex.

3.3. MIWI associates with piRNA-encoding RNAs

We then focused on the cDNA clones that showed no homology to known mRNAs but matched perfectly to the genomic sequence. Since pachytene piRNAs associated with MIWI are exclusively produced by the primary processing pathway, we assumed that the piRNA precursor transcripts would be present in the MIWI-IP products and investigated by homology searching of databases whether the unknown non-coding clones represented piRNA-encoding sequences. We found that approximately 15% of the unknown non-coding clones derived from the MIWI-IP products represented piRNA-encoding sequences, whereas only approximately 2% of those derived from the AGO2-IP products did (Figure 2C). There were eight clones that encoded a single piRNA and four clones that encoded multiple piRNAs (Table 1). Clone Nos. 4 and 6 matched to the genomic sequence of the same piRNA cluster region on chromosome 7, and clone No. 5 matched to another piRNA cluster region on chromosome 7. We considered that these three piRNA-encoding clones might encode piRNA precursors transcribed from a piRNA cluster. These three piRNA-encoding RNAs were highly enriched in the MIWI-IP products compared to housekeeping *Actb* mRNA (Figure 2D). We cloned the 5' terminal region of clone No. 5 using rapid amplification of cDNA ends (RACE) and identified a 322 bp 5' terminal region. We identified 72 piRNA species within the 540 bp length of clone No. 5 and the 5' terminal nucleotide of 92% of the 72 piRNAs was uridine (data not shown). These results suggest that clone No. 5 is a pachytene piRNA precursor transcribed from the piRNA cluster region or an intermediate of a piRNA precursor generated by additional processing.

3.4. A piRNA-encoding RNA associated with MIWI is a pachytene piRNA precursor

We investigated the expression pattern of three piRNA-

encoding RNAs (clone Nos. 4, 5 and 6) derived from chromosome 7 during spermatogenesis. In the mouse testis, pachytene spermatocytes are first found at 14 days postpartum (dpp) and the percentage of pachytene spermatocytes is highest at 18-20 dpp (35). The expression level of these three piRNA-encoding RNAs in mouse testes at 12-24 dpp was compared with the levels of *Miwi* and three known pachytene markers (*Ccna1* (36), *Dmrta2* (37) and *Ovov1* (38)), and *Actb* mRNAs. The expression levels of the piRNA-encoding RNAs tended to increase from 12-20 dpp, similarly to those of *Miwi* and the pachytene marker mRNAs, whereas that of *Actb* mRNA were constant (Figure 3A). Furthermore, Northern blotting analysis showed that one of the piRNAs specifically encoded in clone No. 5, piR-108166, also increased from 12-20 dpp (Figure 3B). These results indicate that piRNA-encoding RNAs enriched in the MIWI-IP products are pachytene piRNA precursors or intermediates of such.

To clarify whether MIWI participates in piR-108166 biogenesis, we compared the RNA levels of the piRNA-encoding clone No. 5 and piR-108166 in *Miwi*^{+/+} and *Miwi*^{-/-} testes at 24 dpp. The RNA level of piR-108166 was undetectable in *Miwi*^{-/-} testes (Figure 3C). In contrast, the RNA level of clone No. 5 did not show such a reduction in *Miwi*^{-/-} testes (Figure 3D). These results suggest that MIWI is essential for biogenesis of pachytene piRNA and is involved in processing of precursor RNA.

3.5. MIWI associates with mRNAs whose expression levels are increased in pachytene spermatocytes

Next, we analyzed the protein-encoding mRNAs present in the AGO2-IP products and the MIWI-IP products comprehensively, by microarray analysis. We identified mRNAs enriched in the IP products by examining the ratio of the signal intensity in AGO2-IP RNA or MIWI-IP RNA to total RNA signal intensity. Based on an IP RNA/total RNA signal ratio ≥ 2.0 , we selected 1,644 and 1,739 mRNAs that were enriched in the AGO2-IP and MIWI-IP products respectively, for further analysis (Figure 4A). Many different mRNAs

Table 1. piRNA-encoding clones in the "genome" (non-mRNA-matching) clones derived from the MIWI-IP products

Clone No.	cDNA length	Chromosome (strand)	Number of encoded piRNA	piRNA cluster region
1	158 base	ch.1 (+)	1	Not hit
2	334 base	ch.2 (+)	1	Not hit
3	189 base	ch.6 (+)	2	Not hit
4	183 base	ch.7 (-)	4	Hit
5	218 base	ch.7 (+)	23	Hit
6	378 base	ch.7 (+)	1	Hit
7	273 base	ch.8 (-)	1	Not hit
8	273 base	ch.8 (-)	1	Not hit
9	480 base	ch.9 (-)	1	Not hit
10	271 base	ch.10 (-)	1	Not hit
11	394 base	ch.14 (-)	1	Not hit
12	61 base	ch.15 (-)	3	Not hit

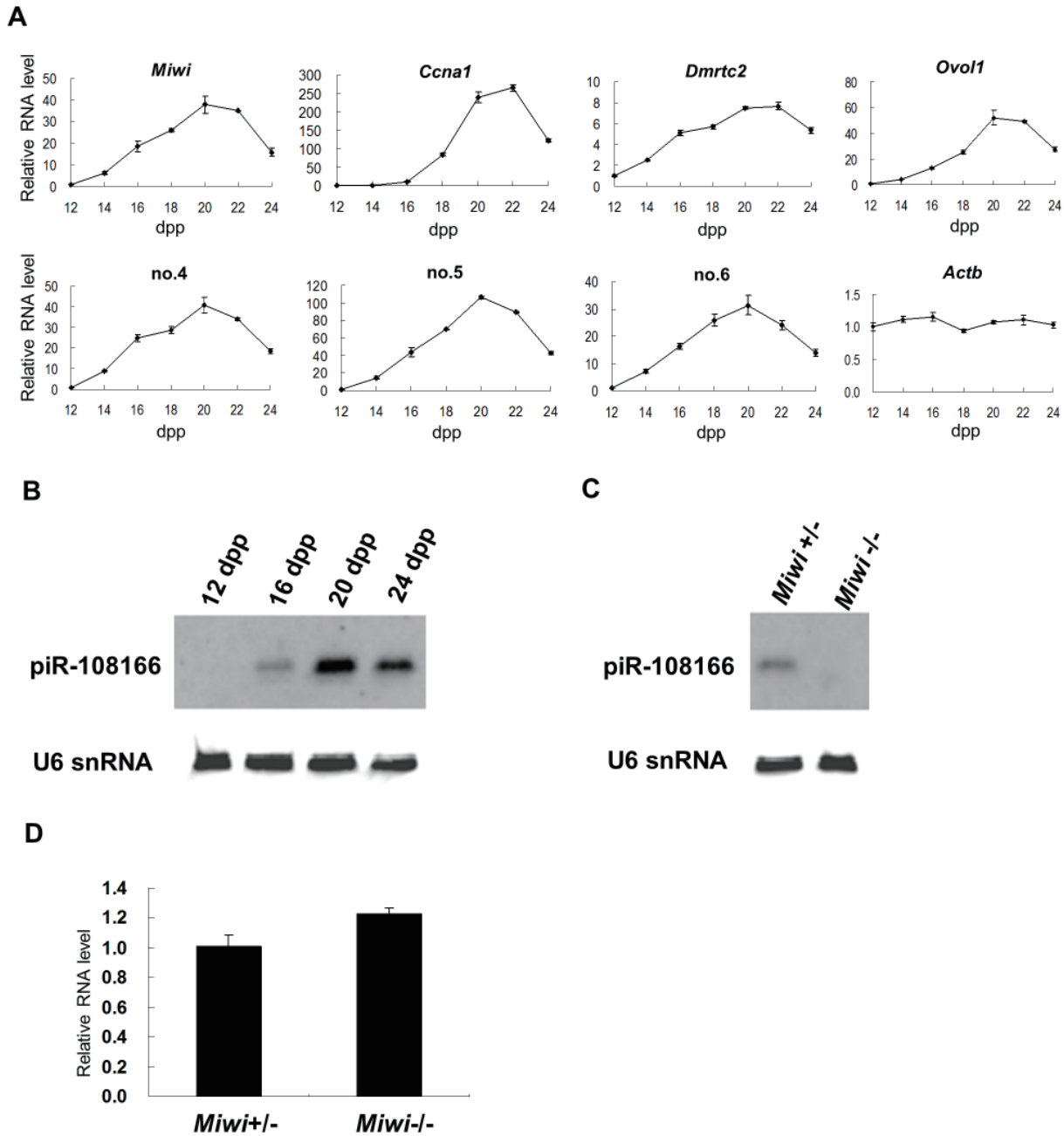


Figure 3. Expression analysis of piRNA-encoding RNAs contained in the MIWI-IP products. (A) Expression pattern of several piRNA-encoding RNAs contained in the MIWI-IP products during spermatogenesis. The expression levels of three piRNA-encoding RNAs (clone Nos. 4, 5 and 6) derived from chromosome 7, *Miwi* mRNA, three known pachytene marker mRNAs (*Ccna1*, *Dmrtc2*, *Ovol1*), and *Actb* mRNA in mouse testes at 12 to 24 days postpartum (dpp) were analyzed by quantitative PCR and normalized to those of *Gapdh*. The normalized levels were compared with those at 12 dpp. **(B)** Expression levels analyzed by Northern blotting of piR-108116, which was specifically encoded in piRNA-encoding RNA clone no. 5 during spermatogenesis in mouse testes at 12 to 24 dpp. **(C)** Comparison of RNA level of piR-108116 in *Miwi*^{+/-} and *Miwi*^{-/-} testes at 24 dpp by Northern blotting. **(D)** Comparison of the RNA levels of the piRNA-encoding RNA clone No. 5 in *Miwi*^{+/-} and *Miwi*^{-/-} testes at 24 dpp. The expression level of the piRNA-encoding RNA clone no. 5 was analyzed by quantitative PCR and normalized to that of *Gapdh*. The normalized level in *Miwi*^{-/-} testes was compared to that in *Miwi*^{+/-} testes.

were enriched in each group (Figure 4B). We selected the top ten mRNAs that were highly and specifically enriched in the AGO2-IP products (AGO2-IP/total RNA signal ratio ≥ 2.0 and MIWI-IP/total RNA signal ratio < 1.5) and MIWI-IP products (MIWI-IP/total RNA signal ratio ≥ 2.0 and AGO2-IP/total RNA signal ratio < 1.5), and investigated the expression level of these mRNAs in mouse testes at 12-24 dpp. We found

that the mRNAs highly and specifically enriched in the MIWI-IP products were present at a higher level at 20 dpp compared to at 12 dpp (Table 2). However, the mRNAs highly and specifically enriched in the AGO2-IP products remained at nearly the same level. This result indicates that MIWI specifically associates with many mRNAs whose expression levels are increased in pachytene spermatocytes.

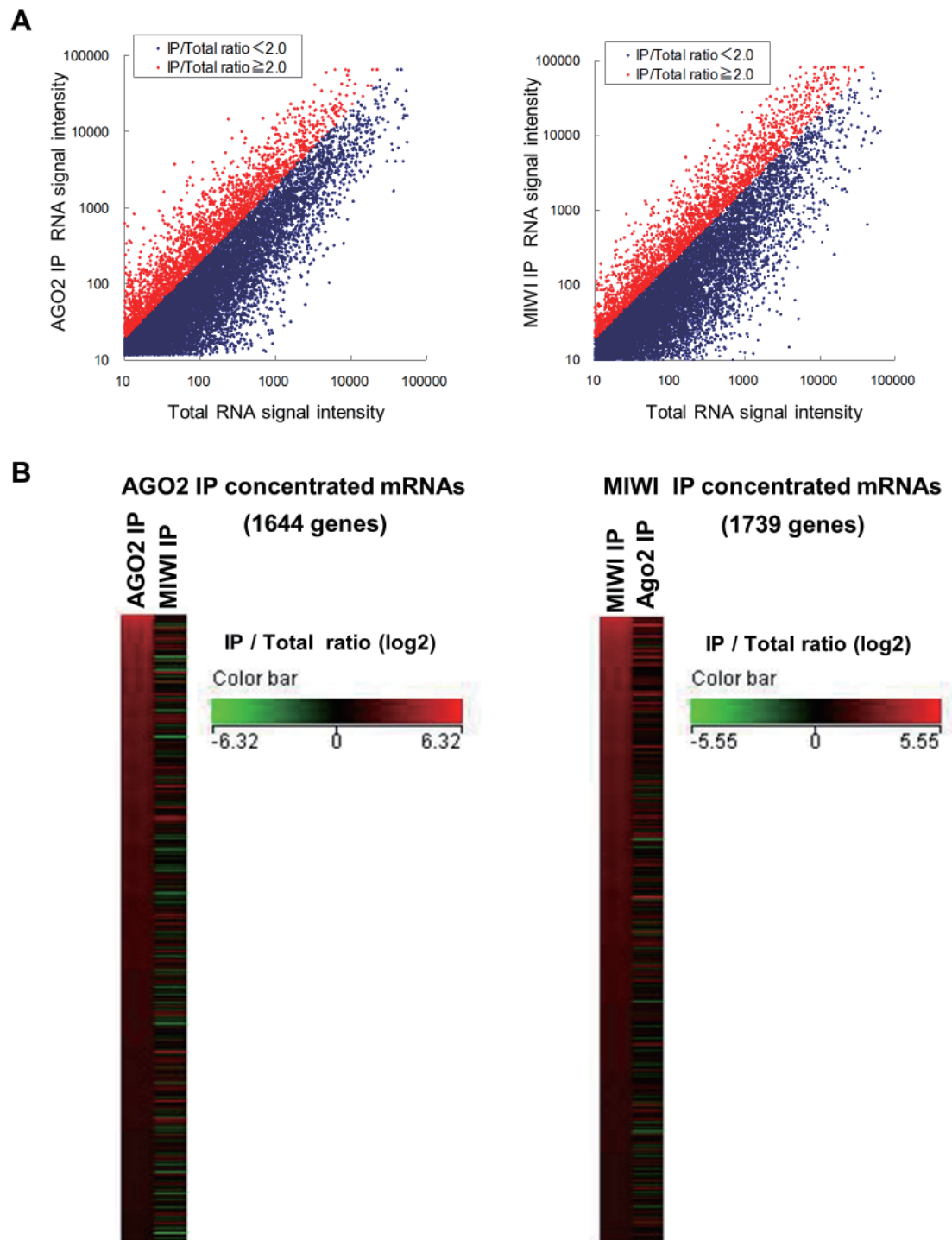


Figure 4. Microarray analysis of mRNAs contained in the MIWI complex. (A) Scatter plot of signal intensity (\log_{10}) between AGO2-IP RNA and total RNA (left) and between MIWI-IP RNA and total RNA (right). Total RNA, AGO2-IP RNA and MIWI-IP RNA were isolated from adult testes. Total RNA labeled with Cy3 and AGO2-IP RNA or MIWI-IP RNA labeled with Cy5 were hybridized onto a 3D-Gene[®] Mouse Oligo chip 25k. The signals for which the IP RNA/total RNA signal ratio was \geq 2.0 are shown in red, and those for signal ratio < 2.0 are shown in blue. (B) Heat map of the ratio of signal intensities of AGO2-IP RNA to total RNA and MIWI-IP RNA to total RNA. We selected 1644 (left) and 1739 (right) mRNAs as enriched mRNA in the AGO2-IP products and the MIWI-IP products, respectively, based on the signal ratio of the IP RNA to total RNA \geq 2.0, and compared the ratio (\log_2) of signal intensities of AGO2-IP RNA to total RNA and MIWI-IP RNA to total RNA.

Interestingly, we found that *Aym1* mRNA, encoding not only a protein but also several piRNAs, was included among the mRNAs highly and specifically enriched in the MIWI-IP products (Figure S6). One of the piRNAs specifically encoded in *Aym1* mRNA,

piR-18928, was generated in the testes and its expression level increased from 12-20 dpp, similarly to *Aym1* mRNA (Figures S7A and S7B). AYM1 protein has been reported to be expressed in pachytene spermatocytes (39). In pachytene spermatocytes, the

Table 2. Expression analysis of mRNAs highly and specifically enriched in the MIWI-IP products during spermatogenesis

Category	Gene symbol	Microarray signal ratio		Relative mRNA level (20 dpp/12 dpp)
		AGO2-IP/Total	MIWI-IP/Total	
AGO2-IP	<i>Gca</i>	26.8	0.1	0.2
	<i>Rgs2</i>	21.7	0.2	0.6
	<i>Cmpk</i>	20.1	0.5	1.1
	<i>Btg3</i>	17.7	0.2	1.2
	<i>Reep1</i>	15.7	0.2	1.2
	<i>Cdc42se2</i>	14.9	0.2	1.0
	<i>8430410K20Rik</i>	14.2	0.3	1.3
	<i>Myadm</i>	13.1	0.8	0.8
	<i>Rnf11</i>	12.3	0.3	1.1
	<i>Mex3c</i>	12.3	1.1	1.1
	Mean	16.9	0.4	1.0
MIWI-IP	<i>Dynlrb2</i>	1.2	22.5	61.9
	<i>Aym1</i>	0.4	19.6	39.8
	<i>Mrps18c</i>	1.1	18.8	3.1
	<i>Chchd1</i>	1.3	17.6	3.8
	<i>Bcmo1</i>	0.5	16.4	13.3
	<i>H2-DMb2</i>	1.3	15.8	1.9
	<i>Ddt</i>	0.9	15.5	9.1
	<i>Wfdc15</i>	1.4	14.7	14.8
	<i>Rpp21</i>	1.2	11.8	8.9
	<i>Cdk5rap1</i>	0.9	11.3	2.5
	Mean	1.0	16.4	15.9

The expression levels of the top ten mRNAs each, highly and specifically enriched in the AGO2-IP and MIWI-IP products, were analyzed by quantitative PCR in mouse testes at 12 and 20 dpp, and normalized to those of Gapdh. The normalized levels at 20 dpp were compared with those at 12 dpp, days postpartum.

Table 3. Pathway analysis of mRNAs enriched in the MIWI-IP products

Category	MAPP name	# measured	# on MAPP	% changed	% present	Z score
AGO2-IP	mRNA_processing_binding_Reactome	378	551	19	69	4.0
	Methionine_metabolism	6	26	50	23	2.8
	Circadian_Exercise	42	49	26	86	2.7
	Electron_Transport_Chain	63	83	22	76	2.3
	2_4_Dichlorobenzoate_degradation	4	32	50	13	2.3
	RNA_transcription_Reactome	38	41	24	93	2.1
MIWI-IP	Electron_Transport_Chain	63	83	51	76	10.2
	Ribosomal_Proteins	49	80	35	61	5.4
	mRNA_processing_binding_Reactome	378	551	16	69	3.1
	RNA_transcription_Reactome	38	41	26	93	3.1
	Hedgehog_Netpath_10	21	21	29	100	2.6
	Small_ligand_GPCRs	19	19	26	100	2.2
	Biotin_metabolism	5	13	40	38	2.1

1,644 and 1,739 mRNAs were selected as enriched mRNA in the AGO2-IP and MIWI-IP products, respectively, based on the signal ratio of the IP RNA to total RNA ≥ 2.0 by microarray expression analysis. These mRNAs were applied to the GenMAPP pathway profiler. The pathways for which the Z score was above 2.0 are listed in the table. From the left-hand side the columns indicate: category; the name of the pathway (MAPP name); the number of mRNAs for which the IP RNA/total RNA signal ratio was ≥ 2.0 (# changed); the number of mRNAs used for the analysis (# measured); the number of mRNAs in the pathway (# on MAPP); the percentage of the number changed per the number measured (% changed); the percentage of the number measured per the number on MAPP (% present); and the Z-score.

Aym1 mRNA appears to generate both the AYM1 protein and the piRNA. Furthermore, piR-18928 was undetectable in *Miwi*^{-/-} testes, whereas *Aym1* mRNA did not show such a reduction in *Miwi*^{-/-} testes (Figures S7C and S7D). These results suggest that MIWI is also involved in pachytene piRNA biogenesis from mRNA-type piRNA precursor.

In addition, mRNAs encoding electron transport

chain, ribosomal and mitochondrial ribosomal proteins were present specifically in the MIWI-IP products (Table 3). This result indicates that MIWI associates with many mRNAs encoding mitochondrial proteins. Since the expression levels of these mRNAs at 20 dpp were higher than that at 12 dpp (Table S2), the expression level of these mRNAs also tends to increase in pachytene spermatocytes.

Table 4. Expression analysis of mRNAs highly and specifically enriched in the MIWI-IP products in Miwi-deficient testes

Category	Gene symbol	Relative mRNA level (<i>Miwi</i> ^{-/-} / <i>Miwi</i> ^{+/-})		
		20 dpp	22 dpp	24 dpp
AGO2-IP	<i>Gca</i>	1.10	1.17	0.97
	<i>Rgs2</i>	1.25	1.08	1.17
	<i>Cmpk</i>	1.00	1.05	1.18
	<i>Btg3</i>	0.95	0.99	1.15
	<i>Reep1</i>	0.92	1.02	0.90
	<i>Cdc42se2</i>	0.95	0.96	0.98
	<i>8430410K20Rik</i>	0.93	1.08	1.08
	<i>Myadm</i>	1.08	0.81	0.96
	<i>Rnf11</i>	0.91	0.95	1.03
	<i>Mex3c</i>	0.95	0.95	0.82
	Mean	1.01	1.01	1.02
MIWI-IP	<i>Dynlrb2</i>	0.64	0.96	1.15
	<i>Aym1</i>	0.82	1.13	1.37
	<i>Mrps18c</i>	0.88	1.04	1.14
	<i>Chchd1</i>	0.72	1.02	1.16
	<i>Bcmo1</i>	0.51	0.82	0.64
	<i>H2-DMb2</i>	0.68	1.16	1.00
	<i>Ddt</i>	0.62	0.89	1.02
	<i>Wfdc15</i>	0.67	0.85	0.97
	<i>Rpp21</i>	0.74	0.87	1.04
	<i>Cdk5rap1</i>	0.75	0.85	0.97
	Mean	0.70	0.96	1.05

The expression levels of ten mRNAs each, highly and specifically enriched in the AGO2-IP products and the MIWI-IP products, were analyzed by quantitative PCR in *Miwi*^{+/-} and *Miwi*^{-/-} testes at 20, 22 and 24 dpp, and normalized to those of Gapdh. The normalized levels in *Miwi*^{-/-} testes were compared with those in *Miwi*^{+/-} testes. dpp, days postpartum.

3.6. Expression of mRNAs enriched in the MIWI-IP products is decreased in *Miwi*-deficient testes

We compared the expression levels of the top ten mRNAs that were highly and specifically enriched in the AGO2-IP and MIWI-IP products in *Miwi*^{+/-} and *Miwi*^{-/-} mice testes at 20, 22, and 24 dpp. mRNAs enriched in the MIWI-IP products were decreased by 20-30% in 20 dpp *Miwi*^{-/-} testes, although these mRNAs did not show a significant reduction in RNA levels at 22 or 24 dpp (Table 4). In contrast, mRNAs enriched in the AGO2-IP products did not show such a reduction in *Miwi*^{-/-} testes. We also performed a similar analysis of mRNAs encoding electron transport chain and ribosomal proteins enriched in MIWI-IP products, and these mRNA levels were decreased by approximately 20% in 20 dpp *Miwi*^{-/-} testes (Table S3). These results indicated that at 20 dpp, *Miwi*^{-/-} testes have reduced MIWI-associated mRNAs, specifically when pachytene spermatocytes are most abundant. We also compared the RNA and protein levels of two mRNAs highly enriched in the MIWI-IP products, *Ssnal* and *Nasp*, in *Miwi*^{+/-} and *Miwi*^{-/-} testes at 20, 22 and 24 dpp. The protein abundance ratio of these mRNAs in *Miwi*^{+/-} and *Miwi*^{-/-} testes correlated approximately with the RNA abundance ratio (Figure S8). These results suggest that MIWI is involved in stabilization of target mRNAs rather than translational regulation in pachytene spermatocytes.

4. Discussion

Since *Miwi*^{-/-} mice display spermatogenic arrest at the round spermatid stage, MIWI has been thought to play an essential role in spermiogenesis (10). Recently, analysis of *Miwi*^{-/-}/*Miwi*^{+/-} double knockout mice revealed that PIWI proteins including MIWI are required for spermatogenesis (40). However, the function of MIWI in spermatogenesis and spermiogenesis is not well understood. In this study, we investigated MIWI-associated poly(A) RNAs, and revealed that MIWI may play an important role in piRNA biogenesis and target mRNA metabolism in pachytene spermatocytes before spermiogenesis.

4.1. MIWI may be directly involved in pachytene piRNA biogenesis

The biogenesis of piRNAs is independent of Dicer in flies and zebrafish, and thus it is thought that piRNAs are generated from single-stranded RNA precursors (41,42). In mice, long precursor RNAs of piRNA-like RNAs, moderately long precursor RNAs of piRNAs and mRNA-type piRNA precursors were identified (43-46). However, it is still unclear whether MIWI is involved in processing of these precursor RNAs. In this study, we show that MIWI associates with non-coding type piRNA precursors, such as clone No. 5, and mRNA-type piRNA precursor, such as *Aym1* mRNA

(Figure 2D and Table 2). The expression level of these piRNA-encoding RNAs was increased in pachytene spermatocytes (Figures 3A and S7A), and mature piRNAs specifically encoded in these piRNA-encoding RNAs were generated in pachytene spermatocytes (Figures 3B and S7B). Moreover, *Miwi*^{-/-} testes did not generate these mature piRNAs (Figures 3C and S7C). Therefore, we conclude that these RNAs are pachytene piRNA precursors, and that MIWI may be involved in processing of these piRNA precursor RNAs. Most recently, the study of MIWI-catalytic activity mutant mice revealed that the slicer activity of MIWI is not required for piRNA biogenesis (27). Hence, not only MIWI but also other factors appear to be required for processing of pachytene piRNA precursors, and further study is required to identify these factors.

4.2. MIWI may play an important role in the positive regulation of target mRNAs in pachytene spermatocytes

In both the MIWI-IP and AGO2-IP products, approximately 70% of poly(A) RNAs encoded known mRNAs (Figure 2B). We compared the mRNA species enriched in the MIWI and AGO2 complexes by microarray analysis. Many mRNA species whose expression level was increased in pachytene spermatocytes were specifically enriched in the MIWI-IP products (Table 2). This result suggests that MIWI may target mRNAs that play important roles in pachytene spermatocytes. In particular, those mRNAs encoding mitochondrial proteins, likely electron transport chain and mitochondrial ribosomal proteins, were enriched in the MIWI-IP products (Table 3). Previous reports show that mitochondrial function is essential for meiosis in yeast and mouse testes (47,48). Furthermore, the mitochondrial membrane protein MITOPLD is essential for nuage formation and piRNA biogenesis, indicating that mitochondrial function is closely related to piRNA biogenesis (49,50). The possibility that MIWI targets a large number of mRNA species encoding mitochondrial proteins provides new insight into MIWI function.

Finally, we investigated the possibility that MIWI is involved in post-transcriptional regulation of target mRNAs. We compared the RNA level of mRNAs enriched in the MIWI-IP products in *Miwi*^{+/-} and *Miwi*^{-/-} testes. These mRNAs were decreased by 20-30% in 20 dpp *Miwi*^{-/-} testes, but did not show any significant reduction at 22 or 24 dpp (Table 4 and S3). Pachytene spermatocytes have high levels of MIWI-associated mRNAs. Therefore, the reduction of MIWI-associated mRNAs in *Miwi*^{-/-} testes at 20 dpp, when pachytene spermatocytes are most abundant, suggests that MIWI is involved in mRNA stabilization in these cells. There remains a possibility that delayed differentiation of pachytene spermatocytes could lead to a significant reduction in RNA levels in 20 dpp *Miwi*^{-/-} testes. Hence,

further study is required to compare mRNA levels in pachytene spermatocytes isolated from *Miwi*^{+/-} and *Miwi*^{-/-} testes. Furthermore, in this study we could not clarify whether piRNAs mediate MIWI binding to its target mRNA. Future studies are also needed to elucidate whether MIWI associates with mRNAs in a piRNA mediated manner.

Acknowledgements

We thank Dr. H. Lin (Yale University) for providing *Miwi* knockout mice, and Hideo Akiyama and Satoshi Kondo (Toray Industries, Inc.) for supporting the microarray analysis. We also thank Takahisa Kobayashi for supporting production of monoclonal antibodies, and Masaki Warashina, Makoto Amano, Taku Funakoshi, and Hitoshi Uemori for valuable discussions and advice.

References

1. Sasaki T, Shiohama A, Minoshima S, Shimizu N. Identification of eight members of the Argonaute family in the human genome small star, filled. *Genomics*. 2003; 82:323-330.
2. Liu J, Carmell MA, Rivas FV, Marsden CG, Thomson JM, Song JJ, Hammond SM, Joshua-Tor L, Hannon GJ. Argonaute2 is the catalytic engine of mammalian RNAi. *Science*. 2004; 305:1437-1441.
3. Meister G, Landthaler M, Patkaniowska A, Dorsett Y, Teng G, Tuschl T. Human Argonaute2 mediates RNA cleavage targeted by miRNAs and siRNAs. *Mol Cell*. 2004; 15:185-197.
4. Pillai RS, Artus CG, Filipowicz W. Tethering of human Ago proteins to mRNA mimics the miRNA-mediated repression of protein synthesis. *RNA*. 2004; 10:1518-1525.
5. Aravin A, Gaidatzis D, Pfeffer S, *et al.* A novel class of small RNAs bind to MILI protein in mouse testes. *Nature*. 2006; 442:203-207.
6. Girard A, Sachidanandam R, Hannon GJ, Carmell MA. A germline-specific class of small RNAs binds mammalian Piwi proteins. *Nature*. 2006; 442:199-202.
7. Grivna ST, Beyret E, Wang Z, Lin H. A novel class of small RNAs in mouse spermatogenic cells. *Genes Dev*. 2006; 20:1709-1714.
8. Lau NC, Seto AG, Kim J, Kuramochi-Miyagawa S, Nakano T, Bartel DP, Kingston RE. Characterization of the piRNA complex from rat testes. *Science*. 2006; 313:363-367.
9. Watanabe T, Takeda A, Tsukiyama T, Mise K, Okuno T, Sasaki H, Minami N, Imai H. Identification and characterization of two novel classes of small RNAs in the mouse germline: Retrotransposon-derived siRNAs in oocytes and germline small RNAs in testes. *Genes Dev*. 2006; 20:1732-1743.
10. Deng W, Lin H. *Miwi*, a murine homolog of piwi, encodes a cytoplasmic protein essential for spermatogenesis. *Dev Cell*. 2002; 2:819-830.
11. Kuramochi-Miyagawa S, Kimura T, Ijiri TW, Isobe T, Asada N, Fujita Y, Ikawa M, Iwai N, Okabe M, Deng W, Lin H, Matsuda Y, Nakano T. *Mili*, a mammalian member

- of piwi family gene, is essential for spermatogenesis. *Development*. 2004; 131:839-849.
12. Carmell MA, Girard A, van de Kant HJ, Bourc'his D, Bestor TH, de Rooij DG, Hannon GJ. MIWI2 is essential for spermatogenesis and repression of transposons in the mouse male germline. *Dev Cell*. 2007; 12:503-514.
 13. Aravin AA, Sachidanandam R, Bourc'his D, Schaefer C, Pezic D, Toth KF, Bestor T, Hannon GJ. A piRNA pathway primed by individual transposons is linked to *de novo* DNA methylation in mice. *Mol Cell*. 2008; 31:785-799.
 14. Unhavaithaya Y, Hao Y, Beyret E, Yin H, Kuramochi-Miyagawa S, Nakano T, Lin H. MILI, a PIWI-interacting RNA-binding protein, is required for germ line stem cell self-renewal and appears to positively regulate translation. *J Biol Chem*. 2009; 284:6507-6519.
 15. Kuramochi-Miyagawa S, Watanabe T, Gotoh K, *et al*. DNA methylation of retrotransposon genes is regulated by Piwi family members MILI and MIWI2 in murine fetal testes. *Genes Dev*. 2008; 22:908-917.
 16. Aravin AA, Sachidanandam R, Girard A, Fejes-Toth K, Hannon GJ. Developmentally regulated piRNA clusters implicate MILI in transposon control. *Science*. 2007; 316:744-747.
 17. Kojima K, Kuramochi-Miyagawa S, Chuma S, Tanaka T, Nakatsuji N, Kimura T, Nakano T. Associations between PIWI proteins and TDRD1/MTR-1 are critical for integrated subcellular localization in murine male germ cells. *Genes Cells*. 2009; 14:1155-1165.
 18. Reuter M, Chuma S, Tanaka T, Franz T, Stark A, Pillai RS. Loss of the Mili-interacting Tudor domain-containing protein-1 activates transposons and alters the Mili-associated small RNA profile. *Nat Struct Mol Biol*. 2009; 16:639-646.
 19. Shoji M, Tanaka T, Hosokawa M, *et al*. The TDRD9-MIWI2 complex is essential for piRNA-mediated retrotransposon silencing in the mouse male germline. *Dev Cell*. 2009; 17:775-787.
 20. Vagin VV, Wohlschlegel J, Qu J, Jonsson Z, Huang X, Chuma S, Girard A, Sachidanandam R, Hannon GJ, Aravin AA. Proteomic analysis of murine Piwi proteins reveals a role for arginine methylation in specifying interaction with Tudor family members. *Genes Dev*. 2009; 23:1749-1762.
 21. Wang J, Saxe JP, Tanaka T, Chuma S, Lin H. Mili interacts with tudor domain-containing protein 1 in regulating spermatogenesis. *Curr Biol*. 2009; 19:640-644.
 22. Frost RJ, Hamra FK, Richardson JA, Qi X, Bassel-Duby R, Olson EN. MOV10L1 is necessary for protection of spermatocytes against retrotransposons by Piwi-interacting RNAs. *Proc Natl Acad Sci U S A*. 2010; 107:11847-11852.
 23. Kuramochi-Miyagawa S, Watanabe T, Gotoh K, *et al*. MVH in piRNA processing and gene silencing of retrotransposons. *Genes Dev*. 2010; 24:887-892.
 24. Zheng K, Xiol J, Reuter M, Eckardt S, Leu NA, McLaughlin KJ, Stark A, Sachidanandam R, Pillai RS, Wang PJ. Mouse MOV10L1 associates with Piwi proteins and is an essential component of the Piwi-interacting RNA (piRNA) pathway. *Proc Natl Acad Sci U S A*. 2010; 107:11841-11846.
 25. Chi YH, Cheng LI, Myers T, Ward JM, Williams E, Su Q, Faucette L, Wang JY, Jeang KT. Requirement for Sun1 in the expression of meiotic reproductive genes and piRNA. *Development*. 2009; 136:965-973.
 26. Ma L, Buchold GM, Greenbaum MP, Roy A, Burns KH, Zhu H, Han DY, Harris RA, Coarfa C, Gunaratne PH, Yan W, Matzuk MM. GASZ is essential for male meiosis and suppression of retrotransposon expression in the male germline. *PLoS Genet*. 2009; 5:e1000635.
 27. Reuter M, Berninger P, Chuma S, Shah H, Hosokawa M, Funaya C, Antony C, Sachidanandam R, Pillai RS. Miwi catalysis is required for piRNA amplification-independent LINE1 transposon silencing. *Nature*. 2011; 480:264-267.
 28. Kotaja N, Bhattacharyya SN, Jaskiewicz L, Kimmins S, Parvinen M, Filipowicz W, Sassone-Corsi P. The chromatoid body of male germ cells: Similarity with processing bodies and presence of Dicer and microRNA pathway components. *Proc Natl Acad Sci U S A*. 2006; 103:2647-2652.
 29. Grivna ST, Pyhtila B, Lin H. MIWI associates with translational machinery and PIWI-interacting RNAs (piRNAs) in regulating spermatogenesis. *Proc Natl Acad Sci U S A*. 2006; 103:13415-13420.
 30. Hayashi K, Chuva de Sousa Lopes SM, Kaneda M, Tang F, Hajkova P, Lao K, O'Carroll D, Das PP, Tarakhovskiy A, Miska EA, Surani MA. MicroRNA biogenesis is required for mouse primordial germ cell development and spermatogenesis. *PLoS One*. 2008; 3:e1738.
 31. Hayashida Y, Nishibu T, Inoue K, Kurokawa T. A useful approach to total analysis of RISC-associated RNA. *BMC Res Notes*. 2009; 2:169.
 32. Iwasaki S, Kobayashi M, Yoda M, Sakaguchi Y, Katsuma S, Suzuki T, Tomari Y. Hsc70/Hsp90 chaperone machinery mediates ATP-dependent RISC loading of small RNA duplexes. *Mol Cell*. 2010; 39:292-299.
 33. Brennecke J, Aravin AA, Stark A, Dus M, Kellis M, Sachidanandam R, Hannon GJ. Discrete small RNA-generating loci as master regulators of transposon activity in *Drosophila*. *Cell*. 2007; 128:1089-1103.
 34. Gunawardane LS, Saito K, Nishida KM, Miyoshi K, Kawamura Y, Nagami T, Siomi H, Siomi MC. A slicer-mediated mechanism for repeat-associated siRNA 5' end formation in *Drosophila*. *Science*. 2007; 315:1587-1590.
 35. Bellve AR. Purification, culture, and fractionation of spermatogenic cells. *Methods Enzymol*. 1993; 225:84-113.
 36. Liu D, Matzuk MM, Sung WK, Guo Q, Wang P, Wolgemuth DJ. Cyclin A1 is required for meiosis in the male mouse. *Nat Genet*. 1998; 20:377-380.
 37. Kawamata M, Nishimori K. Mice deficient in *Dmrt7* show infertility with spermatogenic arrest at pachytene stage. *FEBS Lett*. 2006; 580:6442-6446.
 38. Li B, Nair M, Mackay DR, Bilanchone V, Hu M, Fallahi M, Song H, Dai Q, Cohen PE, Dai X. *Ov11* regulates meiotic pachytene progression during spermatogenesis by repressing *Id2* expression. *Development*. 2005; 132:1463-1473.
 39. Malcov M, Cesarkas K, Stelzer G, Shalom S, Dicken Y, Naor Y, Goldstein RS, Sagee S, Kassir Y, Don J. *Aym1*, a mouse meiotic gene identified by virtue of its ability to activate early meiotic genes in the yeast *Saccharomyces cerevisiae*. *Dev Biol*. 2004; 276:111-123.
 40. Beyret E, Lin H. Pinpointing the expression of piRNAs and function of the PIWI protein subfamily during spermatogenesis in the mouse. *Dev Biol*. 2011; 355:215-226.
 41. Vagin VV, Sigova A, Li C, Seitz H, Gvozdev V, Zamore

- PD. A distinct small RNA pathway silences selfish genetic elements in the germline. *Science*. 2006; 313:320-324.
42. Houwing S, Kamminga LM, Berezikov E, Cronembold D, Girard A, van den Elst H, Filippov DV, Blaser H, Raz E, Moens CB, Plasterk RH, Hannon GJ, Draper BW, Ketting RF. A role for Piwi and piRNAs in germ cell maintenance and transposon silencing in Zebrafish. *Cell*. 2007; 129:69-82.
 43. Iguchi N, Xu M, Hori T, Hecht NB. Noncoding RNAs of the mammalian testis: The meiotic transcripts Nct1 and Nct2 encode piRNAs. *Ann N Y Acad Sci*. 2007; 1120:84-94.
 44. Ro S, Park C, Song R, Nguyen D, Jin J, Sanders KM, McCarrey JR, Yan W. Cloning and expression profiling of testis-expressed piRNA-like RNAs. *RNA*. 2007; 13:1693-1702.
 45. Xu M, You Y, Hunsicker P, Hori T, Small C, Griswold MD, Hecht NB. Mice deficient for a small cluster of Piwi-interacting RNAs implicate Piwi-interacting RNAs in transposon control. *Biol Reprod*. 2008; 79:51-57.
 46. Robine N, Lau NC, Balla S, Jin Z, Okamura K, Kuramochi-Miyagawa S, Blower MD, Lai EC. A broadly conserved pathway generates 3'UTR-directed primary piRNAs. *Curr Biol*. 2009; 19:2066-2076.
 47. Nakada K, Sato A, Yoshida K, Morita T, Tanaka H, Inoue S, Yonekawa H, Hayashi J. Mitochondria-related male infertility. *Proc Natl Acad Sci U S A*. 2006; 103:15148-15153.
 48. Treinin M, Simchen G. Mitochondrial activity is required for the expression of IME1, a regulator of meiosis in yeast. *Curr Genet*. 1993; 23:223-227.
 49. Huang H, Gao Q, Peng X, Choi SY, Sarma K, Ren H, Morris AJ, Frohman MA. piRNA-associated germline nuage formation and spermatogenesis require MitoPLD profusogenic mitochondrial-surface lipid signaling. *Dev Cell*. 2011; 20:376-387.
 50. Watanabe T, Chuma S, Yamamoto Y, Kuramochi-Miyagawa S, Totoki Y, Toyoda A, Hoki Y, Fujiyama A, Shibata T, Sado T, Noce T, Nakano T, Nakatsuji N, Lin H, Sasaki H. MITOPLD is a mitochondrial protein essential for nuage formation and piRNA biogenesis in the mouse germline. *Dev Cell*. 2011; 20:364-375.
- (Received May 9, 2012; Revised August 30, 2012; Accepted September 14, 2012)

Effects of Xiaoqinglong decoction on gene expression profiles in a rat chronic obstructive pulmonary disease model

Caiqing Zhang^{1,#}, Lili Feng^{2,#}, Ming Li^{3,*}, Chongjuan Dong⁴, Wei Zhang^{5,*}

¹ Department of Respiratory Medicine, Qianfoshan Hospital Affiliated to Shandong University, Ji'nan, China;

² Department of Hematology, Provincial Hospital Affiliated to Shandong University, Ji'nan, China;

³ Department of Rheumatology and Clinical Immunology, Provincial Hospital Affiliated to Shandong University, Ji'nan, China;

⁴ Department of Pediatrics, Wendeng Central Hospital of Weihai City Affiliated to Weifang Medical College, Wendeng, China;

⁵ Department of Respiratory, the First Affiliated Hospital of Shandong University of Traditional Chinese Medicine, Ji'nan, China.

Summary

Xiaoqinglong decoction (XQLD) has been used for centuries in Asia to effectively treat patients with chronic obstructive pulmonary disease (COPD). However, its mechanisms remain unknown. To elucidate this problem, we analyzed the effects of XQLD on gene expressions profiles in COPD rats. In the study, 20 male Wistar rats were injected with lipopolysaccharide (LPS), exposed to cigarette smoke and kept at -20°C for 5 min/day for a successive 8 days to establish COPD animals. Trachea ultramicrostructure and histomorphology were observed to determine whether these models were established successfully. Gene expression profiles were detected using cDNA microarrays. We found 56 differentially expressed genes associated with COPD progression, including 32 up-regulated genes and 24 down-regulated genes. These genes were confirmed to be involved in immune and inflammation reactions, metabolism, cell transportation and the cell cycle, signal transduction and gene regulation. Comparison of gene expression between the therapy group and control group showed that there were only 11 differentially expressed genes, including 5 up-regulated genes and 6 down-regulated genes. We concluded that XQLD had therapeutic effects in COPD rats by affecting gene expression. Pharmacological or targeted expression of some genes might be found useful as novel therapy in COPD management.

Keywords: Pulmonary disease, chronic obstructive, Xiaoqinglong decoction (XQLD), cDNA microarrays

1. Introduction

Chronic obstructive pulmonary disease (COPD) is the fourth most common global cause of death and also exerts an enormous toll on patient quality of life

[#]Co-first author: These two authors contributed equally to this work.

^{*}Address correspondence to:

Dr. Ming Li, Department of Rheumatology and Clinical Immunology, Provincial Hospital Affiliated to Shandong University, No. 324 Jingwu Weiqi Road, Ji'nan, 250021, China.

E-mail: simlas2006@yahoo.com.cn

Dr. Wei Zhang, Department of Respiratory, the First Affiliated Hospital of Shandong University of Traditional Chinese Medicine, Ji'nan, 250021, China.

E-mail: wmx1104@163.com

(1). Currently, treatment of COPD is suboptimal. In the past, long-term administration of antibiotics was used to treat acute exacerbations of COPD, but meta-analyses of the studies of antibiotic administration showed no significant benefit (2). A multicenter, cross-sectional, observational study was conducted in 30 Spanish hospitals among COPD patients aged > 40 years who were hospitalized for an acute exacerbation showed that antibiotic use was significantly associated with yellow or green-yellow sputum prior to the exacerbation, a higher number of exacerbations in the previous year, more visits to emergency departments, and bronchiectasis (3). Because of these problems with antibiotic treatment, more and more traditional Chinese physicians are focusing on exploring the therapeutic effect of Chinese herbal medicine in COPD.

Xiaoqinglong decoction (XQLD) was from Shan

Han Lun, a famous formulary in traditional Chinese medicine (4). The components of XQLD included Ma Huang (9 g), Gui Zhi (6 g), Bai Shao (9 g), Gan Jiang (3 g), Xi Xin (3 g), Zhi Gan Cao (6 g), Ban Xia (9 g) and Wu Wei Zi (3 g) and its major active constituents were ephedrine, cinnamic acid, peoniflorin, methyleugenol, glycyrrhizin and schisandrin. XQLD has been used for asthma, chronic bronchitis, allergic rhinitis, pneumonia, COPD, and sick sinus syndrome therapy for many years. The therapeutic effect of XQLD in COPD patients has received most traditional Chinese physicians' approval. Its side effects are fewer than antibiotics and it will not generate resistance as antibiotics do. Based on these advantages, the usage of XQLD in COPD treatment and related mechanisms have acquired wide attention recently. Its functional mechanism may be related to multiple factors (5). It was reported that XQLD could inhibit inflammatory cytokines, including IL-4, IL-8, TNF- α , and IFN- γ (6), rectify imbalance of oxidation/anti-oxidation and alleviate inflammatory reactions in COPD rats (4). And also, it could ameliorate pathological changes of airway inflammation and remodeling in COPD models. We have also documented that XQLD treatment could significantly lower expression of γ -glutamylcysteine synthetase and nuclear factor- κ B in bronchial and alveolar epithelium of COPD rats (4). However, the precise molecular and genetic mechanism of XQLD in COPD therapy remains to be determined.

Gene expression profiles of diseased tissues help us to provide insight into the molecular mechanisms of disease and may eventually lead to the identification of novel therapeutic targets. Gene expression profile analysis has been used in many diseases, including respiratory system diseases, such as acute lung injury (7). In the current study, to evaluate the effect of XQLD on COPD, we established a modified rat COPD model following previous studies described by Nie YC *et al.* (8), Song YP *et al.* (9), and Sun GR *et al.* (10). Differentially expressed genes were screened by a cDNA microarray technique after COPD rats were established to explore effects of XQLD on gene expression profiles. The relationship between alteration of gene expression and disease progress in rats helped us to elucidate the pathogenesis of COPD, understand the mechanisms of XQLD in COPD therapy and explore new potential novel therapeutic targets in COPD.

2. Materials and Methods

2.1. Animals and reagents

Thirty 2-month-old male Wistar rats were purchased from the Center of Medical Experimental Animals of Shandong University (Grade SPF, Certificated SCXK Lu2003004) (Ji'nan, China) and maintained

in accordance with guidelines of the committee on Care and Use of Laboratory Animals of the Institute of Laboratory Resources, National Research Council (DHEW publication No. [NIH] FS-23) on Animal Care. Animals were divided into 3 experimental groups at random. Twenty rats were used to induce COPD models. Ten animals with this disease received XQLD therapy (therapy group) and the other ten were treated with PBS (model group). Ten normal Wistar rats were used as controls (control group). LPS was obtained from Sigma (St. Louis, MO, USA). Pentobarbital sodium was purchased from China National Medicine Group Shanghai Chemical Reagent Company. Reagents for XQLD were purchased from the pharmacy of Shandong University of Traditional Chinese Medicine. All the herbs were decocted with water and the final concentration was 0.6 g/mL. Sterilization of this decoction was carried out by steam sterilizer.

2.2. Experimental procedures

We established a modified rat COPD model following previous studies (8-10) and the treatment schema is shown in Figure 1. At first, a normal rat COPD model was established with LPS injection and cigarette smoke (CS) which has been documented to be a reliable COPD model (8). LPS was injected into rats through the trachea after they were anesthetized with 0.4% pentobarbital sodium (50 mg/kg) at day 1 and day 14. Animals were fixed and their glottises were exposed. An intravenous cannula was inserted into the trachea quickly and its plunger was drawn out. Then it was connected with another syringe. At the zero point two mL (200 μ g) LPS, dissolved in normal saline, was pushed into the trachea. Rats were erected immediately and swiveled to distribute LPS in the lungs. CS was given twice a day from day 2 to day 28 (except day 1 and day 14). Nine point zero three grams of a cigarette was burned and CS lasted for 1 h each time. The second CS was given after 4 h. The normal rat COPD model was then modified by keeping rats at -20°C for 5 min/day from day 22 to day 29 according to the methods described by Sun GR *et al.* (10). Sun GR *et al.* found that there were more inflammatory cell infiltration in the modified rat COPD model than that in the normal rat COPD model from pathological characteristics analysis. Subsequently, rats in the therapy group were drenched with 2 mL XQLD (total dose = $7.5 \times$ clinical dose in adult) from day 30 to day 43 (4). Rats in the model group were treated with PBS and rats in the control group were held under the same conditions without any intervention.

2.3. Observation of trachea ultramicrostructure

At day 44, all animals were sacrificed. 1-1.5 cm upper eminence trachea tissues were collected, and fixed with

2% glutaraldehyde for 2 h at 4°C. After washing with PBS, they were fixed for 1 h with osmium tetroxide at 4°C and then washed twice with double distilled water. Following dehydration with alcohol, they were dried. At last, samples were stuck to a metal sample table with paste which can conduct electricity, covered by a metal membrane and then observed using scanning electron microscopy.

2.4. Histomorphology performances under light microscope

Paraffin-embedded sections of lung tissue were deparaffinized in xylene and ethanol, stained with hematoxylin-eosin (H&E) and observed under a light microscope (Nikon Corporation, Tokyo, Japan). Trachea pathology grade was judged according to a modified criterion designed by Barbera *et al.* (11) (Table 1).

2.5. General appearances observation and body mass growth index calculation

Animal general appearances were observed during the whole process, which included animal movement, fur appearance, weight growth, respiration situation and cough severity. Animal body mass growth index was calculated as follows: Body mass growth index = (body mass before experiment – body mass after experiment) /body mass before experiment.

2.6. Total RNA extraction and cDNA microarray screening

Lung tissues were selected randomly from each group and total RNA was extracted with Trizol (Invitrogen, Carlsbad, CA, USA). RNA was purified with the NucleoSpin RNA clean-up kit (Macherey-Nagel, Düren, Germany). RNA optical density at 260 nm/280 nm was consistently > 1.8. RNA samples were reverse transcribed into single-strand cDNA, synthesized into double-strand cDNA, and transcribed into cRNA *in vitro* using the T7RiboMAX Express Large Scale RNA Production System (Promega, Madison, WI, USA). After reverse transcription with random primers, cRNA products were marked with the Klenow enzyme.

Samples were hybridized using a hybridization solution (25% formamide, 3× standard saline citrate [SSC], 0.2% sodium dodecyl sulfate [SDS], 5× Denhart's) at 42°C overnight in a humid environment. Subsequently, slides were washed with washing solution I (2× SSC, 0.2% SDS) at 42°C for 4 min, followed by washing solution II (2× SSC). Arrays were scanned using CapitalBio's confocal scanner LuxScan 10K-A (Beijing, China). An intensity-dependent lowess program in the R language package was used to normalize two channel ratio values. Statistical data and differential analysis files were generated by SAM software 3.0 (Stanford University, Stanford, CA, USA).

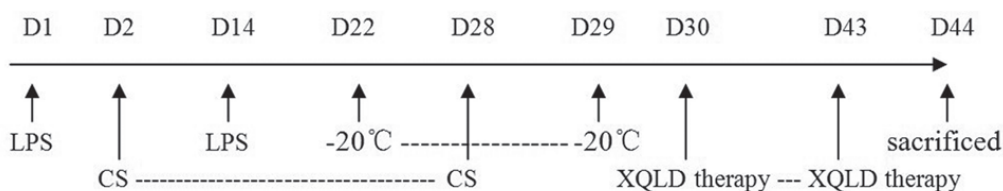


Figure 1. Schema of treatment. LPS (200 µg) was injected into rats through trachea at day 1 and day 14. CS was given twice per day from day 2 to day 28 (except day 14). Animals were kept at –20°C for 5 min/day from day 22 to day 29. Rats received 2 mL of XQLD therapy daily (0.6 g/mL) from day 30 to day 43. All the animals were sacrificed at day 44.

Table 1. Criterion of trachea pathology alteration grades

Histology appearances under microscope	Grade			
	0	1	2	3
Cilia lodging, adhesion and depletion	No	< 1/4 circle	1/4-1/2circle	> 1/2circle
Epithelial cell degeneration, necrosis and desquamate	No	< 1/4 circle	1/4-1/2 circle	> 1/2 circle
Beaker cell proliferation	No	< 1/4 circle	1/4-1/2 circle	> 1/2 circle
Epithelial squamous metaplasia	No	< 1/4 circle	1/4-1/2 circle	> 1/2 circle
Mucous hyperemia and swelling	No	< 1/4 circle	1/4-1/2 circle	> 1/2 circle
Lymphocyte infiltration	No	Lymphocytes can be seen	Follicle can be seen	> 5 follicles
Mononuclear macrophage infiltration	No	< 10 /HP	10-20/HP	> 20/HP
Neutrophil infiltration	No	< 10/HP	10-20/HP	> 20/HP
Eosinophilic cell infiltration	No	< 10/HP	10-20/HP	> 20/HP
Smooth muscle cell breakage/hyperplasia	No	< 1/4 circle	1/4-1/2 circle	> 1/2 circle

Abbreviations: HP, high power microscope.

2.7. Statistical analysis

SPSS 15.0 for Windows was used for all analyses. All data are expressed as mean \pm standard deviation (mean \pm S.D.). One-factor ANOVA was used for measurement data comparison of every group and a *q*-test was used for comparison of two groups. Comparisons of numerical data among groups were performed by χ^2 test. Difference between mean values is judged to be statistically significant when $p < 0.05$.

3. Results

3.1. Trachea morphology and pathology appearances under scanning electron microscope and light microscope

The scanning electron microscope showed that trachea cilia in the control group were uniform and in the same direction. However, there were lodging, adhesion and depletion with large amounts of secretion in the model group. Compared to the model group, the XQLD therapy group was obviously improved (Figure 2A).

We selected bronchioles (diameter: 700-1,200 μm)

and lumen (the shortest diameter/the longest diameter ≥ 0.7) to analyze inflammation responses and small airway modeling. Histomorphology observations under the light microscope in the three groups are shown in Table 2 and Figure 2B. There were severe inflammatory responses in the model group and increased lymphocytes, monocytes and neutrophils can be seen in lung tissues. This phenomenon was accompanied by cilia lodging, adhesion and depletion, epithelial cell degeneration, necrosis and desquamate, goblet cell proliferation, epithelial squamous metaplasia, mucous hyperemia and swelling. These pathological changes confirmed that our COPD models were established successfully. After XQLD therapy, inflammatory responses were obviously relieved and the numbers of inflammatory cells, including lymphocytes, monocytes, and neutrophils, decreased significantly. Meanwhile, pathological changes of cilia, epithelial cells, goblet cells, epithelium and mucous membranes were dramatically relieved.

3.2. General appearances

Rats in the control group were active and restless, with

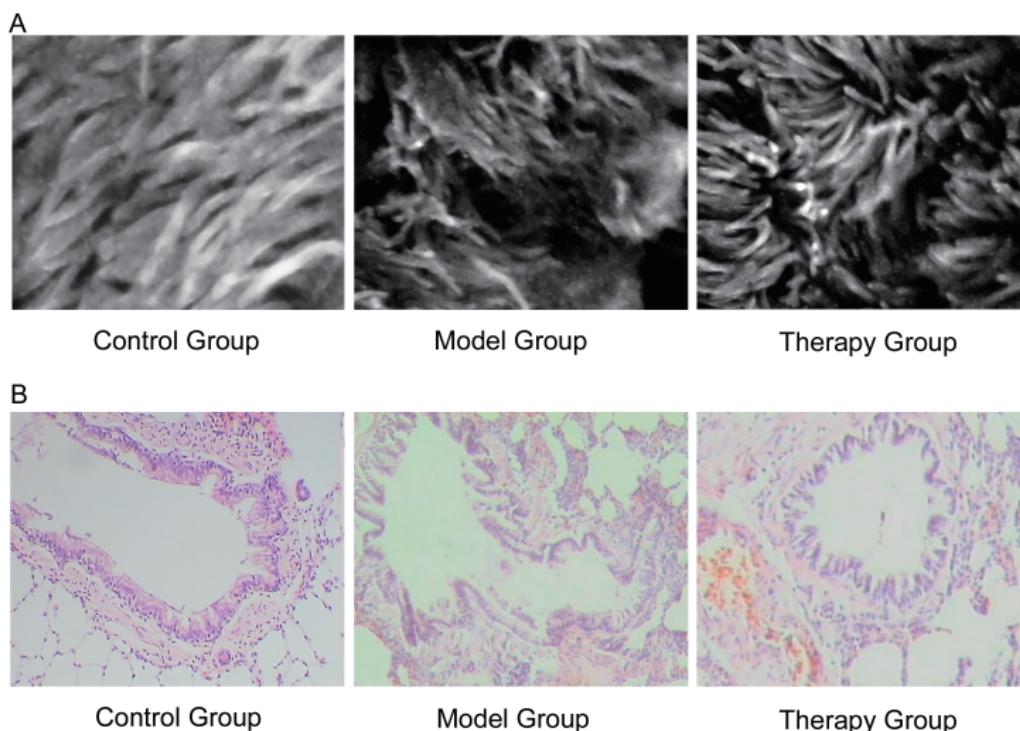


Figure 2. Trachea morphology and pathology appearances under scanning electron microscope and light microscope. Control group, Wistar rats without any treatment; Model group, rat COPD models treated with PBS; Therapy group, rat COPD models received Xiaoqinglong decoction therapy. (A) Alteration of trachea ultramicrostructure. Trachea tissues were collected and observed under scanning electron microscope. Control group (left, magnification $\times 6,000$): Trachea cilia were uniform with same direction. Model group (middle, magnification $\times 6,000$): Trachea cilia diminished dramatically. Depletion and large amounts of secretion can be seen. Therapy group (right, magnification $\times 6,000$): After XQLD therapy, trachea cilia increased in a consistent direction and the secretions were obviously decreased. (B) Pathology appearance of trachea. Control group (left, magnification $\times 100$): Epithelium of bronchiole was smooth and there was no inflammation cell infiltration, no hyperemia or no swelling. Model group (middle, magnification $\times 100$): Bronchial lumen expansion, cilia adhesion and desquamated, goblet cell proliferation, surrounding blood capillary fibrosis hyperplasia were severe. More inflammatory cell infiltration could be found. Therapy group (right, magnification $\times 100$): Inflammation around trachea lessened after XQLD therapy. The number of inflammatory cells decreased dramatically.

Table 2. Inflammation responses and small airway reconstitutions in indicated groups

Histology appearances under microscope	Grade		
	Model group	Therapy group	Control group
Cilia lodging, adhesion and depletion	2-3	1-2	0
Epithelial cell degeneration, necrosis and desquamate	2-3	1-2	0-1
Beaker cell proliferation	1-3	1-2	0
Epithelial squamous metaplasia	2-3	1-2	0
Mucous hyperemia and swelling	1-3	1-2	0
Lymphocyte infiltration	2-3	1-3	0-1
Mononuclear macrophage infiltration	1	1	0-1
Neutrophil infiltration	1-2	1-2	0-1
Eosinophilic cell infiltration	1	1	0
Smooth muscle cell breakage/hyperplasia	1-3	1-2	0

Model group, rat COPD models treated with PBS; Therapy group, rat COPD models received Xiaoqinglong decoction therapy; Control group, Wistar rats without any treatment.

smooth and burnished fur. Their body mass increased gradually and respiration was stable. Before XQLD therapy, rats in the model group and therapy group usually stayed still, extradoed and wriggled with gathered fur. Their body mass increased slowly and respiration was short accompanied by frequent cough. Cough appeared at the first day of CS and lasted to the end of our experiment. At day 28, rats in the model group and therapy group appeared to have shortness of breath. These symptoms of rats in the therapy group were obviously alleviated after XQLD therapy. Body mass growth indexes in the three groups are shown in Figure 3.

3.3. Analysis of gene expression profiles

Genes were judged to be differentially expressed genes when the mean value exceeded 2.5 or lower than 0.375 to increase research reliability. A comparison of gene expression between model group and control group indicated that there were 56 differentially expressed genes which included 32 up-regulated genes and 24 down-regulated genes. The known genes are shown in Table 3. Comparison of gene expression between therapy group and control group showed that there were only 11 differentially expressed genes, including 5 up-regulated genes (3 of them were also up-regulated genes in model group) and 6 down-regulated genes. Our data indicated that expression of 29 up-regulated genes and 24 down-regulated genes were modified by XQLD therapy and there was no difference when these genes expression were compared to their expression in control group.

A functional classification of the differentially expressed genes between model group and control group is shown in Figure 4. The number of differently expressed genes related to immune and inflammation responses is the largest except for not classified and functionally unclassified genes. Other differentially expressed genes were involved in metabolism, gene expression, cell transportation, cell cycle, and cell

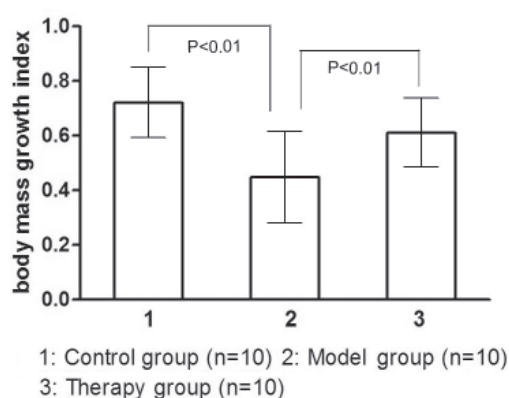


Figure 3. Body mass growth index in three groups. Control group, Wistar rats without any treatment; Model group, rat COPD models treated with PBS; Therapy group, rat COPD models received Xiaoqinglong decoction therapy. Rat body mass growth indexes in indicated groups were measured. It was obviously lower in model group and therapy group than that in the control group. Compared with model group, rat weight growth index increased significantly after XQLD therapy ($p < 0.01$).

proliferation.

4. Discussion

CS represents the most important environmental risk factors for respiratory diseases and it is the first risk for COPD (12,13). However, it needs a long time to establish rat COPD models with CS only. LPS is the major component of Gram-negative bacterium adventitia. It can damage airway epithelium directly, activate macrophages, lymphocytes, and neutrophils, induce bronchi chronic inflammation and cause emphysema formation. It stimulates secretion of specific pro-inflammatory molecules from circulating monocytes, such as IL-6 and monocyte chemotactic protein-1, and thereby aggravates progress of COPD (14). In this study, the COPD model was established by a modified method of combining fumigation and lipopolysaccharide (LPS) intra-tracheal dripping (4). Pathology appearances under a scanning electron

Table 3. Differentially expressed genes in model group when compared with control group

Gene name	Mean ratio	Function
Up-regulated genes		
Immunoglobulin joining chain	6.872	Immune
Fructose-bisphosphate aldolase A	4.708	Metabolism
Immunoglobulin heavy chain, α	4.556	Immune
Fertility related protein WMP1	3.884	Spermatogenesis
Norvegicus nucleoporin 62 (Nup62)	3.832	Gene expression
Immunoglobulin heavy chain 1a (serum IgG2a)	3.813	Immune
Chaperonin containing TCP1, subunit 5 (epsilon)	3.446	Cell transportation and cycle
Complement component 1, s subcomponent	2.967	Immune
CD36 molecule (thrombospondin receptor) (Cd36)	2.901	Signal transduction
Arginase, liver (Arg1)	2.727	Immune and inflammation
Sorting nexin 25 (Snx25)	2.533	Cell transportation and cell cycle
(α -N-acetyl-neuraminyl-2,3- β -galactosyl-1,3)-N-acetylglucosaminide α -2,6-sialyltransferase 3 (St6galnac3)	2.519	Immune and inflammation
Leukotriene A4 hydrolase (Lta4h)	2.504	Immune and inflammation
Down-regulated genes		
6-Pyruvoyl-tetrahydropterin synthase (Pts)	0.371	Metabolism
3'-Phosphoadenosine 5'-phosphosulfate synthase 2 (Papss2)	0.353	Metabolism
Immunoglobulin superfamily, member 10 (Igsf10)	0.351	Immune
FK506 binding protein 9 (Fkbp9)	0.344	Immune and inflammation
Developmental arteries and neural crest EGF-like protein fibulin 5 (Fbln5)	0.343	Signal transduction
CEA-related cell adhesion molecule 1	0.341	Immune and inflammation
Acyl-coenzyme A oxidase 1, palmitoyl (Acox1)	0.340	Metabolism
Group specific component (Gc) vitamin D binding protein	0.330	Metabolism
Vitronectin (Vtn)	0.322	Cell migration and fibrosis
Neuronal PAS domain protein 2 (Npas2)	0.295	Gene expression
Phosphatidylinositol 3-kinase, catalytic, α polypeptide (Pik3ca)	0.244	Signal transduction
Eukaryotic translation initiation factor 2B, subunit 1 α	0.227	Gene expression

microscope and light microscope showed lesions in the rat model closely resemble COPD lesions occurring in humans.

Nutritional status disorders are the most common extra-pulmonary manifestations of COPD. A specific loss of weight, characterized by lean body mass (LBS), is observed in some COPD patients (15). In our study, animals in the model group and therapy group showed lower weight growth indexes than those in the control group ($p < 0.01$). Compared with the model group, the changes of general appearance, including LBS, in the therapy group demonstrated that XQLD was an effective drug which can relieve COPD symptoms.

Modern pharmacology studies have indicated that XQLD could down-regulate expression of γ -glutamylcysteine synthetase and nuclear factor- κ B in bronchial and alveolar epithelium of COPD rats, which maybe responsible for gene expression regulation through multiple mechanisms. Our gene expression profiles analysis showed that the number of differently expressed genes between the model group and control group was 56 while there were only 11 differently expressed genes in the therapy group when compared to the control group. The genes involved were in immune and inflammation reactions, metabolism, cell transportation and cell cycle, signal transduction and gene regulation. Twenty-nine up-regulated genes and 24 down-regulated genes in the model group became non-differentially expressed genes after XQLD therapy. The changes of genes expression after XQLD treatment

reflected that complicated genetic regulations were involved in the progression of COPD.

Differentially expressed genes related to immune response and inflammation mainly included *immunoglobulin heavy chain 1a (serum IgG2a)*, *arginase 1*, *alpha 2,6-sialyltransferase*, *leukotriene A4 hydrolase*, *FK506 binding protein 9 (FKBP9)*, and *CEA-related cell adhesion molecule-1 (CEACAM-1)*. It is known that serum IgG2a (J chain) is a small polypeptide, which regulates polymer formation of immunoglobulin (Ig)A and IgM (16). Arginase-1 is an enzyme in arginine metabolism which plays an important role in asthma by decreasing nitric oxide production and increasing formation of peroxynitrite, polyamines and l-proline (17). Alpha 2,6-sialyltransferase is an acute-phase reactant and it is a Golgi membrane-bound enzyme (18). The leukotrienes are a family of lipid mediators involved in inflammation and allergy. Leukotriene B4 modulates immune responses, participates in the host defense against infections, and is a key mediator of PAF-induced lethal shock. The final step in the biosynthesis of leukotriene B4 is catalyzed by leukotriene A4 hydrolase, a unique bifunctional zinc metalloenzyme with an anion-dependent aminopeptidase activity (19). *Immunoglobulin heavy chain 1a (serum IgG2a)*, *arginase 1*, *alpha 2,6-sialyltransferase* and *leukotriene A4 hydrolase* were up-regulated when COPD occurred. FK506 (tacrolimus), has powerful immunosuppressant properties and it can promote nerve regeneration (20).

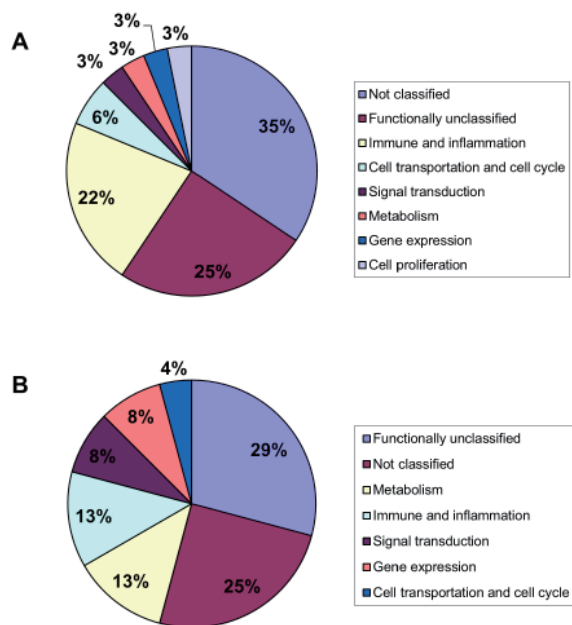


Figure 4. Functional classification of differentially expressed genes between model group and control group. (A) Functional classification of up-regulated genes between model group and control group. These genes were related to immune function and inflammation, cell transportation, cell cycle, signal transduction, metabolism, gene expression, and cell proliferation. (B) Functional classification of down-regulated genes between model group and control group. Most genes involved in metabolism, immune function and inflammation, signal transduction and gene expression.

FKBP9 encodes a protein related to FK506-binding protein 6 (65 kDa, FKBP65) which binds to FK506 (21) and plays an immunosuppression role. *CEACAM1* appears to play a unique role among the neutrophil CEACAMs (22). Both *FKBP9* and *CEACAM1* genes were down-regulated in the model group compared to the control group.

There were also some differentially expressed genes related to gene expression regulation in the model group when compared to the control group. These genes included *nuclear pore protein p62* (*Nup62*), *neuronal PAS domain protein 2* (*NPAS2*) and the α -subunit of eukaryotic initiation factor 2B (*eIF-2B*). Transcription factor *Sp1* plays an important role in the expression of many cellular genes and it must interact with p62, through its C-terminus, to bring transcribeable DNA in contact with the transcription factors (23). In COPD rats, increased expression of p62 suggested up-regulated transcription of some genes. *NPAS2* is a transcription factor expressed primarily in the mammalian forebrain (24) and it is an important transcription factor associated with circadian rhythms (25). Phosphorylation of eIF-2 is one of the best known mechanisms regulating protein synthesis in a wide range of eukaryotic cells, from yeast to human (26). In COPD rat models, *NPAS2* and *eIF-2* were negatively regulated but their roles in COPD are still unclear.

Some other differentially expressed genes

between the model group and control group had a relationship with metabolism and signal transduction. *Fructose-bisphosphate aldolase A* (*Muscle-type aldolase*) involved in glycometabolism, was up-regulated while *6-pyruvoyl-tetrahydropterin synthase*, *3'-phosphoadenosine 5'-phosphosulfate synthetase 2* and *acyl-coA oxidase* were down-regulated. Differentially expressed genes associated with signal transduction included *epidermal growth factor (EGF)-related peptides* and *phosphatidylinositol 3-kinase catalytic subunit α* (*PIK3CA*). Both of these were down-regulated while their expression had no significant difference between the therapy group and control group. And also, there were some genes whose functions were not clear. They perhaps played a novel or important role in COPD genesis and development. Further study is still needed to explore these unknown genes.

5. Conclusion

Our results showed XQLD was an effective drug for COPD treatment and its function was related to gene expression alteration. A functional classification of differentially expressed genes indicated complex mechanisms involved in the genesis and development of COPD. Our results facilitate further investigation of the molecular mechanisms underlying the genesis and development of COPD and help us to understand mechanisms of XQLD in COPD therapy.

Acknowledgements

This study was supported by grant from Shandong science and technology program of China (No. 2002B17) and outstanding scholarship 1020 project of Shandong provincial health system.

References

- Groneberg-Kloft B, Fischer A, Welte T. Fixed combination therapies in COPD – effect on quality of life. *Int J Chron Obstruct Pulmon Dis.* 2007; 2:551-557.
- Siafakas NM. Preventing exacerbations of COPD – advice from Hippocrates. *N Engl J Med.* 2011; 365:753-754.
- Miravittles M, Soler-Cataluña JJ, Baranda F, Cordero P, Greses JV, de la Roza C. Previous outpatient antibiotic use in patients admitted to hospital for COPD exacerbations: Room for improvement. *Infection.* 2012; Epub ahead of print.
- Zhang W, Zhang XY, Shao YM. Effects of TCM treatment according to syndrome differentiation on expressions of nuclear factor- κ B and γ -glutamylcysteine synthetase in rats with chronic obstructive pulmonary disease of various syndrome types. *Zhongguo Zhong Yi Jie He Za Zhi.* 2007; 27:426-430. (in Chinese)
- Fang XM, Li J, Li ZG, Dong XB. Functional mechanism of pingchuanning decoction on adjustment of clara cell secretory protein in airway remodeling of asthmatic rats.

- J Tradit Chin Med. 2012; 32:215-221.
6. Zhang CQ, Liang TJ, Zhang XY, Shao YM, He R, Zhang M, Long F, Li DW. Protective effect of Wenfei Huayin Recipe on lung of rats with chronic obstructive pulmonary diseases. *Zhongguo Zhong Xi Yi Jie He Za Zhi*. 2010; 30:72-75. (in Chinese)
 7. Lesur I, Textoris J, Loriiod B, Courbon C, Garcia S, Leone M, Nguyen C. Gene expression profiles characterize inflammation stages in the acute lung injury in mice. *PLoS One*. 2010; 5:e11485.
 8. Nie YC, Wu H, Li PB, Luo YL, Zhang CC, Shen JG, Su WW. Characteristic comparison of three rat models induced by cigarette smoke or combined with LPS: To establish a suitable model for study of airway mucus hypersecretion in chronic obstructive pulmonary disease. *Pulm Pharmacol Ther*. 2012; 25:349-356.
 9. Song YP, Cui DJ, Mao PY. A new way of establishing a rat chronic obstructive pulmonary disease model and the effects of drugs on them. *Acad J PLA Postgrad Med Sch*. 2001; 22:99-102. (in Chinese)
 10. Sun GR, Xue WG, Gao B. Assessment on rat model of accumulation of cold and harmful fluid in lung with chronic obstructive pulmonary disease. *World J Integr Tradit West Med*. 2008; 3:635-639. (in Chinese)
 11. Barbera JA, Peinado VI, Santos S, Ramirez J, Roca J, Rodriguez-Roisin R. Reduced expression of endothelial nitric oxide synthase in pulmonary arteries of smokers. *Am J Respir Crit Care Med*. 2001; 164:709-713.
 12. Hill AT, Campbell EJ, Bayley DL, Hill SL, Stockley RA. Evidence for excessive bronchial inflammation during an acute exacerbation of chronic obstructive pulmonary disease in patients with $\alpha(1)$ -antitrypsin deficiency (PiZ). *Am J Respir Crit Care Med*. 1999; 160:1968-1975.
 13. Mannino DM. COPD: Epidemiology, prevalence, morbidity and mortality, and disease heterogeneity. *Chest*. 2002; 121:121S-126S.
 14. Aldonyte R, Jansson L, Piitulainen E, Janciauskiene S. Circulating monocytes from healthy individuals and COPD patients. *Respir Res*. 2003; 4:11.
 15. Kuznar-Kaminska B, Batura-Gabryel H, Brajer B, Kaminski J. Analysis of nutritional status disorders in patients with chronic obstructive pulmonary disease. *Pneumonol Alergol Pol*. 2008; 76:327-333.
 16. Johansen FE, Braathen R, Brandtzaeg P. Role of J chain in secretory immunoglobulin formation. *Scand J Immunol*. 2000; 52:240-248.
 17. Maarsingh H, Zaagsma J, Meurs H. Arginine homeostasis in allergic asthma. *Eur J Pharmacol*. 2008; 585:375-384.
 18. Jamieson JC, McCaffrey G, Harder PG. Sialyltransferase: a novel acute-phase reactant. *Comp Biochem Physiol B*. 1993; 105:29-33.
 19. Haeggstrom JZ, Nordlund P, Thunnissen MM. Functional properties and molecular architecture of leukotriene A4 hydrolase, a pivotal catalyst of chemotactic leukotriene formation. *ScientificWorldJournal*. 2002; 2:1734-1749.
 20. Chabas JF, Alluin O, Rao G, Garcia S, Lavaut MN, Legre R, Magalon G, Marqueste T, Feron F, Decherchi P. FK506 induces changes in muscle properties and promotes metabosensitive nerve fiber regeneration. *J Neurotrauma*. 2009; 26:97-108.
 21. Jo D, Lyu MS, Cho EG, Park D, Kozak CA, Kim MG. Identification and genetic mapping of the mouse Fkbp9 gene encoding a new member of FK506-binding protein family. *Mol Cells*. 2001; 12:272-275.
 22. Skubitz KM, Skubitz AP. Interdependency of CEACAM-1, -3, -6, and -8 induced human neutrophil adhesion to endothelial cells. *J Transl Med*. 2008; 6:78.
 23. Han I, Roos MD, Kudlow JE. Interaction of the transcription factor Sp1 with the nuclear pore protein p62 requires the C-terminal domain of p62. *J Cell Biochem*. 1998; 68:50-61.
 24. Reick M, Garcia JA, Dudley C, McKnight SL. NPAS2: An analog of clock operative in the mammalian forebrain. *Science*. 2001; 293:506-509.
 25. Koudo R, Kurokawa H, Sato E, Igarashi J, Uchida T, Sagami I, Kitagawa T, Shimizu T. Spectroscopic characterization of the isolated heme-bound PAS-B domain of neuronal PAS domain protein 2 associated with circadian rhythms. *Febs J*. 2005; 272:4153-4162.
 26. Alcazar A, Rivera J, Gomez-Calcerrada M, Munoz F, Salinas M, Fando JL. Changes in the phosphorylation of eukaryotic initiation factor 2 α , initiation factor 2B activity and translational rates in primary neuronal cultures under different physiological growing conditions. *Brain Res Mol Brain Res*. 1996; 38:101-108.

(Received January 18, 2012; Revised September 3, 2012; Accepted October 18, 2012)

An *in vitro* study of *pcDNA 3.0-hVEGF165* gene transfection in endothelial progenitor cells derived from peripheral blood of rabbits

Xiulian Gu¹, Xiaoyong Miao², Jia Xu², Jianping Cao^{2,*}

¹ Department of Cardiology, Hospital No. 455 of the PLA, Shanghai, China;

² Department of Anesthesiology, Hospital No. 455 of the PLA, Shanghai, China.

Summary

The present study investigated the effect of the *VEGF165* gene on adhesion, migration, and proliferation of endothelial progenitor cells (EPCs) derived from peripheral blood of rabbits. Peripheral blood mononuclear cells were isolated from rabbits by density gradient centrifugation with Ficoll-Plaque Plus. EPCs were characterized by immunofluorescence and immunostaining. A *pcDNA 3.0-hVEGF165* expression vector was constructed and EPCs were transfected with the *pcDNA 3.0-hVEGF165* gene. The EPCs derived from peripheral blood of rabbits were successfully transfected with *pcDNA 3.0-hVEGF165*. ELISA showed that the expression of VEGF165 increased significantly in the EPCs transfected with the *hVEGF165* gene compared to control cells. Compared to control EPCs, EPCs transfected with the *hVEGF165* gene had significantly enhanced adhesion, migration, and proliferative ability *in vitro*.

Keywords: *hVEGF165* gene, endothelial progenitor cells, transfection, adhesion, migration, proliferation

1. Introduction

Asahara *et al.* (1) first reported the role of circulating endothelial progenitor cells (EPCs) in neovascularization and vasculogenesis in 1997. Over the past few decades, several studies have indicated that transplantation of EPCs effectively restored injured endothelia, repaired limb ischemia (2), myocardial ischemia (3), and carotid artery injury (4), and promoted vascular graft survival (5). A recent study by the current authors showed that transplantation of peripheral blood-derived EPCs effectively attenuated endotoxin-induced acute lung injury as a result of the paracrine effect of VEGF (6).

However, low concentrations of EPCs in peripheral blood precluded the extensive use of EPCs. A study indicated that VEGF stimulates the proliferation, migration, and survival of endothelial cells, in turn

facilitating endothelialization with EPCs and recovery of endothelial function (7). VEGF was first discovered by Ferrara (8) and is a glucoprotein isolated from cattle pituitary gland follicle stellate cells. VEGF helps maintain vessel normal shape and integrity, promote vessel permeability, and facilitate endothelial cell proliferation and vessel production (9). Five different VEGF protein isoforms, including VEGF-A, VEGF-B, VEGF-C, VEGF-D, and VEGF-E, have been derived from a single gene by alternative splicing (10). There are five characterized VEGF-A isomers of 121, 145, 165, 189, and 206 amino acids in mammals that are generated by alternative splicing of the mRNA from a single gene consisting of eight exons. VEGF165 is the most powerful function protein that promotes angiogenesis in the VEGF family. However, its short half-life and few natural sources mean that an effective concentration of VEGF165 cannot be maintained in the blood after injection. The use of *ex vivo*-transfected stem cells as vectors for gene therapy has largely solved this problem. A study reported that transplantation of VEGF-transfected EPCs increased vasculogenesis and required fewer EPCs than non-transfected EPCs (11). Moreover, the role of VEGF genes transfected

*Address correspondence to:

Dr. Jianping Cao, Department of Anesthesiology, Hospital No. 455 of the PLA, 338 West Huaihai Road, Shanghai 200052, China.

E-mail: cjpcl221019@sina.com

in EPCs has yet to be fully elucidated. Therefore, the current study sought to investigate the effects of EPCs transfected with the *hVEGF165* gene on the adhesion, migration, and proliferative ability of EPCs *in vitro*.

2. Materials and Methods

2.1. Materials

New Zealand White rabbits were obtained from Shanghai Laboratory Animal Center, Chinese Academy of Sciences. Ficoll-Plaque Plus was purchased from Amersham Pharmacia Biotech AB (Uppsala, Sweden). EGM-2 MV Single Quots were obtained from Lonza Corp (Basel, Switzerland). DiI-acetyl-low density lipoprotein was purchased from Invitrogen (Carlsbad, CA, USA). Fluorescein isothiocyanate-ulex europaeus agglutinin-1 (UEA-1) was from Sigma-Aldrich (St. Louis, MO, USA). VEGFR2 and CD133 were purchased from Santa Cruz Biotechnology (Santa Cruz, CA, USA). A hVEGF165 ELISA detection kit was provided by Chemicon International Inc., Temecula, CA, USA.

2.2. Isolation and culture of peripheral blood EPCs

Approval was obtained from the Animal Care and Use Committee of Hospital No. 455 of the PLA. Peripheral blood was obtained from an ear artery of New Zealand White rabbits (10 mL/kg). Peripheral blood mononuclear cells were isolated by density gradient centrifugation with Ficoll-Plaque Plus. Mononuclear cells were then washed and plated on six-well plates supplemented with EGM-2 MV Single Quots. Mononuclear cells were incubated at 37°C, 5% CO₂ and supplied daily with EGM-2. The nonadherent cells were removed after 48 h of culture. On day 7 of culturing, the adherent cells (known as early EPCs) were detached with 0.025% trypsin containing 0.02% EDTA and used for analysis or transplantation.

2.3. Characterization of EPCs

The EPCs isolated from rabbits were characterized as previously described (8). Cells were incubated with 10 µg/mL DiI-acetyl-low density lipoprotein (LDL) and 5 µg/mL fluorescein isothiocyanate-*Ulex europaeus* agglutinin-1 (UEA-1). The staining of acetyl-LDL and UEA-1 in cultured EPCs was detected under fluorescence confocal microscopy at the absorption wavelengths of 555 and 490 nm, respectively. Dual fluorescent staining positive for both fluorescein isothiocyanate-labeled UEA-1 and DiI-labeled acetyl-LDL (double-positive cells) served to identify differentiating EPCs. Immunostaining of vascular endothelial growth factor receptor 2 and CD133 was performed as previously described.

2.4. Construction and identification of a pcDNA 3.0-hVEGF165 expression vector

The recombinant retroviral vectors pLXSN-KDRp-VEGF165 and pcDNA 3.0 vectors were constructed in this laboratory. PLXSN-KDRp-VEGF165 was digested by Bam HI and XhoI to release KDRp-VEGF165. The KDRp-VEGF165 fragment was ligated with Bam HI and XhoI digested pcDNA 3.0 to form a pcDNA 3.0-KDRp-VEGF165 recombinant vector. Then, pcDNA 3.0-KDRp-VEGF165 was digested with EcoR I to remove KDRp and self-ligated to generate a pcDNA 3.0-VEGF165 recombinant plasmid. pcDNA 3.0-VEGF165 was verified by XhoI and Hind III digestion and sequencing analysis.

2.5. Transfection of EPCs with the pcDNA 3.0-hVEGF165 expression vector

After EPCs were cultured for 7 days according to the manufacturer's instructions in the DOTAP Liposomal kit, EPCs were transfected with pcDNA 3.0-hVEGF165 and eGFP (group A). EPCs transfected with null-plasmid (group B) and nontransfected EPCs (group C) served as controls. After 24 h, the EPCs were detected using fluorescent microscopy.

2.6. ELISA detection of VEGF165 expression *in vitro*

pcDNA 3.0-hVEGF165-transfected EPCs were grown in six-well plates at a cell density of 1×10^5 cells per well, using EPCs transfected with null-plasmid and nontransfected MSCs as controls. The supernatant were harvested at two-day intervals from day 1 to day 7 post-transfection. The samples were centrifuged and then stored at -70°C until the assay. A human VEGF165 ELISA kit was used to detect the VEGF165 protein secreted from transfected EPCs in accordance with the manufacturer's instructions.

2.7. Detection of the adhesive ability of EPCs

pcDNA 3.0-hVEGF165-transfected EPCs and null-plasmid and nontransfected EPCs were washed with PBS and gently detached with 0.25% trypsin. After centrifugation and resuspension in EGM-2, identical cell numbers were replated onto fibronectin-coated culture dishes and incubated for 30 min at 37°C. Adherent cells were counted.

2.8. Migration assay

EPC migration was evaluated using a transwell chamber assay. In brief, the pcDNA 3.0-hVEGF165-transfected EPCs and null-plasmid and nontransfected EPCs were detached with 0.25% trypsin, and then 1×10^5 EPCs in 200 µL EGM-2 were seeded in the upper chamber of a

transwell cell culture insert (5 μm pore size). VEGF (50 ng/mL, PeproTech, Rocky Hill, NJ, USA) in EGM-2 was placed in the lower chamber. After incubation for 6 h at 37°C, the membranes were washed with phosphate buffer solution (PBS) and fixed with methanol. EPCs were stained with 4,6-diamidino-2-phenylindole (DAPI) solution. Light microscopy (400-fold magnification) was used to count the numbers of EPCs that had migrated to the lower surface of the membrane from five random fields in five domains.

2.9. MTT assay of EPC proliferation

The 3-(4,5-dimethylthiazol-2-yl)-2,5-diphenyl-tetrazolium bromide (MTT) assay was used to determine EPC proliferation. pcDNA 3.0-hVEGF165-transfected EPCs and null-plasmid and nontransfected EPCs were digested with 0.25% trypsin and then cultured in 96-well plates (200 μL /well). EPCs were supplemented with 10 μL MTT (5 g/L, Sigma-Aldrich) and incubated for another 4h. The supernatant was then discarded by aspiration and the EPC preparation was shaken with 150 μL dimethyl sulfoxide (DMSO) for 10 min before the OD value was measured at 490 nm.

2.10. Statistical analysis

All data are presented as mean \pm S.D. Parametric data were analyzed using one-way ANOVA and variations in different groups were compared using the Turkey *post hoc* test. $p < 0.05$ was considered statistically significance.

3. Results

3.1. Characterization of EPCs

Seven days after cultivation, EPCs (approximately $2-3 \times 10^6$ cells) proliferated from 20 mL peripheral blood of each rabbit. Formation of monolayer colonies with a "cobblestone" appearance was also observed after 2 weeks of culturing in endothelial basic medium 2 (Figure 1A). The EPCs also displayed expression of endothelial markers vascular endothelial growth factor receptor 2 (Figure 1B) and CD133 (Figure 1C). Fluorescence confocal microscopy showed that these early EPCs exhibited phenotyping of endothelial cells, including incorporation of DiI-ac-LDL and binding of fluorescein isothiocyanate-UEA-1. Dual fluorescent staining positive for both fluorescein isothiocyanate labeled UEA-1 and DiI-ac-LDL (double-positive cell) served to identify differentiating EPCs (Figures 1D-1F).

3.2. Identification of the pcDNA 3.0-hVEGF165 expression vector

3.2.1. Fluorescence detection of hVEGF165-eGFP-transfected EPCs

In inverted fluorescence microscopy, EPCs had little green fluorescence 1 day after transfection with hVEGF165-eGFP (Figure 2A). Forty-eight h after transfection with hVEGF165-eGFP, EPCs fluoresced green (Figure 2B). Moreover, after day 3 hVEGF165-eGFP-transfected EPCs had substantial green

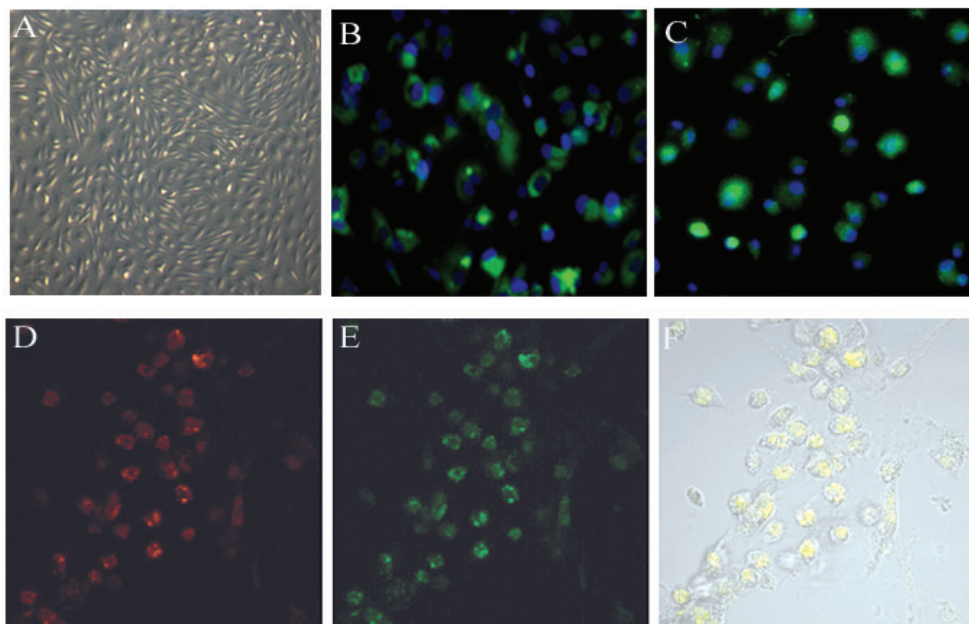


Figure 1. Characterization of EPCs. Cultured for 14 days, EPCs grew into monolayer with a "cobblestone" appearance (A, 100 \times magnification). Immunofluorescent EPCs were positive for cytoplasmic vascular endothelial growth factor receptor 2 and CD133 (B, 200 \times magnification, and C, 200 \times magnification, green fluorescence). Nuclei were counterstained in blue fluorescence. Fluorescence confocal microscopy (200 \times magnification) revealed that after day 7 the endothelial progenitors were positive for the uptake of DiI-acLDL (D, red fluorescence) and for staining of FITC-UEA-1 (E, green fluorescence). D and E results are superimposed in panel F (yellow fluorescence).

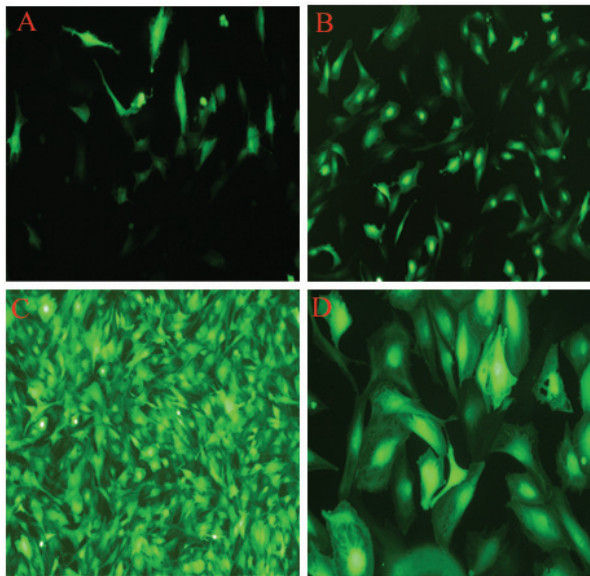


Figure 2. Fluorescence detection of hVEGF165-eGFP-transfected EPCs. Fluorescence microscopy revealed little green fluorescence 1 day after EPCs were transfected with hVEGF165-eGFP (A, 200 \times magnification). Two days after transfection with hVEGF165-eGFP, EPCs fluoresced green (B, 200 \times magnification). Moreover, after day 3 hVEGF165-eGFP-transfected EPCs had substantial green fluorescence (C, 200 \times magnification; D, 400 \times magnification).

fluorescence (Figures 2C and 2D).

3.2.2. VEGF165 protein levels in EPCs

VEGF protein expression was confirmed by ELISA. As shown in Figure 3, the VEGF protein level in group A was higher than that in group B ($p < 0.05$) and group C ($p < 0.05$). Moreover, the level increased significantly after 3 days, reaching 1,255 pg/mL after 7 days.

3.3. Assay of EPC adhesion

To investigate the possibility that pcDNA 3.0-hVEGF165-transfected EPCs alter the adhesion of EPCs, an adhesion assay was performed. EPC adhesion was significantly enhanced in the pcDNA 3.0-hVEGF165-transfected EPCs (66.2 ± 6.4 , Figure 4) compared to the null-plasmid-transfected EPCs (33.5 ± 4.4) and nontransfected EPCs (35.7 ± 6.3).

3.4. Assay of EPC migration

The influence of VEGF165-transfected EPC migration was analyzed in a transwell chamber assay. As shown in Figure 5, the migration of EPCs was significantly enhanced in group A (43.6 ± 2.5) compared to group B (19.8 ± 2.8) and group C (17.6 ± 3.2) ($p < 0.01$).

3.5. Assay of EPC proliferation

The MTT assay was used to detect the proliferative activity of transfected EPCs. The *in vitro* proliferative

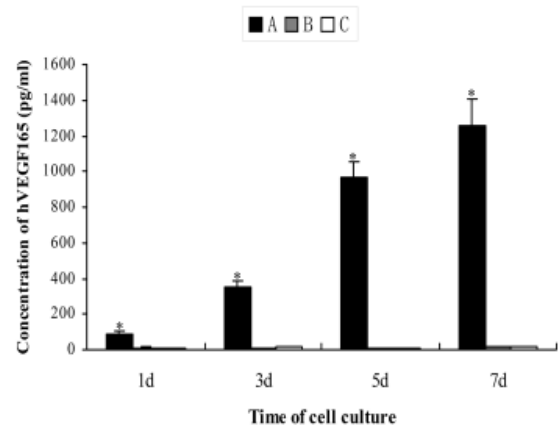


Figure 3. ELISA detection of VEGF165 protein levels in EPCs. VEGF protein expression was detected with ELISA. VEGF protein level in group A was higher than that in group B and group C. Moreover, the VEGF protein level increased significantly ($*p < 0.05$, A vs. B and C; $n = 5$ different samples in each group) after 3 days, reaching 1,255 pg/mL after 7 days. Data are presented as mean \pm S.D. Statistical analysis was performed using ANOVA followed by the Turkey multiple comparison test.

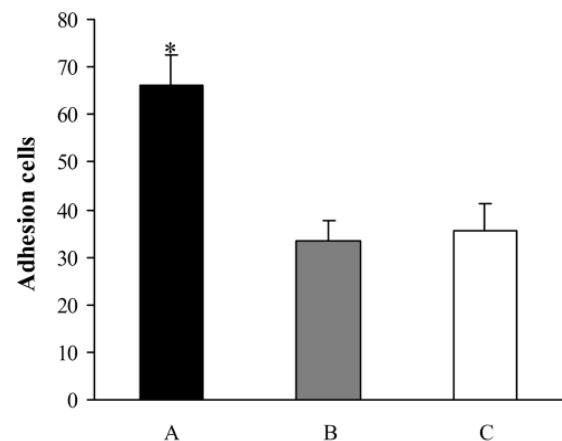


Figure 4. Assay of EPC adhesion. To investigate the possibility that the pcDNA 3.0-hVEGF165-transfected EPCs alters the adhesion of EPCs, an adhesion assay was performed. Compared with the null-plasmid transfected EPCs and nontransfected EPCs, EPC adhesion was significantly enhanced ($*p < 0.05$, A vs. B and C; $n = 5$ different samples in each group) in the pcDNA 3.0-hVEGF165-transfected EPCs. Data are presented as mean \pm S.D. Statistical analysis was performed using ANOVA followed by the Turkey multiple comparison tests.

activity of the pcDNA 3.0-hVEGF165-transfected EPCs (0.53 ± 0.04) was greater than that of the null-plasmid-transfected EPCs (0.35 ± 0.02) and nontransfected EPCs (0.31 ± 0.02) ($p < 0.05$). The proliferative activity of null-plasmid-transfected EPCs was similar to that of nontransfected EPCs (Figure 6).

4. Discussion

In the present study, EPCs derived from peripheral blood of rabbits were successfully transfected with the pcDNA 3.0-hVEGF165 gene. The expression of

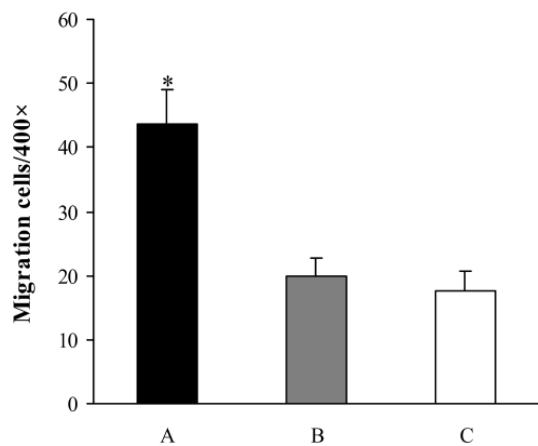


Figure 5. Assay of EPC migration. The influence of VEGF165-transfected EPC migration was analyzed in a transwell chamber assay. Using light microscopy (400-fold magnification), the numbers of EPCs that had migrated to the lower surface of the membrane were counted in five random fields in five domains. EPC migration was significantly enhanced ($*p < 0.05$, A vs. B and C; $n = 5$ different fields in each group) in group A compared to group B and group C. Data are presented as mean \pm S.D. Statistical analysis was performed using ANOVA followed by the Turkey multiple comparison test.

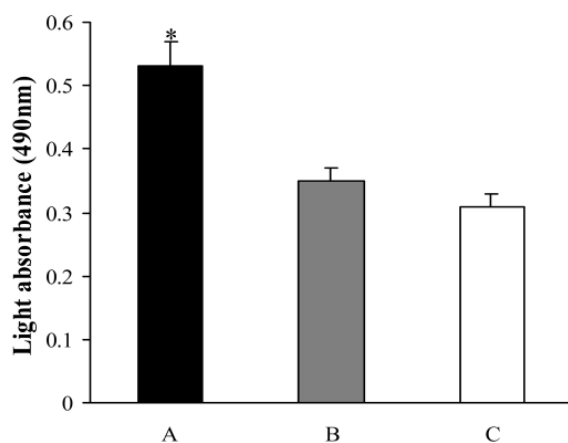


Figure 6. MTT assay of EPC proliferation. The MTT assay was used to detect the proliferative activity of transfected EPCs. The *in vitro* proliferative activity of pcDNA 3.0-hVEGF165-transfected EPCs was greater than that of null-plasmid transfected EPCs and nontransfected EPCs. The proliferative activity of null-plasmid transfected EPCs was similar to that of nontransfected EPCs ($*p < 0.05$, A vs. B and C; $n = 6$ different samples in each group). Data are presented as mean \pm S.D. Statistical analysis was performed using ANOVA followed by the Turkey multiple comparison test.

VEGF165 increased significantly in EPCs transfected with the *hVEGF165* gene. Moreover, EPCs transfected with the *hVEGF165* gene had significantly enhanced adhesion, migration, and proliferative ability.

Previous studies indicated that EPCs harvested from the peripheral circulation proliferated *ex vivo* and EPCs transplanted *in vivo* play an important role in angiogenesis and repair of injured endothelium (12-14). More recent findings suggest that transplantation of circulating EPCs into an injured vascular wall has

beneficial effects on vascular structure and function (15-18). Transplantation of EPCs derived from peripheral blood thus constitutes a novel therapeutic strategy that could provide a robust source of viable endothelial cells to supplement the contribution of endothelial cells. However, healthy adults only have 2-3/mL of EPCs in peripheral blood. Patients with diabetes who are receiving a transplantation of EPCs have fewer, dysfunctional, and rapidly aging EPCs. Although culture and amplification of EPCs *ex vivo* can increase the quantity and purity of EPCs, EPC dysfunction in the peripheral blood restricted the extensive use of EPCs. Therefore, an important challenge was to provide EPCs of sufficient quantity and function for transplantation.

Gene transfer of EPCs during *in vitro* expansion could be used to achieve phenotypic modulation of EPCs. Furthermore, phenotypic modulation of EPCs might also reduce the number of EPCs required for optimal transplantation after *in vitro* expansion and thus serve to address a practical limitation of EPC transplantation, namely the volume of blood required to extract an optimal number of EPCs for autologous transplantation. A study indicated that VEGF stimulates proliferation, migration, and survival of endothelial cells, in turn facilitating endothelialization with EPCs and recovery of endothelial function (7). A recent study found that EPCs produced and secreted more proangiogenic cytokines, such as VEGF, promoting angiogenesis (6). Because of its short half-life, however, an effective concentration of VEGF cannot be maintained in the blood after injection. The use of *in vitro*-transfected stem cells as vectors for gene therapy has largely solved this problem. A study reported that transplantation of VEGF gene-modified EPCs reduced limb ischemia and improved neovascularization compared to control EPCs. The dose of VEGF-transfected EPCs transplanted was 30 times lower than that of nontransfected EPCs (11).

The current findings showed that hVEGF165 gene-modified EPCs increased the levels of VEGF protein and enhanced the ability of EPCs to adhere, migrate, and proliferate. The results of *in vitro* studies provided potential insights into the mechanisms responsible for the *in vivo* outcomes. First, EPCs transfected with the hVEGF165 may increase overexpression of VEGF, which has paracrine effects that promote the restoration of injured endothelial cells. Previous studies demonstrated that VEGF induced upregulation of certain endothelial cell integrins and matrix proteins (19). Second, EPCs transfected with the *hVEGF165* gene enhance the adhesion, migration, and proliferation of EPCs in the quiescent endothelial cell monolayer, and the survival of EPCs is probably due to the reduced requirement for harvested EPCs. Therefore, EPCs likely operate as vector stem cells, promoting local overexpression of VEGF that may in

turn promote migration, proliferation, and remodeling of differentiated endothelial cells residing in the target tissue.

In conclusion, *in vitro*, EPCs were successfully transfected with the *hVEGF165* gene. The expression of VEGF165 increased and adhesion, migration, and proliferative ability were significantly enhanced in EPCs transfected with the *hVEGF165* gene.

Acknowledgements

This work was supported by the Military, Scientific, and Technological Creativity Fund (Grant No. 11MA022).

References

- Asahara T, Murohara T, Sullivan A, Silver M, van der Zee R, Li T, Witzenbichler B, Schatteman G, Isner JM. Isolation of putative progenitor endothelial cells for angiogenesis. *Science*. 1997; 275:964-967.
- Aicher A, Heeschen C, Mildner-Rihm C, Urbich C, Ihling C, Technau-Ihling K, Zeiher AM, Dimmeler S. Essential role of endothelial nitric oxide synthase for mobilization of stem and progenitor cells. *Nat Med*. 2003; 9:1370-1376.
- Lee SH, Wolf PL, Escudero R, Deutsch R, Jamieson SW, Thistlethwaite PA. Early expression of angiogenesis factors in acute myocardial ischemia and infarction. *N Engl J Med*. 2000; 342:626-633.
- He T, Smith LA, Harrington S, Nath KA, Caplice NM, Katusic ZS. Transplantation of circulating endothelial progenitor cells restores endothelial function of denuded rabbit carotid arteries. *Stroke*. 2004; 35:2378-84.
- Kaushal S, Amiel GE, Guleserian KJ, Shapira OM, Perry T, Sutherland FW, Rabkin E, Moran AM, Schoen FJ, Atala A, Soker S, Bischoff J, Mayer JE Jr. Functional small-diameter neovessels created using endothelial progenitor cells expanded *ex vivo*. *Nat Med*. 2001; 7:1035-1040.
- Cao JP, He XY, Xu HT, Zou Z, Shi XY. Autologous transplantation of peripheral blood-derived circulating endothelial progenitor cells attenuates endotoxin-induced acute lung injury in rabbits by direct endothelial repair and indirect immunomodulation. *Anesthesiology*. 2012; 116:1278-1287.
- He T, Smith LA, Harrington S, Nath KA, Caplice NM, Katusic ZS. Transplantation of circulating endothelial progenitor cells restores endothelial function of denuded rabbit carotid arteries. *Stroke*. 2004; 35:2378-2384.
- Ferrara N, Henzel WJ. Pituitary follicular cells secrete a novel heparin-binding growth factor specific for vascular endothelial cells. *Biochem Biophys Res Commun*. 1989; 161:851-858.
- Ennett AB, Kaigler D, Mooney DJ. Temporally regulated delivery of VEGF *in vitro* and *in vivo*. *J Biomed Mater Res A*. 2006; 79:176-184.
- Ferrara N, Houck K, Jakeman L, Leung DW. Molecular and biological properties of the vascular endothelial growth factor family of proteins. *Endocr Rev*. 1992; 13:18-32.
- Iwaguro H, Yamaguchi J, Kalka C, *et al*. Endothelial progenitor cell vascular endothelial growth factor gene transfer for vascular regeneration. *Circulation*. 2002; 105:732-738.
- Kawamoto A, Gwon H-C, Iwaguro H, *et al*. Therapeutic potential of *ex vivo* expanded endothelial progenitor cells for myocardial ischemia. *Circulation*. 2001; 103:634-637.
- Walter DH, Rittig K, Bahlmann FH, Kirchmair R, Silver M, Murayama T, Nishimura H, Losordo DW, Asahara T, Isner JM. Statin therapy accelerates reendothelialization: a novel effect involving mobilization and incorporation of bone marrow-derived endothelial progenitor cells. *Circulation*. 2002; 105:3017-3024.
- Strehlow K, Werner N, Berweiler J, Link A, Dirnagl U, Priller J, Laufs K, Ghaeni L, Milosevic M, Bohm M, Nickenig G. Estrogen increases bone marrow-derived endothelial progenitor cell production and diminishes neointima formation. *Circulation*. 2003; 107:3059-3065.
- Gulati R, Jevremovic D, Peterson TE, Witt TA, Kleppe LS, Mueske CS, Lerman A, Vile RG, Simari RD. Autologous culture-modified mononuclear cells confer vascular protection after arterial injury. *Circulation*. 2003; 108:1520-1526.
- Griese DP, Ehsan A, Melo LG, Kong D, Zhang L, Mann MJ, Pratt RE, Mulligan RC, Dzau VJ. Isolation and transplantation of autologous circulating endothelial cells into denuded vessels and prosthetic grafts: Implications for cell-based vascular therapy. *Circulation*. 2003; 108:2710-2715.
- Werner N, Junk S, Laufs U, Link A, Walenta K, Bohm M, Nickenig G. Intravenous transfusion of endothelial progenitor cells reduces neointima formation after vascular injury. *Circ Res*. 2003; 93:17-24.
- Lam CF, Liu YC, Hsu JK, Yeh PA, Su TY, Huang CC, Lin MW, Wu PC, Chang PJ, Tsai YC. Autologous transplantation of endothelial progenitor cells attenuates acute lung injury in rabbits. *Anesthesiology*. 2008; 108:392-401.
- Senger DR, Ledbetter SR, Claffey KP, *et al*. Stimulation of endothelial cell migration by vascular permeability factor/vascular endothelial growth factor through cooperative mechanisms involving the $\alpha v \beta 3$ integrin, osteopontin, and thrombin. *Am J Pathol*. 1996; 149:293-305.

(Received September 19, 2012; Revised October 25, 2012; Accepted October 26, 2012)

Increased cerebrovascular resistance after retrograde cerebral perfusion: A Doppler study

Nobuhide Kin^{1,*}, Nagara Ono², Yoshiteru Mori¹, Jun Ninagawa¹, Yoshitsugu Yamada¹

¹Department of Anesthesiology, The University of Tokyo, Bunkyo, Tokyo, Japan;

²Department of Anesthesiology, Mitsui Memorial Hospital, Chiyoda, Tokyo, Japan.

Summary

Deep hypothermic circulatory arrest (DHCA) with retrograde cerebral perfusion (RCP) under high central venous pressure (CVP) is often used in aortic arch surgery under cardiopulmonary bypass (CPB). We hypothesized that DHCA with RCP under high CVP causes cerebral vascular compression because of increased perivascular pressure due to extravasation of fluid into intracranial tissue. In a retrospective study, we evaluated the pulsatility index (PI) and resistance index (RI) of the internal carotid arteries (ICA) and external carotid arteries (ECA) before and after CPB in 15 patients who underwent DHCA/RCP (group 1) and 17 patients who underwent regular CPB without DHCA/RCP (group 2). Both indices are known to reflect vascular resistance distal to the measurement point. The PI and RI of the ICA increased significantly after the procedure in group 1 but did not change in group 2. The PI and RI of the ECA did not change in either group. In group 1, the rate of increase in PI and RI correlated with the duration of RCP, which was significantly higher in patients who had postoperative delirium than in patients who did not experience postoperative delirium. As increases in PI/RI after DHCA/RCP occurred only in the ICA, we concluded that the changes were due to compression of vessels as a result of increased perivascular pressure. The greater increase in the PI/RI in patients who experienced postoperative delirium indicates that increased perivascular pressure plays a role in the occurrence of postoperative delirium after DHCA/RCP.

Keywords: Pulsatility index, resistance index, transesophageal echocardiography, delirium

1. Introduction

In complicated thoracic aortic surgeries using cardiopulmonary bypass (CPB), circulatory arrest is needed to obtain a bloodless surgical field (1). During circulatory arrest, either selective cerebral perfusion (SCP) or retrograde cerebral perfusion (RCP) with deep hypothermia is performed for cerebral protection (2). SCP is employed in many institutions but requires extra arterial cannulation and, in some cases, an extra arterial pump; thus, it is relatively complicated and time-consuming (3). In contrast, RCP can be instituted easily just by clamping the venous drainage tube of the inferior vena cava (IVC), snaring the superior vena

cava (SVC) cannula, and counter-rotating the CPB pump (4). However, this method is associated with two major concerns: insufficient cerebral oxygen supply (5) and cerebral edema with increased intracranial pressure due to high venous pressure (6). Cerebral edema caused by RCP has been found in animal models (6,7) but not specifically in humans. Because the intracranial space is limited by the cranium, cerebral edema can cause pressurization of the non-parenchymal area, vessels, and cerebral ventricles. When intracranial vessels are pressurized from the outside, their vascular resistance increases (8,9).

In the current study, Doppler echocardiography was used to evaluate the carotid arteries to determine whether cerebral vessel resistance increases after RCP. Intra-operative transesophageal echocardiography (TEE) was performed during the surgeries except where contraindicated. Carotid artery flow was detected with a TEE probe at the pharynx (10,11). In some patients, blood flow was followed distal to the carotid

*Address correspondence to:

Dr. Nobuhide Kin, Department of Anesthesiology, The University of Tokyo, 7-3-1 Hongo, Bunkyo, Tokyo, 113-8655, Japan.

E-mail: nkin-tyk@umin.net

bifurcation between the ICA and ECA. The peak systolic velocity (PSV), end-diastolic velocity (EDV), and mean velocity (MV) were measured using pulsed-wave Doppler ultrasound (12,13). The pulsatility index (PI) and resistance index (RI) are known to reflect vascular resistance distal to the position where the Doppler signal is received (14,15). PI is calculated as $(PSV-EDV)/MV$ and RI as $(PSV-EDV)/PSV$. PI and RI were used to determine whether signs of increased cerebral vascular resistance were present after RCP.

2. Materials and Methods

2.1. Patients

This study was approved by the internal review board of the University of Tokyo Hospital. Informed consent was waived because of the retrospective nature of the study. Written informed consent for intra-operative TEE was obtained preoperatively. Data used were from carotid artery Doppler flow studies of 32 adult patients who underwent cardiovascular surgery at this institution between July 2008 and October 2010.

2.2. Data collection

Baseline Doppler data were collected when the TEE probe was inserted into the patient's esophagus. Post-CPB Doppler data were obtained just before the TEE probe was withdrawn from the patient's esophagus at the end of surgery. The carotid arteries were evaluated whenever they were easily visualized at the time of probe insertion and withdrawal to ensure that no pathology in these vessels was missed before surgery and that no new lesion was present after the surgery. The carotid artery was identified on one side or the other and traced peripherally towards the carotid bulb using color flow Doppler imaging. After the bifurcation at the carotid bulb, the vessel with flow parallel to the Doppler beam was the ICA, and the vessel with flow at an oblique angle to the Doppler beam was the ECA (11). Blood flow in the ICA and ECA was recorded using pulsed-wave Doppler. At least three consecutive heartbeats were recorded and the average PI and RI calculated. Heart rate (HR), mean arterial blood pressure (MAP), hematocrit, and PaCO₂ were also recorded at the time of the Doppler measurements. Data from patients who were not in sinus or atrial pacing rhythm were excluded from analysis.

RCP was used in all cases in which deep hypothermic circulatory arrest (DHCA) was employed (group 1). When the tympanic temperature reached 18°C, CPB pump flow was stopped and the aortic aneurysm opened. RCP was performed by perfusing oxygenated blood through the SVC cannula as the IVC cannula was occluded and the SVC snared (16). The CPB flow rate was adjusted and periodically

changed from 150 mL/min to 800 mL/min every 30 sec to vary the SVC pressure from 25 mmHg to 35 mmHg. This is designated 'RCP with intermittent pressure augmentation (IPA-RCP)' (17,18) and was used in all RCP cases. The target for the lowest rectal temperature during regular CPB without DHCA (group 2) was 32°C. In both groups, general anesthesia was induced with 5 mg/kg thiopental and 2 mcg/kg fentanyl, and end-tracheal intubation was facilitated with 0.1 mg/kg vecuronium. Anesthesia was maintained with 1% to 2% of sevoflurane and supplemental fentanyl. No additional medication for neuroprotection was given. The α -stat method of pH control was used in all cases. At the time of aorta cross-clamp release, low doses of catecholamine (dopamine 3-5 mcg/kg/min) and vasodilators (nitroglycerin 0.3-0.5 mcg/kg/min, nicardipine 0.5-1 mg/h) were started and continued until after the patients were transferred to the intensive care unit.

Bilateral cerebral oxygen saturation (ScO₂) was monitored continuously in all patients using near infrared spectroscopy (NIRO 200, Hamamatsu Photonics, Hamamatsu, Japan). ScO₂ values usually decrease during CPB and return to pre-operative values after termination of CPB. The change from the baseline, when initial PI and RI data were collected, was calculated for the minimal value during CPB and for the value at the end of surgery, when post-CPB PI and RI data were collected. The presence of postoperative delirium was determined by reviewing patient records from the intensive care unit after surgery.

2.3. Statistical analysis

Analysis of variance (ANOVA) with the Best-Hsu's MCB test was used to compare groups 1 and 2. Wilcoxon matched-pair sign-rank tests were used to compare the baseline and post-CPB values in each group.

3. Results

3.1. Patient demographics

The mean patient age was 65.3 ± 17.5 years. Of the 32 patients, 22 (69%) were male. Twenty-two patients underwent thoracic aortic surgery ($n = 15$ in group 1 and $n = 7$ in group 2). Ten patients underwent valve surgery with regular CPB ($n = 15$ in group 1 and $n = 17$ in group 2). Operating time, CPB time, and the total amount of fentanyl did not differ in groups 1 and 2 (Table 1). In both groups, HR was higher and the bispectral index (BIS) was lower after CPB compared to the baseline, but MAP, hematocrit, end-tidal sevoflurane, nasopharyngeal temperature, and PaCO₂ did not differ before and after CPB in either group or between the two groups (Table 2). The doses

Table 1. Operating, CPB, and RCP time

Items	Group 1 (n = 15)	Group 2 (n = 17)	p-value
Operating time (min)	435 ± 119	381 ± 108	0.2545
CPB time (min)	213 ± 55	188 ± 79	0.2847
Total amount of fentanyl (mcg/kg)	19 ± 18	23 ± 11	0.3626
DHCA time (min)	61 ± 23	N/A	N/A
RCP time (min)	53 ± 35	N/A	N/A

Data reported as means ± standard deviation. CPB, cardiopulmonary bypass; RCP, retrograde cerebral perfusion; DHCA, deep hypothermic circulatory arrest; N/A, not applicable.

Table 2. Vital signs and blood gas analysis

Items	Group 1 (n = 15)		Group 2 (n = 17)	
	Baseline	Post CPB	Baseline	Post CPB
HR (beat/min)	61 ± 10	81 ± 13*	62 ± 8	88 ± 15*
MAP (mmHg)	63 ± 15	79 ± 18	72 ± 16	76 ± 13
Hematocrit (%)	32.9 ± 3.8	32.2 ± 3.3	32.4 ± 3.7	32.0 ± 3.9
PaCO ₂ (mmHg)	39.5 ± 5.8	37.6 ± 6.2	38.5 ± 3.6	39.9 ± 4.8
EtSEV (%)	1.0 ± 0.4	1.0 ± 0.9	1.2 ± 0.6	1.1 ± 0.8
BIS	53 ± 8.2	41 ± 9.5*	49 ± 10.1	39 ± 11.3*
TEMP naso (°C)	35.5 ± 0.6	36.0 ± 0.9	35.9 ± 0.7	36.1 ± 0.8

Data reported as mean ± standard deviation. HR, heart rate; MAP, mean arterial pressure; EtSEV, end-tidal sevoflurane; BIS, bispectral index; TEMP naso, nasopharyngeal temperature; CPB, cardiopulmonary bypass; DHCA, deep hypothermic circulatory arrest; RCP, retrograde cerebral perfusion. * $p < 0.05$ between the baseline and post-CPB in each group.

of catecholamine and vasodilators administered in the operating room did not differ for the groups.

3.2. PI and RI of ICA and ECA

The baseline PI and RI of the ICA did not differ between groups 1 and 2, but the post-CPB PI and RI of the ICA were higher in group 1 than in group 2. In the ECA, neither the baseline indices nor post-CPB PI and RI differed between the two groups. In group 1, the PI and RI of the ICA increased significantly after CPB compared to the baseline, but in group 2 the indices did not change after CPB. The PI and RI of the ECA did not change significantly after CPB in either group (Table 3, Figure 1). No patient suffered permanent neurological damage after the procedure. However, eight patients (four in each group) had temporary postoperative delirium while in the intensive care unit. Patients who experienced delirium were significantly older (75.0 vs. 61.4 years old, $p < 0.05$) than patients who did not experience delirium. The operating time, CPB time, hematocrit, MAP, ScO₂, and BIS did not differ between the patients who experienced delirium and patients who did not. In group 1, the patients who experienced delirium tended to be older (68.8 vs. 58.0 years, $p > 0.05$) and have a longer RCP time (37.8 vs. 87.5 min, $p < 0.05$) than the patients who did not experience delirium. Patients with delirium tended to have a higher post-CPB PI and RI of the ICA, and the increase in the PI and RI of the ICA after CPB was significantly higher

Table 3. Pulsatility and resistance indices of the internal carotid artery (a) and the external carotid artery (b)

(a)	PI		RI	
	Baseline	Post-CPB	Baseline	Post-CPB
ICA				
Group 1 (n = 15)	1.53 ± 0.48	2.13 ± 0.67*	0.73 ± 0.11	0.84 ± 0.09*
Group 2 (n = 17)	1.78 ± 0.50	1.73 ± 0.48 [#]	0.77 ± 0.08*	0.75 ± 0.07 [#]

(b)	PI		RI	
	Baseline	Post-CPB	Baseline	Post-CPB
ECA				
Group 1 (n = 15)	2.05 ± 0.53	1.97 ± 0.54	0.83 ± 0.06	0.82 ± 0.07
Group 2 (n = 17)	1.87 ± 0.51	1.95 ± 0.58	0.83 ± 0.09	0.85 ± 0.10

Data reported as mean ± standard deviation. ICA, internal carotid artery; PI, pulsatility index; RI, resistance index; CPB, cardiopulmonary bypass; ECA, external carotid artery. * $p < 0.05$ between the baseline and post-CPB. [#] $p < 0.05$ between group 1 and group 2.

than that in patients who did not experience delirium (Table 4). Moderate correlations were found between RCP time and increased ICA PI and RI (Figure 2). In group 2, the PI/RI of the patients who experienced delirium did not differ from the PI/RI of the patients who did not experience delirium.

3.3. ScO₂ changes

The average change in right and left ScO₂ from the baseline to the minimum value during CPB was significantly larger in group 1 than in group 2, but it did not differ between the two groups from the baseline to the end of surgery (Table 5). In group 1, the average change in right and left ScO₂ from the baseline to the minimum value during CPB did not differ between patients who experienced delirium and patients who did not (39.2 vs. 34.4%, $p > 0.05$). No correlation was found between the extent of the increase in PI/RI and the average change in ScO₂ from the baseline to the minimum value during CPB in group 1.

4. Discussion

In the present retrospective study, the PI and RI of the ICA, but not of the ECA, increased after CPB when DHCA with RCP was used. As the PI and RI are known to reflect resistance distal to the measurement point (14,15), results indicated that DHCA with RCP, but not regular CPB without DHCA, increases the resistance of cerebral vessels distal to the ICA.

Cerebral blood flow and cerebrovascular resistance are affected by many factors, including cerebral electrophysiological activity, MAP, hematocrit, PaCO₂, temperature, anesthetics, catecholamines, and vasodilators (20-23). BIS decreased during CPB, possibly reflecting reduced cerebral electrophysiological activity. Such activity can reduce cerebral blood flow and increase cerebrovascular resistance. The increase in HR after CPB may have

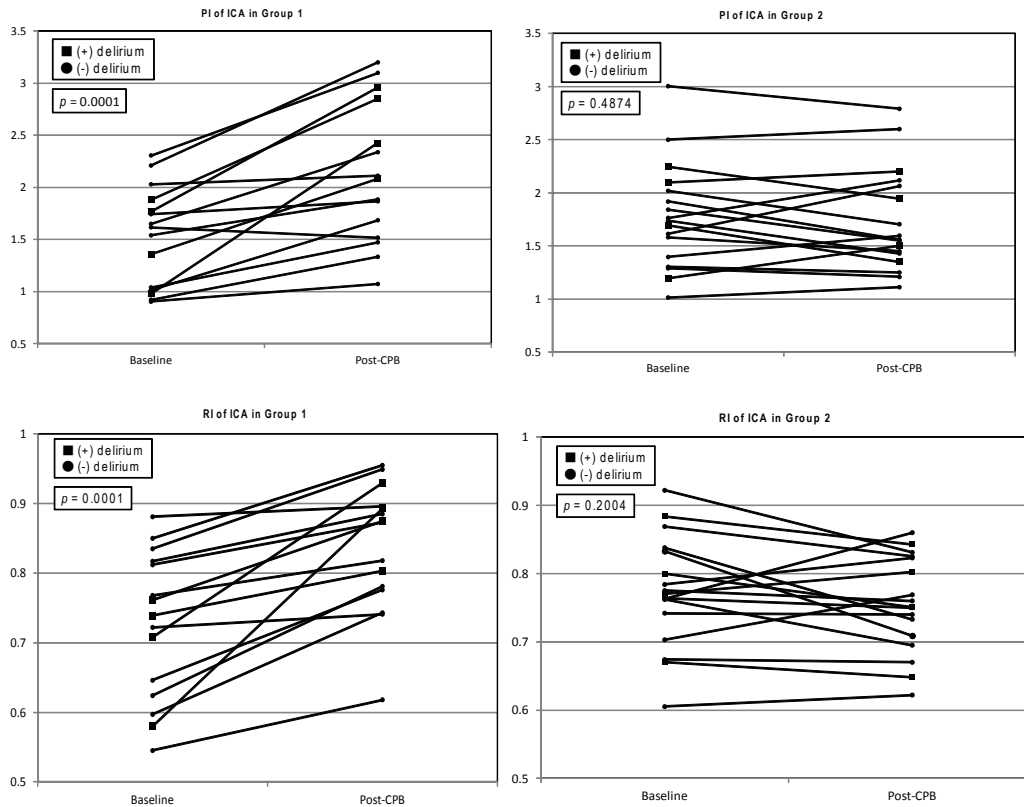


Figure 1. Pulsatility indices (PI) and resistance indices (RI) of the internal carotid artery (ICA) in group 1 (CPB with DHCA/RCP) and in group 2 (regular CPB without DHCA/RCP) patients.

Table 4. Pulsatility and resistance indices of the internal carotid artery of the patients in Group 1

Items	PI			RI		
	Baseline	Post-CPB	PI ratio	Baseline	Post-CPB	RI ratio
Delirium (-) (n = 11)	1.54 ± 0.51	2.16 ± 0.29*	1.30 ± 0.22	0.74 ± 0.12	0.81 ± 0.03*	1.12 ± 0.08
Delirium (+) (n = 4)	1.50 ± 0.41	2.43 ± 0.46*	1.80 ± 0.46 [#]	0.70 ± 0.08	0.87 ± 0.05*	1.27 ± 0.20 [#]

Data reported as mean ± standard deviation. PI, pulsatility index; RI, resistance index; CPB, cardiopulmonary bypass. PI ratio = (post-CPB PI)/(baseline PI); RI ratio = (post-CPB RI)/(baseline RI). * $p < 0.05$ between the baseline and post-CPB. [#] $p < 0.05$ between Delirium (-) and Delirium (+).

affected the PI and RI, but the similar changes in BIS and HR in both groups do not explain why the PI and RI of the ICA increased only in group 1. Similar doses of fentanyl, catecholamine, and vasodilators were given to patients in both groups, so they should not have affected the groups differently. In addition, MAP, hematocrit, PaCO₂, end-tidal sevoflurane, and nasopharyngeal temperature did not differ between the baseline and the end of surgery. Thus, the increase in cerebrovascular resistance after DHCA with RCP was a result of some other factor(s).

One explanation is that DHCA with RCP may have increased the basic tone of the vessels. If vessels become hypercontractile, the PI and RI of the ECA would be similarly affected by the elevated capillary pressure. Since the indices did not change significantly after CPB in group 1, increased vascular tone is not likely to be a major mechanism. Another possible explanation is an increase in perivascular interstitial

pressure around the vessel. During RCP, the SVC pressure was increased up to 35 mmHg. With this high pressure, fluid extravasation probably occurs from the venous lumen through the vessel wall into the extravascular space. Because the intracranial space is limited, extravasation of fluid into the cerebral parenchyma would cause an exaggerated increase in the perivascular pressure and compress the extraparenchymal arteries and parenchymal arterioles, which are major resistance vessels (24,25). This scenario would lead to increased PI and RI in the ICA. DHCA with RCP could also have caused edema in the extracranial tissue, but unlike the intracranial space, the extracranial space is not limited by the cranium. Thus, tissue edema would not pressurize the arteries and arterioles and the PI and RI of the ECA would not increase.

Four of the five patients who had a RCP time of more than one hour experienced postoperative delirium.

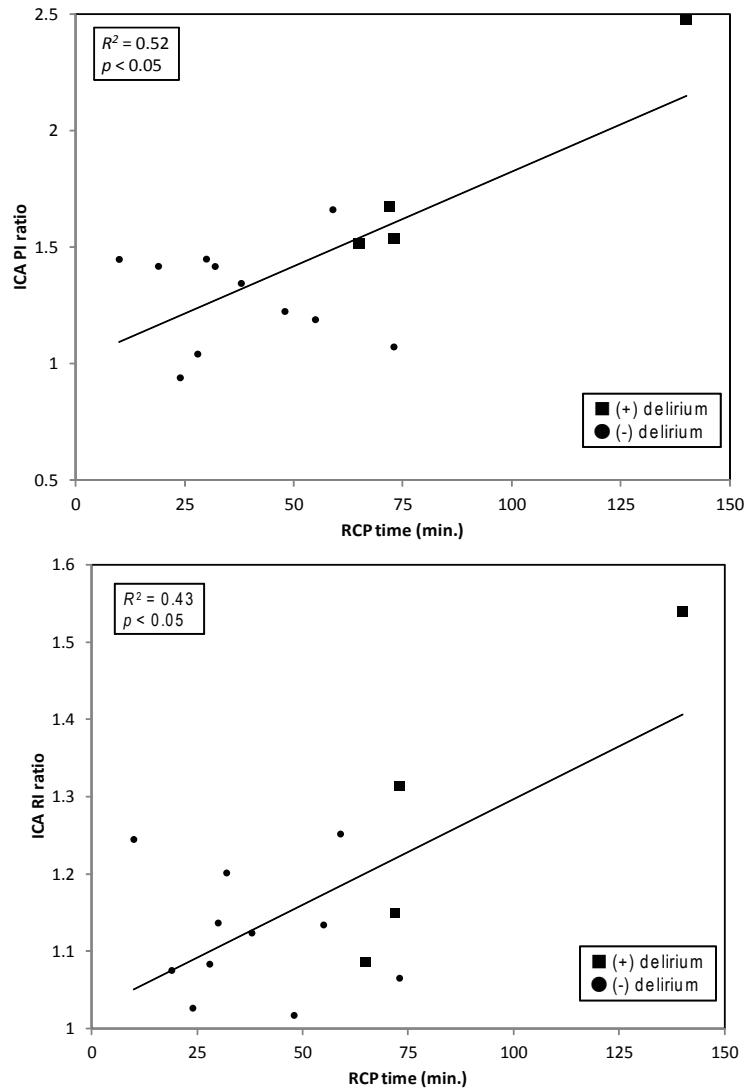


Figure 2. Relationship between the retrograde cerebral perfusion (RCP) time and the pulsatility index ratio (PI) and resistance index (RI) ratio of the post-CPB to the baseline.

Table 5. Change in ScO₂ from the baseline (%)

Items	Min. during CPB	End of surgery
Group 1 (n = 15)	-35.6 ± 14.3	-1.1 ± 9.4
Group 2 (n = 17)	-20.0 ± 8.4 [#]	-4.4 ± 8.4

Data reported as mean ± standard deviation. Min. = the minimum value. [#]p < 0.05 between group 1 and 2.

A moderate correlation was found between the change in the PI/RI of the ICA and the duration of RCP. Moreover, four of the five patients whose PI increased more than 50% after DHCA with RCP experienced postoperative delirium. This finding indicates that increased perivascular pressure may play some role in causing delirium after DHCA with RCP. RCP causes cerebral edema in animal models (6,7). Although this trend has not been verified in humans, a central venous pressure (CVP) as high as 35 mmHg is speculated to cause extravasation of fluid from intracranial blood vessels. In both groups, the patients who experienced delirium tended to be older. Patient age has been

shown to be an important factor in the occurrence of delirium after cardiac surgery. Other factors associated with postoperative delirium include renal impairment, chronic lung disease, extracardiac arteriopathy, poor mobility, and electrolyte disturbances (26). In the present retrospective study, RCP duration tended to be longer for older patients. Most likely, patient age and other factors, and not the increased perivascular pressure itself, were the major causes of postoperative delirium.

ScO₂ was monitored with near infrared spectroscopy in all cases. A number of studies have shown that RCP may not provide enough oxygen to the brain during DHCA (27-30), which is consistent with the current findings although the two groups had a similar incidence of postoperative delirium. In group 1, the decrease in ScO₂ during CPB was not related to the occurrence of postoperative delirium. Thus, cerebral ischemia during DHCA with RCP may not be a major cause of postoperative delirium.

No patient underwent DHCA without RCP because performing DHCA without any measure aimed at providing oxygen to the brain is not standard practice. As selective antegrade cerebral perfusion was not performed at this institution during the period studied, data on this method are not available.

The PI and RI data for the ICA and ECA were collected from only some of the patients who underwent intra-operative TEE. Some patients had a high bifurcation of the ICA and ECA and each vessel could not be followed with the TEE probe. In addition, only one side of the carotid artery could be examined in some patients, which was probably due to the acoustic effect of the endotracheal tube. Therefore, the laterality of the change could not always be assessed.

Doppler flow data can be obtained for the ICA and ECA by transcutaneous carotid artery sonography rather than a TEE probe, but using a hand-held probe under all the surgical drapes and instruments is cumbersome and carries the risk of contaminating the sterile surgical field. In addition, checking the carotid artery flow intra-operatively, especially during aortic arch surgery, has other advantages, such as the detection of carotid malperfusion during CPB, finding a carotid dissection resulting from aortic cannulation, and confirming that debris is not flowing distally in the carotid artery at the time of aortic manipulation (31). Such intra-operative carotid monitoring can also be used during cannulation of the internal jugular vein (32). The current study suggests that monitoring carotid artery flow could also be used to detect potentially abnormal cerebrovascular dynamics.

In conclusion, the PI and RI of the ICA, but not of the ECA, increased after DHCA with RCP. These indices did not change after regular CPB without DHCA. Because the PI and RI are indicators of vascular resistance distal to the measurement site, these results indicate that cerebral vascular resistance increases after DHCA with RCP but does not change after regular CPB. This phenomenon can be explained by increased perivascular pressure, which potentially contributes to delirium after cardiac surgery with DHCA and RCP.

References

1. Graham JM, Stinnett DM. Operative management of acute aortic arch dissection using profound hypothermia and circulatory arrest. *Ann Thorac Surg.* 1987; 44:192-198.
2. Bachet J, Guilmet D. Brain protection during surgery of the aortic arch. *J Card Surg.* 2002; 17:115-124.
3. Ogino H, Sasaki H, Minatoya K, Matsuda H, Tanaka H, Watanuki H, Ando M, Kitamura S. Evolving arch surgery using integrated antegrade selective cerebral perfusion: Impact of axillary artery perfusion. *J Thorac Cardiovasc Surg.* 2008; 136:641-648.
4. Ergin MA, Griep RB, Lansman SL, Galla JD, Levy M, Griep RB. Hypothermic circulatory arrest and other methods of cerebral protection during operations on the

- thoracic aorta. *J Card Surg.* 1994; 9:525-537.
5. Griep RB, Juvonen T, Griep EB, McCollough JN, Ergin MA. Is retrograde cerebral perfusion an effective means of neural support during deep hypothermic circulatory arrest? *Ann Thorac Surg.* 1997; 64:913-916.
6. Usui A, Oohara K, Liu TL, Murase M, Tanaka M, Takeuchi E, Abe T. Determination of optimum retrograde cerebral perfusion conditions. *J Thorac Cardiovasc Surg.* 1994; 107:300-308.
7. Oshikiri N, Watanabe T, Saitou H, Iijima Y, Minowa T, Inui K, Shimazaki Y. Retrograde cerebral perfusion: experimental approach to brain oedema. *Perfusion.* 1999; 14:257-262.
8. Lupetin AR, Davis DA, Beckman I, Dash N. Transcranial Doppler sonography. Part 1. Principles, technique, and normal appearances. *Radiographics.* 1995; 15:179-191.
9. Bellner J, Romner B, Reinstrup P, Kristiansson KA, Ryding E, Brandt L. Transcranial Doppler sonography pulsatility index (PI) reflects intracranial pressure (ICP). *Surg Neurol.* 2004; 62:45-51
10. Nanda NC, Miller AP, Nekkanti R, Aaluri S. Transpharyngeal echocardiographic imaging of the right and left carotid arteries. *Echocardiography.* 2001; 18:711-716.
11. Khanna D, Sinha A, Nanda NC, Gupta R, Sidhu M, Vengala S, Dod HS, Ilgenli TF. Transesophageal and transpharyngeal ultrasound demonstration of reversed diastolic flow in aortic arch branches and neck vessels in severe aortic regurgitation. *Echocardiography.* 2004; 21:349-353.
12. Juul R, Aakhus S, Bjornstad K, Gisvold SE, Brubakk AO, Edvinsson L. Calcitonin gene-related peptide (human α -CGRP) counteracts vasoconstriction in human subarachnoid haemorrhage. *Neurosci Lett.* 1994; 170:67-70.
13. Touati GD, Roux N, Carmi D, Carmi D, Szymanski C, Barry M, Trojette F, Caus T. Totally normothermic aortic arch replacement without circulatory arrest. *Ann Thorac Surg.* 2003; 76:2115-2117.
14. Albayrak R, Degirmenci B, Acar M, Haktanir A, Colbay M, Yaman M. Doppler sonography evaluation of flow velocity and volume of the extracranial internal carotid and vertebral arteries in healthy adults. *J Clin Ultrasound.* 2007; 35:27-33.
15. Bor-Seng-Shu E, Hirsch R, Teixeira MJ, De Andrade AF, Marino R. Cerebral hemodynamic changes gauged by transcranial Doppler ultrasonography in patients with posttraumatic brain swelling treated by surgical decompression. *J Neurosurg.* 2006; 104:93-100.
16. Reich DL, Uysal S, Ergin MA, Griep RB. Retrograde cerebral perfusion as a method of neuroprotection during thoracic aortic surgery. *Ann Thorac Surg.* 2001; 72:1774-1782.
17. Kawata M, Sekino M, Takamoto S, Ueno S, Yamaguchi S, Kitahori K, Tsukihara H, Suematsu Y, Ono M, Motomura N, Morota T, Murakami A. Retrograde cerebral perfusion with intermittent pressure augmentation provides adequate neuroprotection: Diffusion- and perfusion-weighted magnetic resonance imaging study in an experimental canine model. *J Thorac Cardiovasc Surg.* 2006; 132:933-940.
18. Kitahori K, Takamoto S, Takayama H, Suematsu Y, Ono M, Motomura N, Morota T, Takeuchi, K. A novel protocol of retrograde cerebral perfusion with intermittent pressure augmentation for brain protection. *J*

- Thorac Cardiovasc Surg. 2005; 130:363-370.
19. Yasuura K, Takagi Y, Oohara Y, Takami Y. Total body retrograde perfusion during operations on the descending thoracic aorta. *J Thorac Cardiovasc Surg.* 1999; 118:559-561.
 20. Bruder N, Cohen B, Pellissier D, Francois G. The effect of hemodilution on cerebral blood flow velocity in anesthetized patients. *Anesth Analg.* 1998; 86:320-324.
 21. Doblar DD, Frenette L, Poplawski S, Gelman S, Boyd G, Ranjan D, Halsey JH. Middle cerebral artery transcranial Doppler velocity monitoring during orthotopic liver transplantation: Changes at reperfusion—a report of six cases. *J Clin Anesth.* 1993; 5:479-485.
 22. Sulek CA, Blas ML, Lobato EB. Milrinone increases middle cerebral artery blood flow velocity after cardiopulmonary bypass. *J Cardiothorac Vasc Anesth.* 2002; 16:64-69.
 23. Mahmood MA, Voorhees ME, Parnell M, Zweifler RM. Transcranial Doppler ultrasonographic evaluation of middle cerebral artery hemodynamics during mild hypothermia. *J Neuroimaging.* 2005; 15:336-340.
 24. Faraci FM, Heistad DD. Regulation of large cerebral arteries and cerebral microvascular pressure. *Circ Res.* 1990; 66:8-17.
 25. Ngai AC, Nguyen TS, Meno JR, Britz GW. Posts ischemic augmentation of conducted dilation in cerebral arterioles. *Stroke.* 2007; 38:124-130.
 26. Koster S, Oosterveld FG, Hensens AG, Wijma A, van der Palen J. Delirium after cardiac surgery and predictive validity of a risk checklist. *Ann Thorac Surg.* 2008; 86:1883-1887.
 27. Higami T, Kozawa S, Asada T, Obo H, Gan K, Iwahashi K, Nohara H. Retrograde cerebral perfusion *versus* selective cerebral perfusion as evaluated by cerebral oxygen saturation during aortic arch reconstruction. *Ann Thorac Surg.* 1999; 67:1091-1096.
 28. Duebener L, Hagino I, Schmitt K, Sakamoto T, Stamm C, Zurakowski D, Schafers H, Jonas R. Direct visualization of minimal cerebral capillary flow during retrograde cerebral perfusion: An intravital fluorescence microscopy study in pigs. *Ann Thorac Surg.* 2003; 75:1288-1293.
 29. Bonser RS, Wong CH, Harrington D, Pagano D, Wilkes M, Clutton-Brock T, Faroqui M. Failure of retrograde cerebral perfusion to attenuate metabolic changes associated with hypothermic circulatory arrest. *J Thorac Cardiovasc Surg.* 2002; 123:943-950.
 30. Reich DL, Uysal S, Ergin MA, Bodian C, Hossain S, Griep R. Retrograde cerebral perfusion during thoracic aortic surgery and late neuropsychological dysfunction. *Eur J Cardiothorac Surg.* 2001; 19:594-600.
 31. Augoustides JG. Transpharyngeal imaging of the carotid artery and internal jugular vein: Possible roles in cerebral perfusion management during adult aortic arch repair. *J Cardiothorac Vasc Anesth.* 2007; 21:318-319.
 32. Bevilacqua S, Romagnoli S, Ciappi F, Ridolfi N, Codecasa R, Rostagno C, Sorbara C. Transpharyngeal ultrasonography for cannulation of the internal jugular vein. *Anesthesiology.* 2005; 102:873-874.

(Received June 5, 2012; Revised October 2, 2012; Accepted October 16, 2012)

Guide for Authors

1. Scope of Articles

BioScience Trends is an international peer-reviewed journal. BioScience Trends devotes to publishing the latest and most exciting advances in scientific research. Articles cover fields of life science such as biochemistry, molecular biology, clinical research, public health, medical care system, and social science in order to encourage cooperation and exchange among scientists and clinical researchers.

2. Submission Types

Original Articles should be well-documented, novel, and significant to the field as a whole. An Original Article should be arranged into the following sections: Title page, Abstract, Introduction, Materials and Methods, Results, Discussion, Acknowledgments, and References. Original articles should not exceed 5,000 words in length (excluding references) and should be limited to a maximum of 50 references. Articles may contain a maximum of 10 figures and/or tables.

Brief Reports definitively documenting either experimental results or informative clinical observations will be considered for publication in this category. Brief Reports are not intended for publication of incomplete or preliminary findings. Brief Reports should not exceed 3,000 words in length (excluding references) and should be limited to a maximum of 4 figures and/or tables and 30 references. A Brief Report contains the same sections as an Original Article, but the Results and Discussion sections should be combined.

Reviews should present a full and up-to-date account of recent developments within an area of research. Normally, reviews should not exceed 8,000 words in length (excluding references) and should be limited to a maximum of 100 references. Mini reviews are also accepted.

Policy Forum articles discuss research and policy issues in areas related to life science such as public health, the medical care system, and social science and may address governmental issues at district, national, and international levels of discourse. Policy Forum articles should not exceed 2,000 words in length (excluding references).

Case Reports should be detailed reports of the symptoms, signs, diagnosis, treatment, and follow-up of an individual patient. Case reports may contain a demographic profile of the patient but usually describe an unusual or novel occurrence. Unreported or unusual

side effects or adverse interactions involving medications will also be considered. Case Reports should not exceed 3,000 words in length (excluding references).

News articles should report the latest events in health sciences and medical research from around the world. News should not exceed 500 words in length.

Letters should present considered opinions in response to articles published in BioScience Trends in the last 6 months or issues of general interest. Letters should not exceed 800 words in length and may contain a maximum of 10 references.

3. Editorial Policies

Ethics: BioScience Trends requires that authors of reports of investigations in humans or animals indicate that those studies were formally approved by a relevant ethics committee or review board.

Conflict of Interest: All authors are required to disclose any actual or potential conflict of interest including financial interests or relationships with other people or organizations that might raise questions of bias in the work reported. If no conflict of interest exists for each author, please state "There is no conflict of interest to disclose".

Submission Declaration: When a manuscript is considered for submission to BioScience Trends, the authors should confirm that 1) no part of this manuscript is currently under consideration for publication elsewhere; 2) this manuscript does not contain the same information in whole or in part as manuscripts that have been published, accepted, or are under review elsewhere, except in the form of an abstract, a letter to the editor, or part of a published lecture or academic thesis; 3) authorization for publication has been obtained from the authors' employer or institution; and 4) all contributing authors have agreed to submit this manuscript.

Cover Letter: The manuscript must be accompanied by a cover letter signed by the corresponding author on behalf of all authors. The letter should indicate the basic findings of the work and their significance. The letter should also include a statement affirming that all authors concur with the submission and that the material submitted for publication has not been published previously or is not under consideration for publication elsewhere. The cover letter should be submitted in PDF format. For example of Cover Letter, please visit <http://www.biosciencetrends.com/downcentre.php> (Download Centre).

Copyright: A signed JOURNAL PUBLISHING AGREEMENT (JPA) form must be provided by post, fax, or as a scanned file before acceptance of the article. Only forms with a hand-written signature are accepted. This copyright will ensure the widest possible dissemination of information. A form facilitating transfer of copyright can be downloaded by clicking the

appropriate link and can be returned to the e-mail address or fax number noted on the form (Please visit [Download Centre](#)). Please note that your manuscript will not proceed to the next step in publication until the JPA Form is received. In addition, if excerpts from other copyrighted works are included, the author(s) must obtain written permission from the copyright owners and credit the source(s) in the article.

Suggested Reviewers: A list of up to 3 reviewers who are qualified to assess the scientific merit of the study is welcomed. Reviewer information including names, affiliations, addresses, and e-mail should be provided at the same time the manuscript is submitted online. Please do not suggest reviewers with known conflicts of interest, including participants or anyone with a stake in the proposed research; anyone from the same institution; former students, advisors, or research collaborators (within the last three years); or close personal contacts. Please note that the Editor-in-Chief may accept one or more of the proposed reviewers or may request a review by other qualified persons.

Language Editing: Manuscripts prepared by authors whose native language is not English should have their work proofread by a native English speaker before submission. If not, this might delay the publication of your manuscript in BioScience Trends.

The Editing Support Organization can provide English proofreading, Japanese-English translation, and Chinese-English translation services to authors who want to publish in BioScience Trends and need assistance before submitting a manuscript. Authors can visit this organization directly at <http://www.iacmhr.com/iac-eso/support.php?lang=en>. IAC-ESO was established to facilitate manuscript preparation by researchers whose native language is not English and to help edit works intended for international academic journals.

4. Manuscript Preparation

Manuscripts should be written in clear, grammatically correct English and submitted as a Microsoft Word file in a single-column format. Manuscripts must be paginated and typed in 12-point Times New Roman font with 24-point line spacing. Please do not embed figures in the text. Abbreviations should be used as little as possible and should be explained at first mention unless the term is a well-known abbreviation (e.g. DNA). Single words should not be abbreviated.

Title Page: The title page must include 1) the title of the paper (Please note the title should be short, informative, and contain the major key words); 2) full name(s) and affiliation(s) of the author(s), 3) abbreviated names of the author(s), 4) full name, mailing address, telephone/fax numbers, and e-mail address of the corresponding author; and 5) conflicts of interest (if you have an actual or potential conflict of interest to disclose, it must be included as a footnote on the title page of the manuscript; if no conflict of

interest exists for each author, please state "There is no conflict of interest to disclose"). Please visit [Download Centre](#) and refer to the title page of the manuscript sample.

Abstract: A one-paragraph abstract consisting of no more than 250 words must be included. The abstract should briefly state the purpose of the study, methods, main findings, and conclusions. Abbreviations must be kept to a minimum and non-standard abbreviations explained in brackets at first mention. References should be avoided in the abstract. Key words or phrases that do not occur in the title should be included in the Abstract page.

Introduction: The introduction should be a concise statement of the basis for the study and its scientific context.

Materials and Methods: The description should be brief but with sufficient detail to enable others to reproduce the experiments. Procedures that have been published previously should not be described in detail but appropriate references should simply be cited. Only new and significant modifications of previously published procedures require complete description. Names of products and manufacturers with their locations (city and state/country) should be given and sources of animals and cell lines should always be indicated. All clinical investigations must have been conducted in accordance with Declaration of Helsinki principles. All human and animal studies must have been approved by the appropriate institutional review board(s) and a specific declaration of approval must be made within this section.

Results: The description of the experimental results should be succinct but in sufficient detail to allow the experiments to be analyzed and interpreted by an independent reader. If necessary, subheadings may be used for an orderly presentation. All figures and tables must be referred to in the text.

Discussion: The data should be interpreted concisely without repeating material already presented in the Results section. Speculation is permissible, but it must be well-founded, and discussion of the wider implications of the findings is encouraged. Conclusions derived from the study should be included in this section.

Acknowledgments: All funding sources should be credited in the Acknowledgments section. In addition, people who contributed to the work but who do not meet the criteria for authors should be listed along with their contributions.

References: References should be numbered in the order in which they appear in the text. Citing of unpublished results, personal communications, conference abstracts, and theses in the reference list is not recommended but these sources may be mentioned in the text. In the reference list, cite the names of all authors when there are fifteen or fewer authors; if there are sixteen or more authors, list the first three

followed by *et al.* Names of journals should be abbreviated in the style used in PubMed. Authors are responsible for the accuracy of the references. Examples are given below:

Example 1 (Sample journal reference):

Inagaki Y, Tang W, Zhang L, Du GH, Xu WF, Kokudo N. Novel aminopeptidase N (APN/CD13) inhibitor 24F can suppress invasion of hepatocellular carcinoma cells as well as angiogenesis. *Biosci Trends*. 2010; 4:56-60.

Example 2 (Sample journal reference with more than 15 authors):

Darby S, Hill D, Auvinen A, *et al.* Radon in homes and risk of lung cancer: Collaborative analysis of individual data from 13 European case-control studies. *BMJ*. 2005; 330:223.

Example 3 (Sample book reference):

Shalev AY. Post-traumatic stress disorder: diagnosis, history and life course. In: *Post-traumatic Stress Disorder, Diagnosis, Management and Treatment* (Nutt DJ, Davidson JR, Zohar J, eds.). Martin Dunitz, London, UK, 2000; pp. 1-15.

Example 4 (Sample web page reference):

Ministry of Health, Labour and Welfare of Japan. Dietary reference intakes for Japanese. <http://www.mhlw.go.jp/houdou/2004/11/h1122-2a.html> (accessed June 14, 2010).

Tables: All tables should be prepared in Microsoft Word or Excel and should be arranged at the end of the manuscript after the References section. Please note that tables should not in image format. All tables should have a concise title and should be numbered consecutively with Arabic numerals. If necessary, additional information should be given below the table.

Figure Legend: The figure legend should be typed on a separate page of the main manuscript and should include a short title and explanation. The legend should be concise but comprehensive and should be understood without referring to the text. Symbols used in figures must be explained.

Figure Preparation: All figures should be clear and cited in numerical order in the text. Figures must fit a one- or two-column format on the journal page: 8.3 cm (3.3 in.) wide for a single column, 17.3 cm (6.8 in.) wide for a double column; maximum height: 24.0 cm (9.5 in.). Please make sure that the symbols and numbers appeared in the figures should be clear. Please make sure that artwork files are in an acceptable format (TIFF or JPEG) at minimum resolution (600 dpi for illustrations, graphs, and annotated artwork, and 300 dpi for micrographs and photographs). Please provide all figures as separate files. Please note that low-resolution images are one of the leading causes of article resubmission and schedule delays. All color figures will be reproduced in full color in the online edition of the journal at no cost to authors.

Units and Symbols: Units and symbols conforming to the International System

of Units (SI) should be used for physicochemical quantities. Solidus notation (*e.g.* mg/kg, mg/mL, mol/mm²/min) should be used. Please refer to the SI Guide www.bipm.org/en/si/ for standard units.

Supplemental data: Supplemental data might be useful for supporting and enhancing your scientific research and BioScience Trends accepts the submission of these materials which will be only published online alongside the electronic version of your article. Supplemental files (figures, tables, and other text materials) should be prepared according to the above guidelines, numbered in Arabic numerals (*e.g.*, Figure S1, Figure S2, and Table S1, Table S2) and referred to in the text. All figures and tables should have titles and legends. All figure legends, tables and supplemental text materials should be placed at the end of the paper. Please note all of these supplemental data should be provided at the time of initial submission and note that the editors reserve the right to limit the size and length of Supplemental Data.

5. Submission Checklist

The Submission Checklist will be useful during the final checking of a manuscript prior to sending it to BioScience Trends for review. Please visit [Download Centre](#) and download the Submission Checklist file.

6. Online Submission

Manuscripts should be submitted to BioScience Trends online at <http://www.biosciencetrends.com>. The manuscript file should be smaller than 5 MB in size. If for any reason you are unable to submit a file online, please contact the Editorial Office by e-mail at office@biosciencetrends.com.

7. Accepted Manuscripts

Proofs: Galley proofs in PDF format will be sent to the corresponding author via e-mail. Corrections must be returned to the editor (proof-editing@biosciencetrends.com) within 3 working days.

Offprints: Authors will be provided with electronic offprints of their article. Paper offprints can be ordered at prices quoted on the order form that accompanies the proofs.

Page Charge: Page charges will be levied on all manuscripts accepted for publication in BioScience Trends (\$140 per page for black white pages; \$340 per page for color pages). Under exceptional circumstances, the author(s) may apply to the editorial office for a waiver of the publication charges at the time of submission.

(Revised October 2011)

Editorial and Head Office:

Pearl City Koishikawa 603
2-4-5 Kasuga, Bunkyo-ku
Tokyo 112-0003 Japan
Tel: +81-3-5840-8764
Fax: +81-3-5840-8765
E-mail: office@biosciencetrends.com

JOURNAL PUBLISHING AGREEMENT (JPA)

Manuscript No.:

Title:

Corresponding Author:

The International Advancement Center for Medicine & Health Research Co., Ltd. (IACMHR Co., Ltd.) is pleased to accept the above article for publication in BioScience Trends. The International Research and Cooperation Association for Bio & Socio-Sciences Advancement (IRCA-BSSA) reserves all rights to the published article. Your written acceptance of this JOURNAL PUBLISHING AGREEMENT is required before the article can be published. Please read this form carefully and sign it if you agree to its terms. The signed JOURNAL PUBLISHING AGREEMENT should be sent to the BioScience Trends office (Pearl City Koishikawa 603, 2-4-5 Kasuga, Bunkyo-ku, Tokyo 112-0003, Japan; E-mail: office@biosciencetrends.com; Tel: +81-3-5840-8764; Fax: +81-3-5840-8765).

1. Authorship Criteria

As the corresponding author, I certify on behalf of all of the authors that:

- 1) The article is an original work and does not involve fraud, fabrication, or plagiarism.
- 2) The article has not been published previously and is not currently under consideration for publication elsewhere. If accepted by BioScience Trends, the article will not be submitted for publication to any other journal.
- 3) The article contains no libelous or other unlawful statements and does not contain any materials that infringes upon individual privacy or proprietary rights or any statutory copyright.
- 4) I have obtained written permission from copyright owners for any excerpts from copyrighted works that are included and have credited the sources in my article.
- 5) All authors have made significant contributions to the study including the conception and design of this work, the analysis of the data, and the writing of the manuscript.
- 6) All authors have reviewed this manuscript and take responsibility for its content and approve its publication.
- 7) I have informed all of the authors of the terms of this publishing agreement and I am signing on their behalf as their agent.

2. Copyright Transfer Agreement

I hereby assign and transfer to IACMHR Co., Ltd. all exclusive rights of copyright ownership to the above work in the journal BioScience Trends, including but not limited to the right 1) to publish, republish, derivate, distribute, transmit, sell, and otherwise use the work and other related material worldwide, in whole or in part, in all languages, in electronic, printed, or any other forms of media now known or hereafter developed and the right 2) to authorize or license third parties to do any of the above.

I understand that these exclusive rights will become the property of IACMHR Co., Ltd., from the date the article is accepted for publication in the journal BioScience Trends. I also understand that IACMHR Co., Ltd. as a copyright owner has sole authority to license and permit reproductions of the article.

I understand that except for copyright, other proprietary rights related to the Work (e.g. patent or other rights to any process or procedure) shall be retained by the authors. To reproduce any text, figures, tables, or illustrations from this Work in future works of their own, the authors must obtain written permission from IACMHR Co., Ltd.; such permission cannot be unreasonably withheld by IACMHR Co., Ltd.

3. Conflict of Interest Disclosure

I confirm that all funding sources supporting the work and all institutions or people who contributed to the work but who do not meet the criteria for authors are acknowledged. I also confirm that all commercial affiliations, stock ownership, equity interests, or patent-licensing arrangements that could be considered to pose a financial conflict of interest in connection with the article have been disclosed.

Corresponding Author's Name (Signature):

Date:

